

63
62

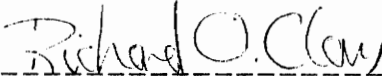
**CERAMIC COATINGS
FOR
SILICA AND SAPPHIRE
OPTICAL WAVEGUIDES FOR HIGH TEMPERATURE
EMBEDDING AND SENSING**

by
Ayesha R. Raheem-Kizchery

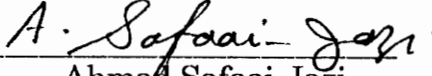
Thesis submitted to the Faculty of the
Virginia Polytechnic Institute and State University
in partial fulfillment of the requirements for the degree of

**Master of Science
in
Electrical Engineering**

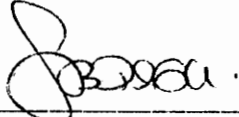
Approved



Richard O. Claus



Ahmad Safaai-Jazi



Seshu B. Desu

**May 1990
Blacksburg, Virginia**

c.2

LD

5655

V855

1990

R344

c.2

Ceramic Coatings for Silica and Sapphire Optical Waveguides for High Temperature Embedding and Sensing

by

Ayesha Rubiath Raheem-Kizchery

**Richard O. Claus, Chairman
Fiber & Electro-Optics Research Center**

(ABSTRACT)

Glass, sapphire and polymer fibers transparent to visible and infrared electromagnetic frequencies are extensively used in communication and sensing. The lifetimes of these waveguides are extended considerably by suitably coating them. Plastic coated silica waveguides are gradually replacing metal coaxial cables used in communications and they have been used successfully in various types of sensing. Unfortunately plastic coatings cannot withstand very high temperatures. In order to perform contact or invasive sensing in the medium to high temperature range and in harsh environments, other appropriate coating materials have to be used. This thesis examines various refractory materials as candidate coating materials.

Coating materials should not react chemically with the waveguide material but should have matching thermal expansion coefficients. Refractory materials are examined in detail for thermodynamic suitability for both sapphire and silica waveguide cores and claddings. The candidate coating materials selected are alumina, silicon carbide, zirconia and metal niobium. Experimental verification of the chemical inertness of these materials with silica and sapphire in very low pressure and at 857°C temperature is studied. The materials found suitable for coating can be coated using the various methods discussed. Fibers suitably coated with these materials would be suitable for high temperature sensing in harsh

environments and in situ within advanced high temperature composites.

Metal niobium does not react with sodium and is thermodynamically compatible with alumina which is also a very stable refractory material. Multilayer coatings of niobium and alumina on sapphire exposed to harsh environmental conditions can prolong the life of the sapphire waveguide.

X-ray diffraction and electron microprobe analyses of the single oxides and carbides, namely, alumina, silicon carbide and zirconia and the metal niobium, were conducted. It was found that sapphire did not react with any of the selected ceramics; the silica fiber underwent structural change in the silicon carbide matrix and the change was macroscopic. Within the restricted environment, the silica fiber appeared not to react with the alumina, zirconia and niobium matrices.

This thesis specifically considers the possibility of using the various ceramics as coating materials without analyzing the nature of the phases present. Hence detailed analyses of phases were not made when macroscopic change in fiber structure was observed or as observed during the x-ray analyses and microprobe analyses.

Acknowledgements

To my graduate advisor Dr. Richard O. Claus I express my gratitude for giving me the opportunity to work in the Fiber & Electro-Optics Research Center, for the subject of this thesis, his constant guidance and encouragement. Dr. Seshu B. Desu gave me valuable suggestions and plenty of encouragement. To Dr. Desu and Dr. Ahmad Safaai-Jazi I extend my thanks for serving on my committee and for being there for all the questions.

Dr. Paul Ribbe and Dr. Jim Craig of the department of Geology allowed me to use their equipment and invested time on some of the experiments. Without their help this project would not have been completed and I have a lot to thank them for. Todd Solberg gave me very valuable suggestions at the beginning of my work and helped me with the electron microprobe. Dr. David Hewitt unhesitatingly loaned me the first piece of platinum to start my experiment.

Tom S. Smithwick from the Radiation Safety Office came to conduct the Radiation Safety Test - a requirement to obtain permission to work on X-ray equipment. Neil Johnson, a postdoctoral student and Dr. Jim Light of the department of Geology helped me get started on their wonderful X-ray diffraction equipment. To all these wonderful people, especially from the department of Geology I express my gratitude.

Kathy Rohr from Materials Engineering taught me sample preparation for the microprobe. Thank you Kathy.

Evelyn Graybeal and Michael Cramer taught me to do a literature search on the data base.

To all the staff members of the **Fiber & Electro-Optics Research Center**,

Linda Jones and Ann Goette for the loan of their office keys, Berndt Zimmermann, Russ G. May, Kent Murphy, Mike Gunther and Kim Bennett for orienting me to the use of different equipment in the laboratories I am most grateful.

I thank the department of Electrical Engineering for giving me the opportunity to do my graduate studies and work on my thesis.

Lastly and most importantly I acknowledge the **Virginia Center for Innovative Technology**, the **US Department of Energy** and **The McDonnell Douglas Corporation** for their sponsorship of this project.

I thank one and all even remotely connected for their contribution to this thesis.

TABLE OF CONTENTS

1.0	Introduction.. .. .	1
2.0	The Coating Materials.. .. .	5
2.1	Alumina.. .. .	7
2.2	Silicon Carbide.. .. .	22
2.3	Zirconia.. .. .	23
2.4	Niobium.. .. .	31
3.0	Phase Diagrams and Analysis	32
3.1	Introduction.. .. .	32
3.2	Phases of selected ceramics.. .. .	40
4.0	Silica and Sapphire Fibers	46
4.1	Silica	46
4.2	Sapphire	54
4.3	Fiber Embedding	61
5.0	The Experiment	63
5.1	Description	63
5.2	X-ray Diffraction Analyses	64
5.3	The Electron Microprobe Analyses	90
6.0	Results and Conclusion	97
	Appendix	107
	Bibliography	109

LIST OF ILLUSTRATIONS

Chapter Two

Figure	2.1	Specific heat of alumina	9
Figure	2.2	Young's modulus of alumina as affected by temperature and density	10
Figure	2.3	Linear thermal expansion of single crystal and polycrystalline alumina	11
Figure	2.4	Thermal conductivity of polycrystalline alumina as a function of density	12
Figure	2.5	Thermal stress resistance of polycrystalline alumina	13
Figure	2.6	Compressive strength of polycrystalline alumina as affected by temperature and density.. .. .	14
Figure	2.7	Tensile strength of polycrystalline alumina as affected by temperature	15
Figure	2.8	Temperature dependence of hardness for polycrystalline alumina	16
Figure	2.9	Shear modulus of polycrystalline alumina as affected by temperature and density	17
Figure	2.10	Phase diagram of the system $K_2O-Al_2O_3-SiO_2$	18
Figure	2.11	Reaction layer height including depth of penetration for various alumina -corundum refractories reacted with soda vapors at 1350C for 12 hours	19
Figure	2.12	$KAlO_2-Al_2O_3$ phase diagram proposed by Moya et al ..	20
Figure	2.13	Phase diagram of $NaAlO_2-Al_2O_3$ proposed by Weber and Venero	21
Figure	2.14	Young's and shear modulus of zirconia	26
Figure	2.15	Linear thermal expansion of single-crystal zirconia as compared to unstabilized polycrystalline zirconia ..	27
Figure	2.16	Linear thermal expansion of zirconia	28

Figure	2.17	Specific heat of Zirconia	29
Figure	2.18	Thermal Conductivity of Zirconia as a function of Temperature	30

Chapter Three

Figure	3.1	Schematic G-P-T diagram showing origin of P-T diagram	37
Figure	3.2	Schematic diagram of the system H ₂ O at ordinary pressure.. .. .	38
Figure	3.3	Intersection of plane of constant pressure with three dimensional (p-T-x) binary system	39
Figure	3.4	System SiO ₂ - Al ₂ O ₃	41
Figure	3.5	System Al ₂ O ₃ - ZrO ₂ in Ar	42
Figure	3.6	SiO ₂ - ZrO ₂ system	43
Figure	3.7	Pt - Nb Phase diagram	44
Figure	3.8	Nb - O Phase diagram	45

Chapter Four

Figure	4.1	Linear thermal expansions of fused silica and quartz	48
Figure	4.2	Young's modulus, shear modulus and Poisson's ratio of bulk fused silica	49
Figure	4.3	Crack propagation velocity in water saturated air as a function of stress intensity factor for fused silica	50
Figure	4.4	Thermal conductivity of quartz and fused silica	51
Figure	4.5	Relative volume expansions of crystalline and amorphous phases of silica	52
Figure	4.6	Specific heat for quartz and fused silica	53
Figure	4.7	Tensile strength of sapphire filaments and whiskers as affected by temperature	56

Figure	4.8	Sapphire - Refractive index vs wavelength	57
Figure	4.9	Sapphire - Thermal Expansion vs temperature	58
Figure	4.10	Sapphire - Thermal conductivity vs temperature	59
Figure	4.11	Sapphire - absorption coefficient vs wavelength	60

Chapter Five

Figure	5.1	Alumina - Silica powder before heating	66
Figure	5.2	Alumina - Silica powder heated at 857°C for 120 hours ..	67
Figure	5.3	Alumina - Silica powder heated at 857°C for 240 hours ..	68
Figure	5.4	Alumina - Silica powder heated at 857°C for 360 hours ..	69
Figure	5.5	Alumina - Silicon carbide before heating	70
Figure	5.6	Alumina - Silicon carbide heated at 857°C for 120 hours ..	71
Figure	5.7	Alumina - Silicon carbide heated at 857°C for 240 hours ..	72
Figure	5.8	Alumina - Silicon carbide heated at 857°C for 360 hours ..	73
Figure	5.9	Alumina - Zirconia powder before heating	74
Figure	5.10	Alumina - Zirconia powder heated at 857°C for 120 hours	75
Figure	5.11	Alumina - Zirconia powder heated at 857°C for 240 hours	76
Figure	5.12	Alumina - Zirconia powder heated at 857°C for 360 hours	77
Figure	5.13	Silica - Silicon carbide before heating	78
Figure	5.14	Silica - Silicon carbide heated at 857°C for 120 hours ..	79
Figure	5.15	Silica - Silicon carbide heated at 857°C for 240 hours ..	80
Figure	5.16	Silica - Silicon carbide heated at 857°C for 360 hours ..	81
Figure	5.17	Silica - Zirconia powder before heating	82
Figure	5.18	Silica - Zirconia powder heated at 857°C for 120 hours ..	83
Figure	5.19	Silica - Zirconia powder heated at 857°C for 240 hours ..	84
Figure	5.20	Silica - Zirconia powder heated at 857°C for 360 hours ..	85
Figure	5.21	Silica - Niobium powder before heating	82
Figure	5.22	Silica - Niobium powder heated at 857°C for 120 hours ..	83
Figure	5.23	Silica - Niobium powder heated at 857°C for 240 hours ..	84
Figure	5.24	Silica - Niobium powder heated at 857°C for 360 hours ..	85

Figure	5.25	Schematic diagram of an Electron Microprobe	92
Figure	5.26	Silica fiber in Alumina heated for 360 hours at 857°C	94
Figure	5.27	Silica fiber in Zirconia heated for 360 hours at 857°C	95
Figure	5.28	Sapphire fiber in niobium heated for 360 hours at 857°C ..	96

Chapter Six

Figure	6.1	Alumina - Silica series	101
Figure	6.2	Alumina - Silicon carbide series	102
Figure	6.3	Alumina - Zirconia series	103
Figure	6.4	Silica - Silicon carbide series	104
Figure	6.5	Silica - Zirconia series	105
Figure	6.6	Silicon - Niobium series	106
Figure	6.7	Comparative chart of the selected materials	107

Appendix

Appendix A	Samples prepared for heat treatment	108
Appendix B	Samples of fiber cross section for microprobe	110
Appendix C	Silica in silicon carbide cross section	112

1.0 INTRODUCTION

The potential for sensing using fiber-optic technology has escalated since the first successful optical fibers were made available in the 1960s. Since the mid-1970s optical fiber technology has had considerable impact in the measurement of strain, temperature, magnetic and electric fields, acoustic waves and chemical concentrations. Areas of application include process control, laboratory tests and instrumentation, general industrial, medical and biological applications, and environmental, military and aerospace research. More recently, embedded optical fibers have been applied to the measurement of the effects of fatigue, cracks and material failure within different classes of materials. In the embedded form, optical fiber sensors may provide a potentially reliable method for the 'cure monitoring' of composites as well as vibration and internal defect detection in composites and other host materials.

Research in the area of 'smart skins and structures' and sensing using optical waveguides continues to be carried out at the Fiber & Electro-Optics Research Center (FEORC) at Virginia Tech. Differential interferometric and modal domain fiber methods for the measurement of strain, pressure and heat flow during cure, temperature insensitive fiber interferometry, polarimetric strain sensing, structural vibration and bend sensing are a few of the programs underway at FEORC.

The optical transmission and mechanical performance of optical fibers are very sensitive to the presence of impurities and structural and surface damage. Highly pure forms of silica glass fiber waveguide regions have minimized signal absorption and scattering losses. Protective coatings on the silica fiber waveguide help increase the lifetime and the flexibility of the fiber. They also help minimize abrasion and the alteration of surface characteristics, and prevent the long term deterioration of strength and stiffness at elevated

temperatures. Suitable fiber coatings also allow the possible enhancement of fiber/matrix wettability - an important consideration for embedded fibers.

Coatings for fibers to be used at high temperature must have the additional following qualities besides those of corrosion resistance and abrasion resistance.

1. The materials selected should have melting points much higher than that of the temperature range of interest.
2. The coating must adhere to the substrate by mechanical bonding.
3. Chemical or diffusion bonding between the fiber substrate and the coating material should be avoided because it would introduce detrimental changes in the fiber surface characteristics.

Other relations between the fiber waveguide material and the coating material are equally important. Thermal coefficient mismatch between the fiber and the coating can give rise to residual stresses. Growth-induced stresses caused by the imperfections in the coating during processing can cause debonding or cracks. Additionally, if the coating is a permeable material, the diffusion of oxygen through it can result in gaseous products that ultimately may rupture the coating.

A coating material which is thermodynamically matched to the waveguide material can be selected using a phase diagram analysis of the system. For multilayer coatings the choice of the coating materials can become very complicated because the thermodynamic compatibility must be established among three or more materials. When the sensor fiber also must be exposed to a wide range of temperature and pressure conditions, the choice of materials becomes even more limited.

The mechanical properties of the coating material and its chemical and

thermal expansion characteristics are all equally important considerations. The material must form a protective noninteracting layer between the waveguide and the environment. Several ceramic materials and one metal which appear to satisfy most of the material requirements have been selected for detailed analysis.

The selected materials are among those used for the refractory linings of coal gasification chambers, discharge tube materials, blast furnaces and glass melts on the basis of the following considerations.

- They may be exposed to large temperature fluctuation without degradation.
- In some cases they may be exposed to large pressure fluctuations without degradation.
- They are durable in the presence of harsh chemicals.
- They may be subjected to high strain due to sudden thermal changes without degradation.

The experimental study designed explores the bulk chemical interaction of these materials with alumina and silica. X-ray diffraction pattern, light microscope and electron microprobe analyses of the samples provide detailed information on the phase and chemical changes in the mixture.

Some of the sensing experiments for which these metal and ceramic coated waveguides can be used are as follows.

- Particulate build up monitoring and failure detection of ceramic filters used in coal gasifiers
- Strain, cracks and failure detection of high temperature composite materials

- High temperature and pressure sensing
- Vibration, strain and other mechanical sensing in harsh environments
- Temperature and pressure sensing in atmospheres limited by conventional fiber and coating material properties

Phase diagrams, their significance and the analysis of the available materials, a brief outline of the properties of each coating material, followed by some introduction to sapphire and silica waveguides, fiber embedding, a discussion about the experiments - the x-ray diffraction analyses and the electron microprobe analyses and the results and the conclusions are presented in the following chapters.

2.0 THE COATING MATERIALS

Oxides, nitrides, carbides, borides and similar materials which form the basis for all ceramics exhibit a high degree of chemical stability over a wide range of temperature and environmental conditions. The compactness of the crystal structure and the directed chemical bonding (mostly ionic or covalent in nature) account for the stability of ceramics [5, 6,13]. The specific heat capacity of ceramics in general is relatively unaffected by the microstructure of the material. Thermal conductivity is a tensor property, which depends strongly on the crystallographic orientation and the bond character of the solid. Hence it is different for different density, porosity and phases of the ceramic. The thermal expansion coefficient is also a structure - dependent quantity. Although ceramic materials in general do not have high thermal shock resistance because of their brittle nature, it can be improved by a low thermal expansion coefficient and high thermal conductivity. In applications involving rapid changes in temperature the thermal shock resistance becomes an important consideration. The elastic modulus of ceramic materials is quite complex for polycrystalline ceramics. The elastic properties depend upon the type of bonding, material homogeneity and isotropy. For monocrystalline ceramics the modulus is a linear function of temperature. The strength of a polycrystalline ceramic is also a very complex quantity, strongly influenced by the past history, temperature and environment as well as the size, shape and geometry of the article being tested.

Silica and single crystal alumina (sapphire) waveguides are both being considered for high temperature sensing. The refractory materials selected for analysis as possible waveguide coatings include the following.

Polycrystalline alumina (PCA)

Silicon carbide (SiC)

Zirconia (ZrO_2)

Zircon (ZrO_2SiO_2)

Niobium metal

Depending upon the particular gasification process, the materials may be subjected to temperatures between 700°C - 1000°C and pressures between 100-10,000 kPa (1 - 100 atmospheres). They are exposed to acids, alkali ashes, steam, CO_2 , hydrogen, methane sulphides and other contaminants without degradation. Surely, if these refractory materials have been applied in such atmospheres, they should be appropriate for reliable protection of the sensor fibers in less harsh environments for example, in temperatures of about 857°C and pressure of about 1000 kPa (10 atmospheres).

The refractory materials selected for blast furnaces and coal gasifiers have the following properties [1, 2, 3, 4].

- high thermal conductivity
- minimum rate of chemical reaction
- good resistance to abrasion, cracking and spalling

Discharge tube materials for HPS lamps must have the following properties [7, 8, 9, 10, 11].

- gas tight
- resistant to sodium vapor for vapor pressure between 5 - 100 kPa and for temperatures between 725°C - 1725°C
- low evaporation rate
- sufficient mechanical strength and resistance to thermal shock

In general the extent of chemical attack on any refractory linings are attributed to the porosity and purity of the material and the surface area exposed.

Polycrystalline alumina meets all of the above requirements. Metal niobium which is used in HPS lamp seals has thermal expansion very close to that of PCA and has been used successfully at temperatures up to 1000°C. A multilayered coating of metal niobium and alumina on sapphire fiber would be ideal to protect the fiber over a large range of temperatures, pressures and environments.

2.1 Alumina

Aluminum oxide (Al_2O_3), also called alumina, has a number of transitional structures depending on temperature. Above 1199°C alpha alumina is the only stable phase. It has the following important characteristics.

- hexagonal crystal structure
- theoretical density of about 3.98 g/cc
- melting point of about 2054°C
- thermal expansion coefficient at 1000°C is $8.1 \times 10^{-6}/^\circ\text{C}$

The thermal properties of alumina are depicted in the figures 2.1 - 2.13 in the next few pages [2, 3, 12].

The mechanical properties of alumina depend on the grain size, porosity and purity of the material. The compressive strength, tensile strength, hardness, shear modulus and Young's modulus as a function of temperature are also given. Several different commercially available samples are compared in some of the graphs. References indicate that alumina brick samples with 0% porosity exhibited little or no aggravation in alkali environment [1,2,3]. All grades of high - alumina bricks are better refractories and provide high chemical stability. The addition of a certain correct amount

of CaO, Y₂O₃ or La₂O₃ to densely sintered PCA increases its density nearer to its theoretical limit and inhibits discontinuous grain growth. This could influence the material properties [7]. The mechanical strength and related thermal shock resistance of the PCA depends on the microstructure which in turn is influenced by the dopant. Sodium diffusion takes place mainly along the grain boundaries, resulting in chemical reactions and microcracking. This is true for very high sodium vapor pressure and at very high temperatures. The reactions can be minimized if the temperature is kept below 1100°C. The temperature of interest to us is below 900°C and hence the question of microcracking should not arise. Figures 2.10[12], 2.11 [3], 2.12 and 2.13[2] provide some information on the reaction of alumina containing bricks and the phase diagrams of alumina and aluminates, respectively. As can be seen from the phase diagrams, most phase changes take place at temperatures far above the range considered in this project.

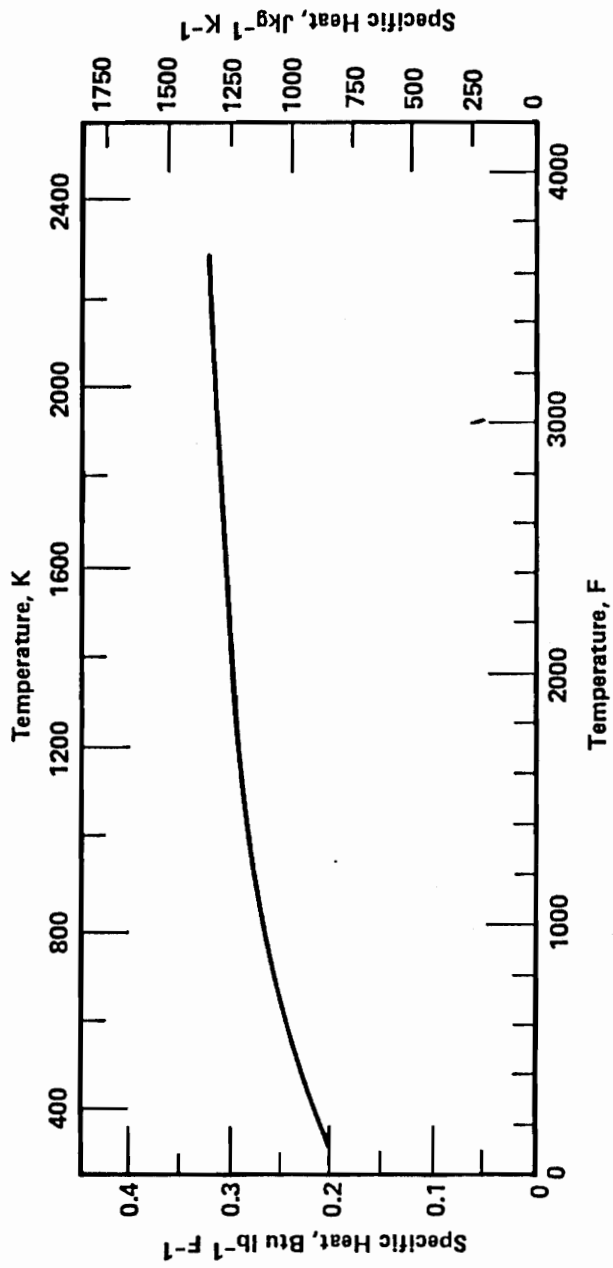


Figure 2.1 Specific Heat of Alumina [12]

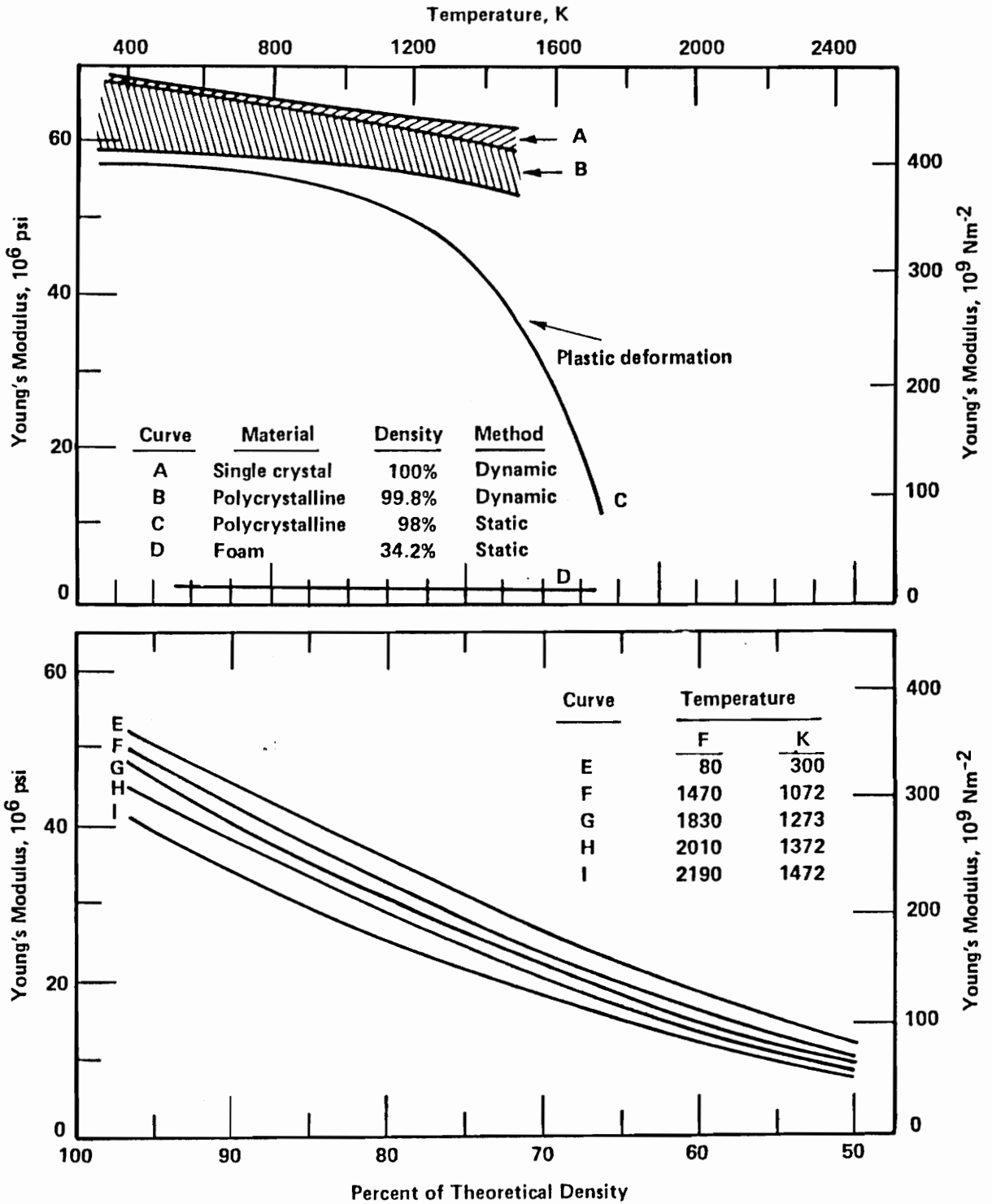


Figure 2.2 Young's Modulus of Alumina as Affected by Temperature and Density [12]

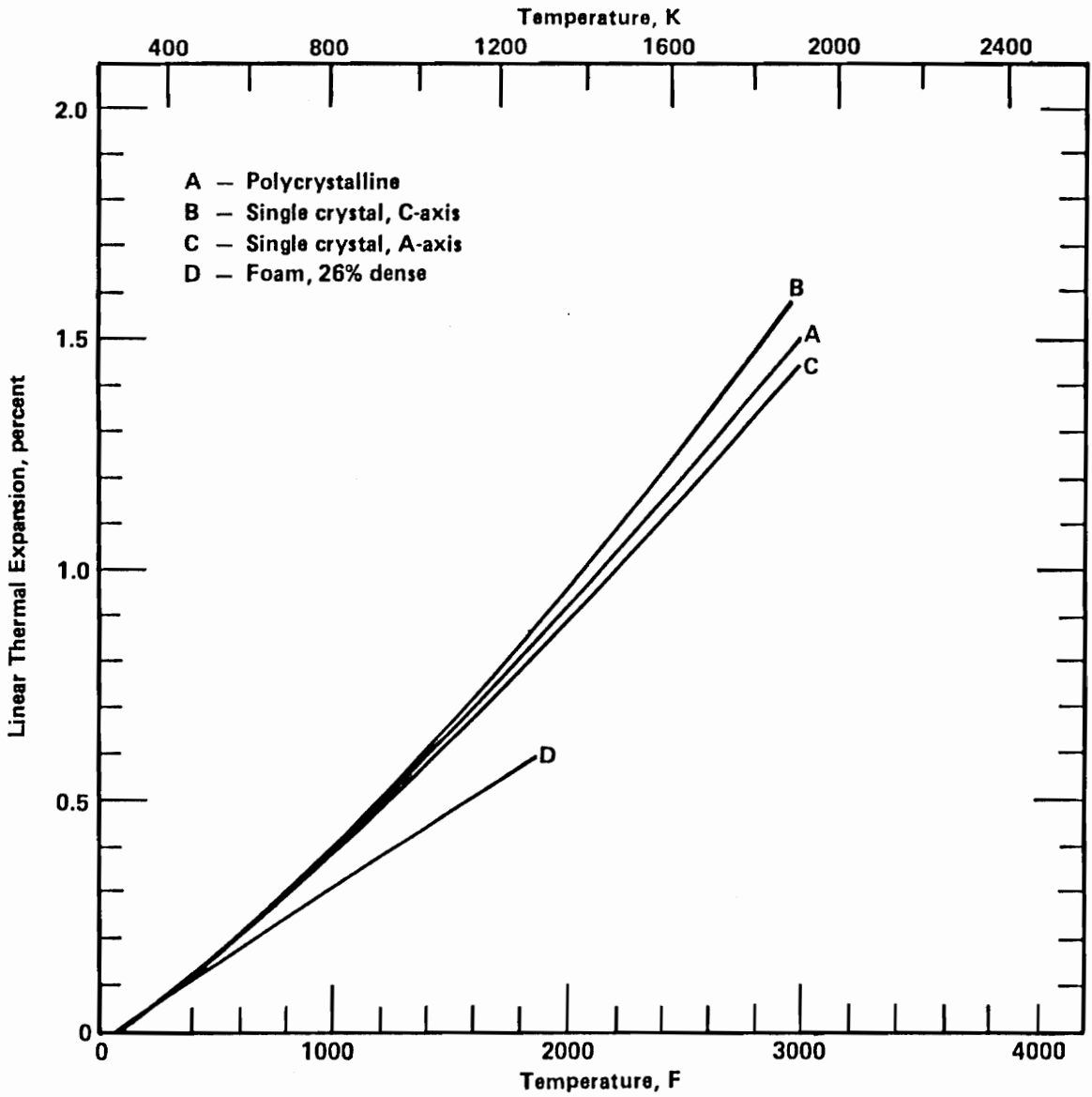


Figure 2.3 Linear Thermal Expansion of Single - crystal and Polycrystalline Alumina [12]

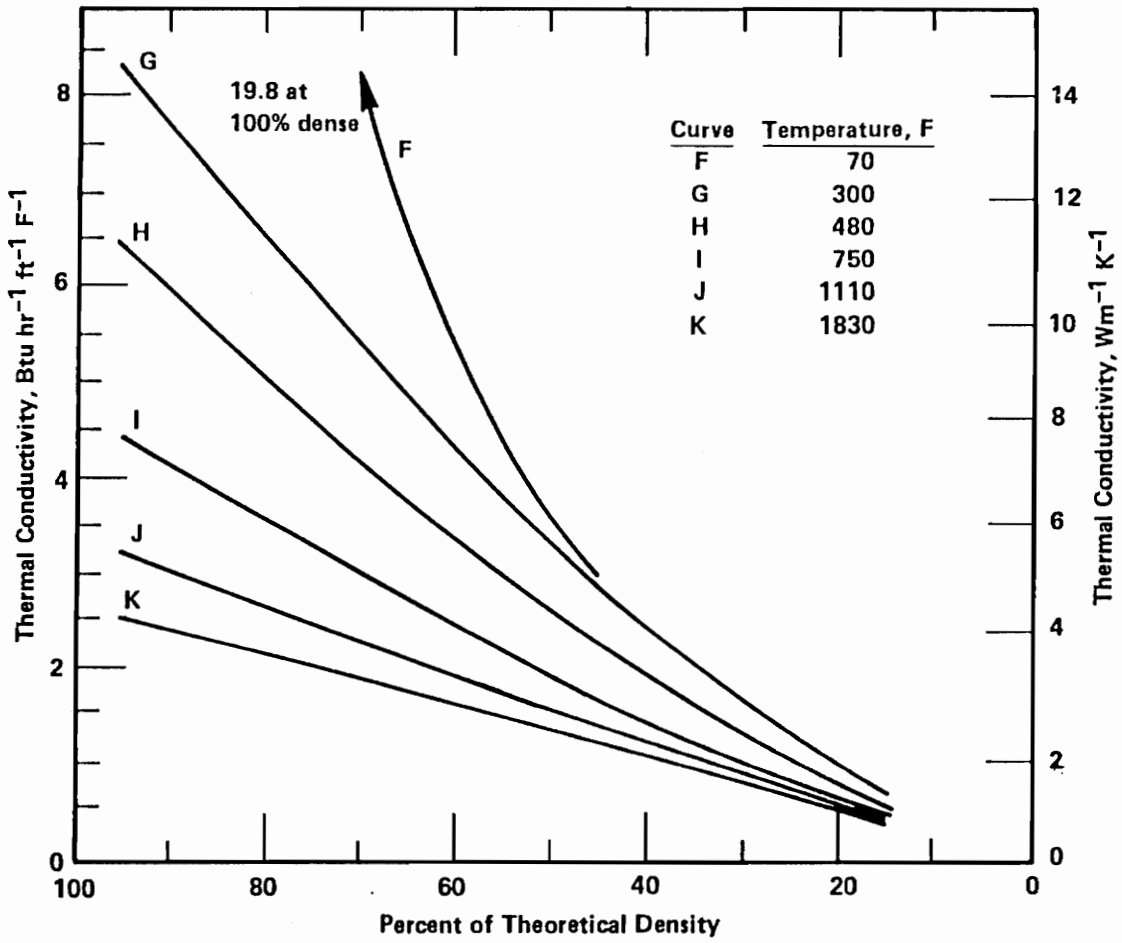


Figure 2.4 Thermal Conductivity of Polycrystalline Alumina as a Function of Density [12]

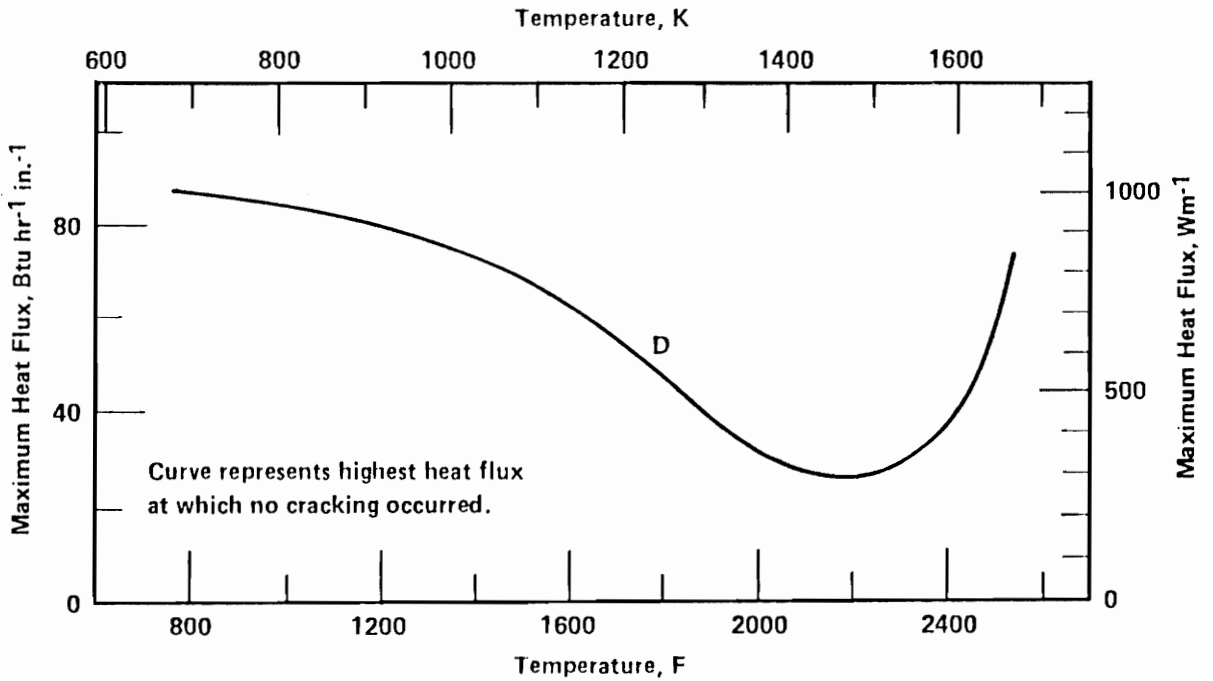
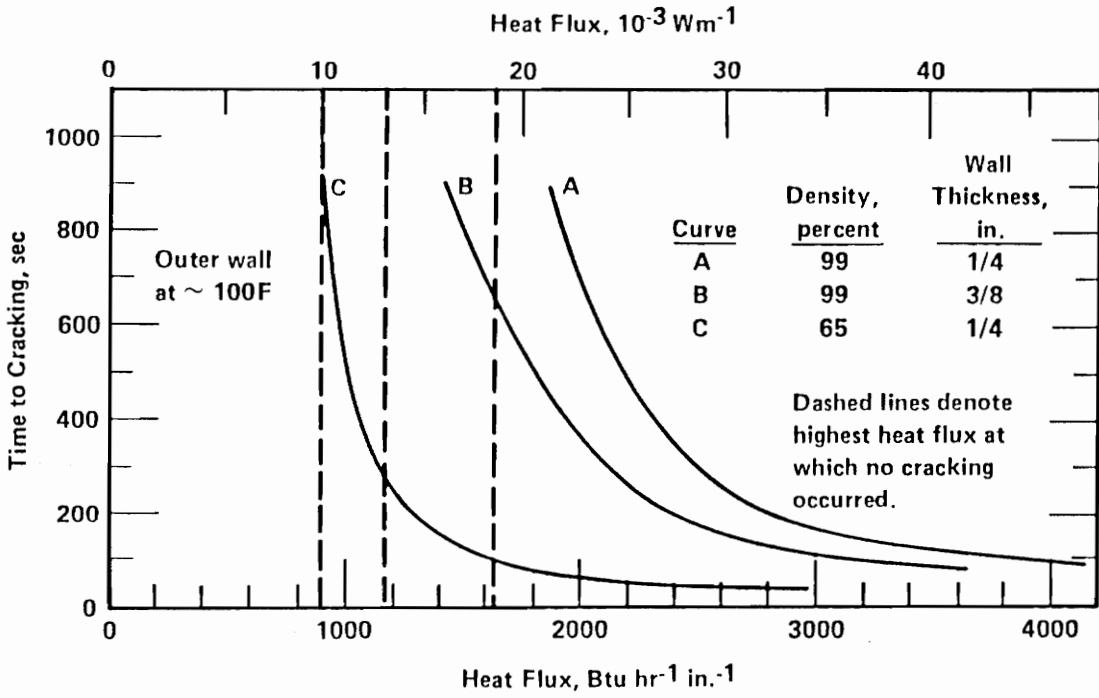


Figure 2.5 Thermal Stress Resistance of Polycrystalline Alumina [12]

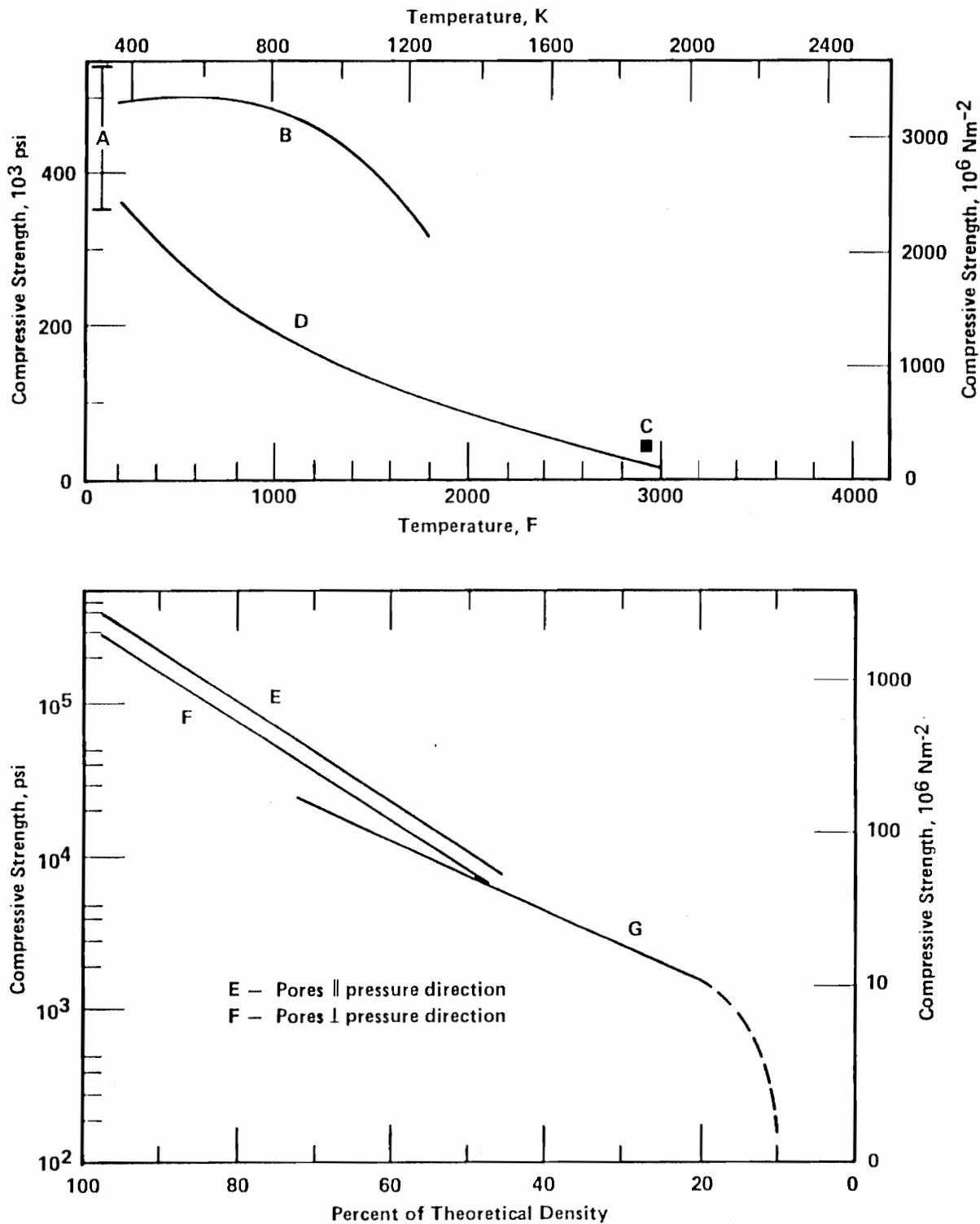


Figure 2.6 Compressive Strength of Polycrystalline Alumina as Affected by Temperature and Density [12]

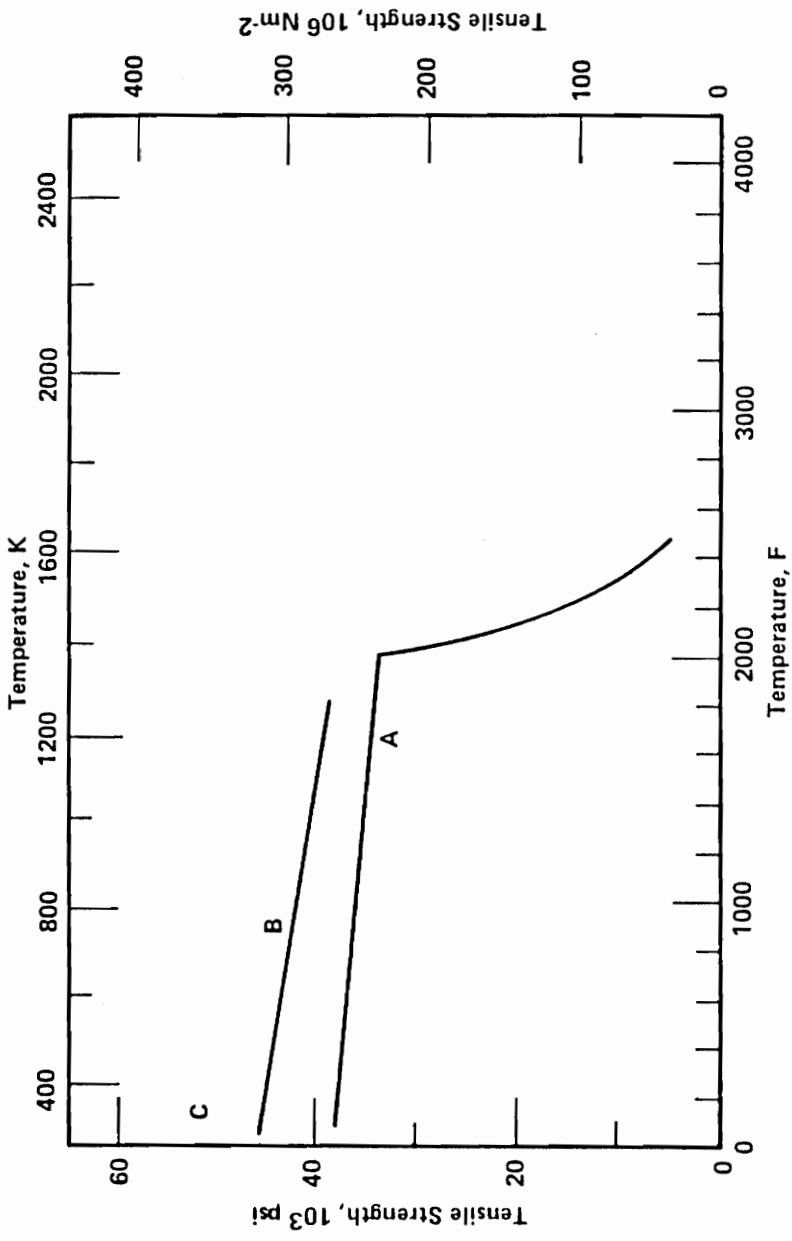


Figure 2.7 Tensile Strength of Polycrystalline Alumina as Affected by Temperature [12]

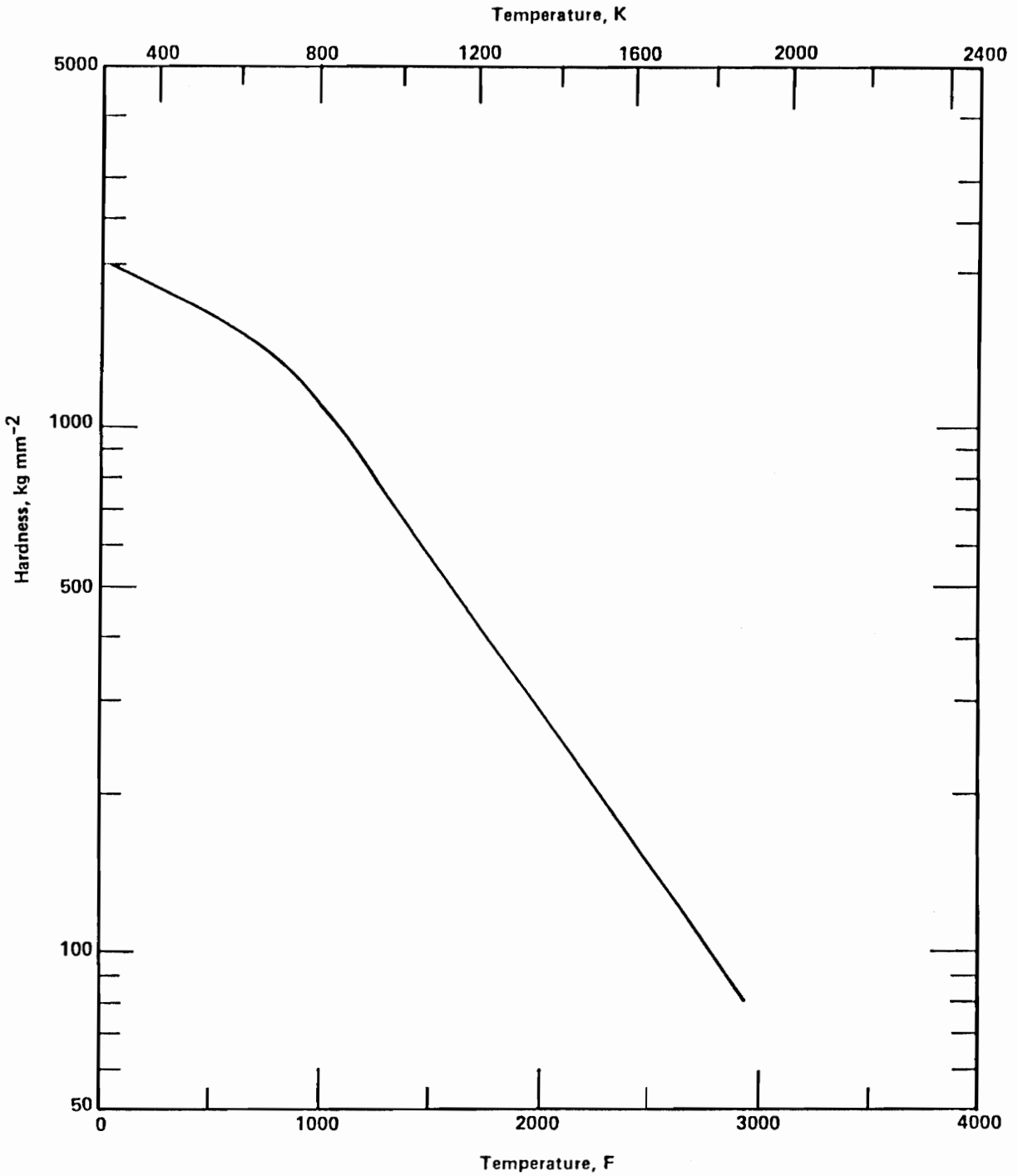


Figure 2.8 Temperature Dependence of Hardness for Polycrystalline Alumina

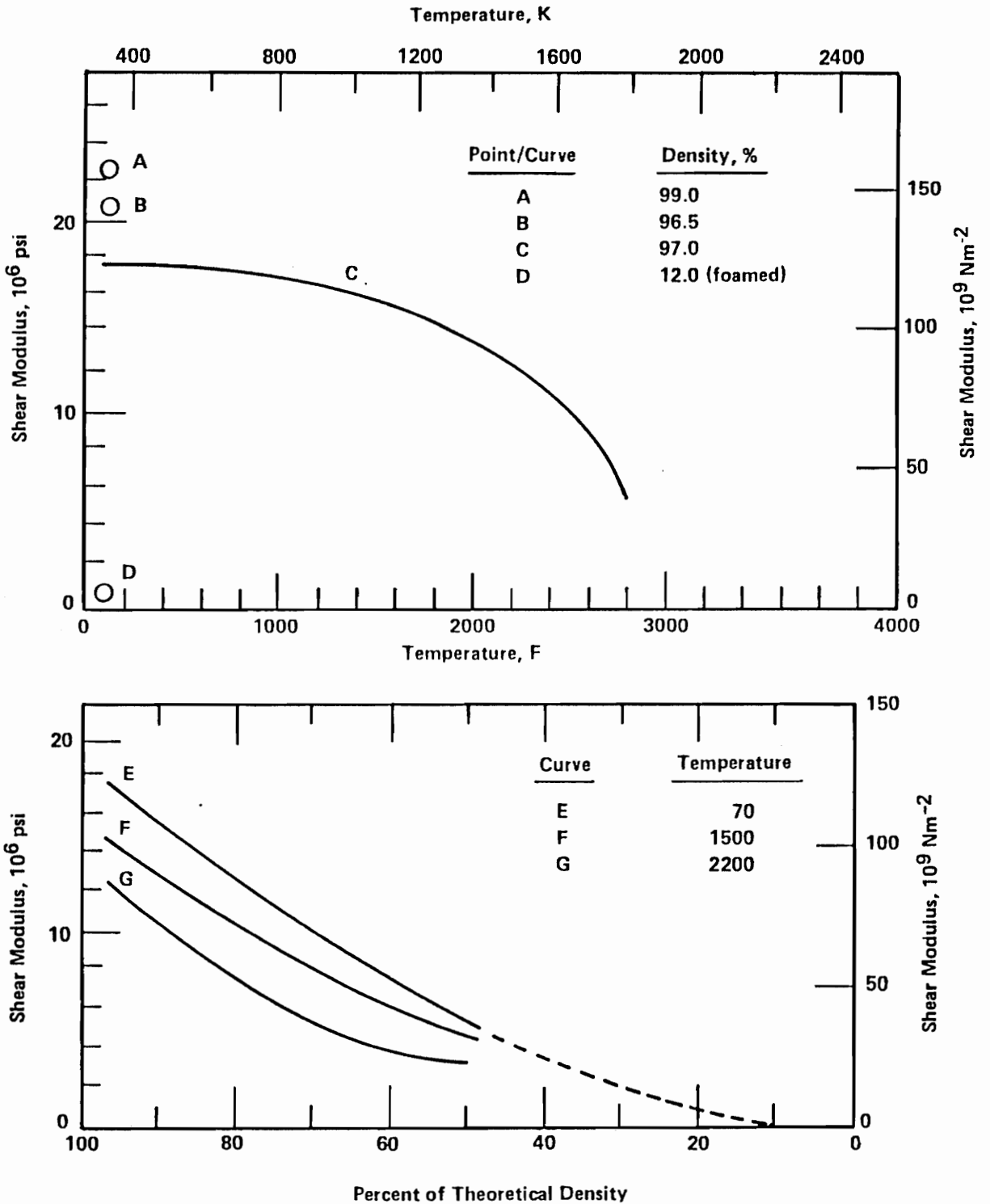


Figure 2.9 Shear Modulus of Polycrystalline Alumina as Affected by Temperature and Density [12]

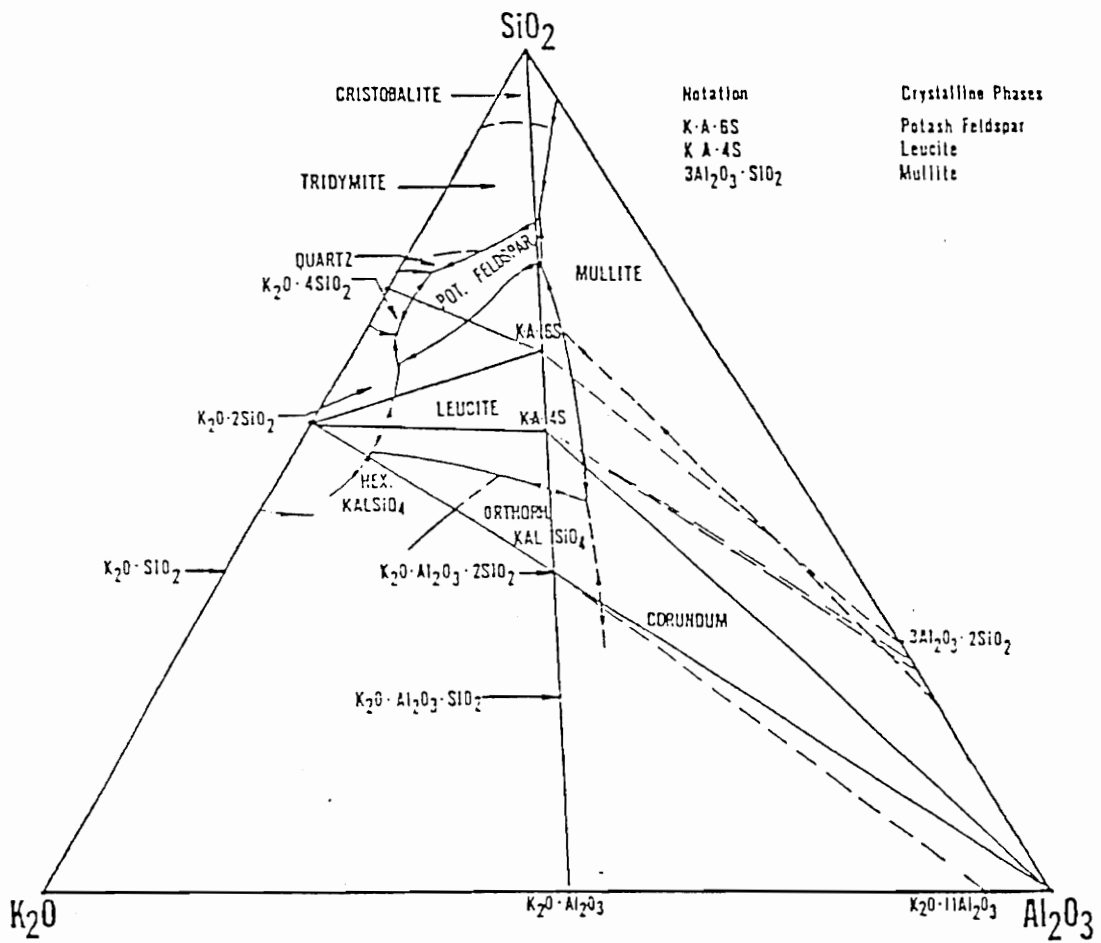


Figure 2.10 Phase Diagram of the System K₂O - Al₂O₃ - SiO₂ [3]

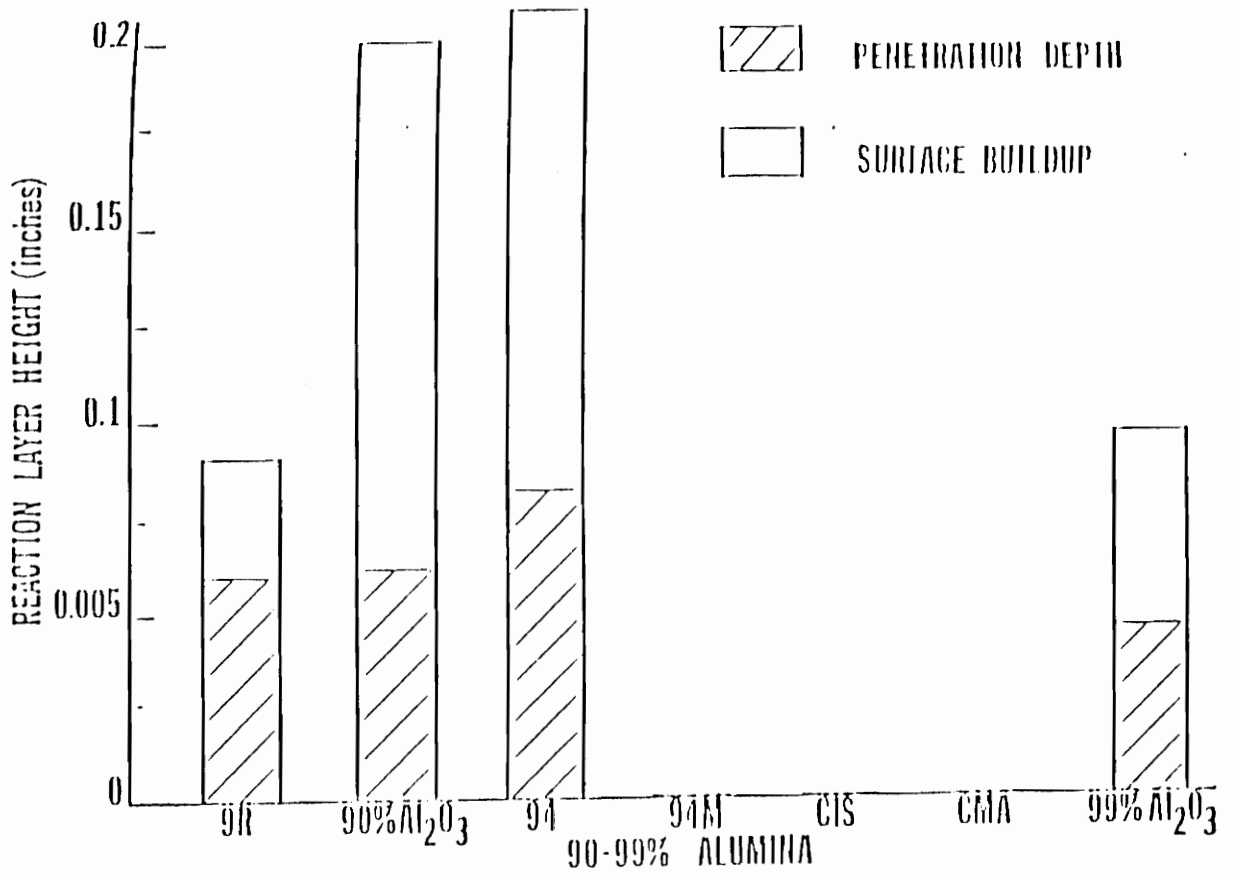


Figure 2.11 Reaction layer height including depth of penetration for various 90% alumina-corundum refractories reacted with soda vapors at 1350°C for 12 hours [3]

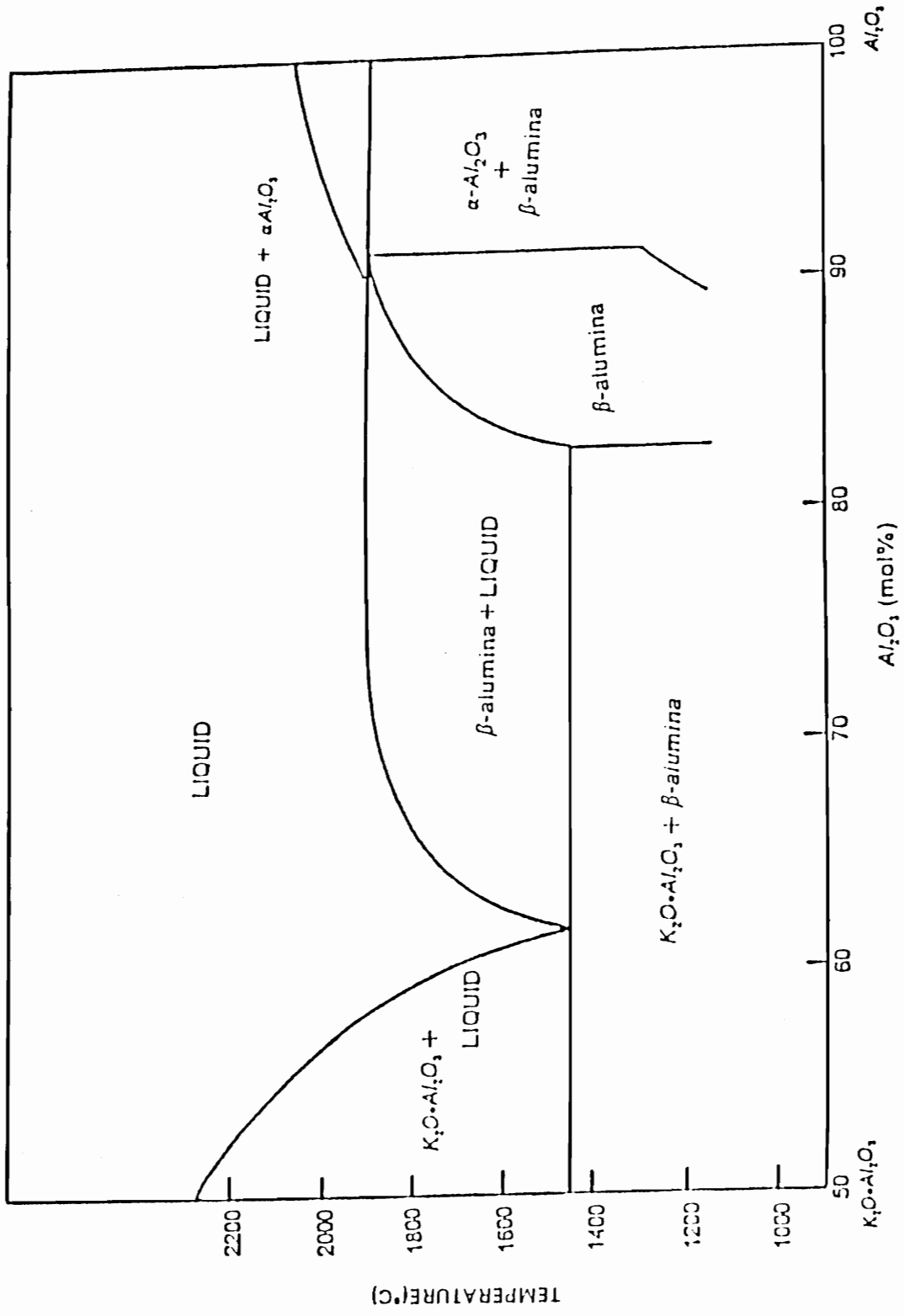


Figure 2.12 $KAlO_2 - Al_2O_3$ phase diagram proposed by Moya et al [2]

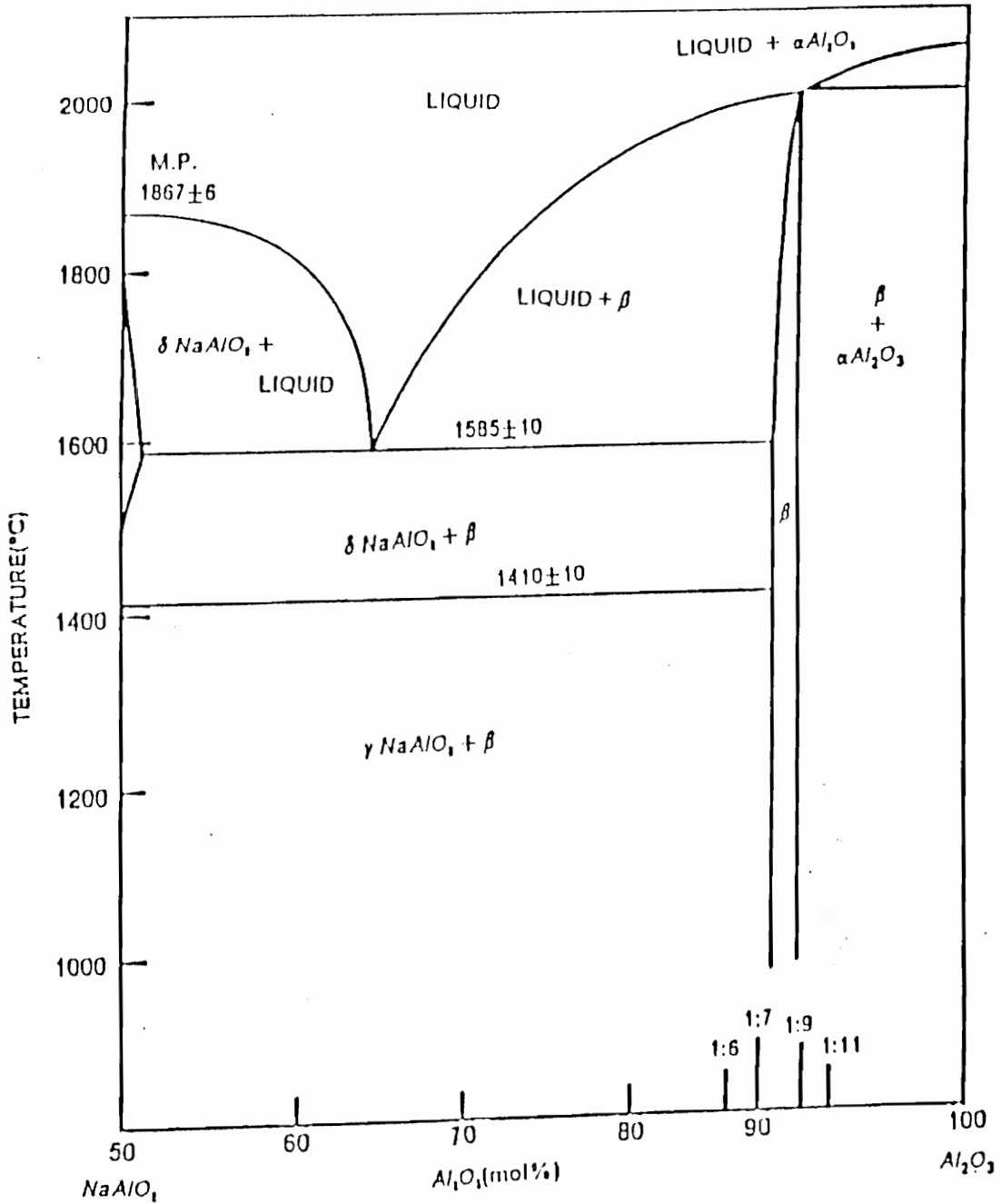


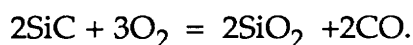
Figure 2.13 Phase diagram of NaAlO₂-Al₂O₃ proposed by Weber and Venero [2]

2.2 Silicon carbide

Electrofusion of silica sand and carbon produces SiC. It is a hard material and is highly resistant to abrasion. It is relatively stable and has a high thermal conductivity. At temperatures above 1400°C it has a tendency to oxidize. The important properties of bulk beta-SiC for this application are as follows [14].

- crystallographic structure fcc
a = 0.436 nm
- melting point
at 3.55 MPa (35 atm.) 2830°C
- density 3.21 gm/cc
- coefft. of thermal expansion $3.8 \times 10^{-6}/^{\circ}\text{C}$ at 200°C
 $5.8 \times 10^{-6}/^{\circ}\text{C}$ at 1000°C
- thermal conductivity 0.25W/cm/°C at 200°C
0.15W/cm/°C at 1000°C
- Young's modulus 450 GPa at room temp.
420 GPa at 1000°C
- fracture toughness 3 - 4.5 MN^{-3/2}
- Poisson's ratios 0.17 at room temp.
0.18 at 1000°C

The high thermal conductivity and the low thermal expansion of SiC makes it a strong, dense and thermally shock resistant material. SiC has been extensively used as an embedded fiber in metal matrix composites. Thermodynamically SiC is very prone to oxidation [15], yet it can exhibit excellent resistance to oxidation due to the formation of a stable protective layer of silica, ie.



It is best used in a reducing atmosphere. SiC refractories are not attacked by most acidic fluxes but molten steel can attack it. Direct bonded SiC bricks are relatively free of porosity and hence have enhanced temperature strength and chemical resistance.

2.3 Zirconia

ZrO₂ is the only stable oxide of the zirconium - oxygen system. It crystallizes in the monoclinic form at room temperature and inverts to tetragonal form at 945°C - 1225°C. This change of phase is accompanied by about a 9% volume change. A stable cubic structure can be induced using CaO, Y₂O₃ and MgO as stabilizers. The physical properties of zirconia are as follows [12].

- crystal system theoretical density
monoclinic 5.56g/cc
tetragonal 6.1g/cc
- melting point
tetragonal 2775°C ± 70°C

The melting point and the density of stabilized zirconia depends on the quantity of the stabilizer. The effect of the stabilizer is to lower the melting point of the material.

Most of the thermal and physical properties of zirconia are represented graphically in the figures which follow [12]. The discontinuities in the linear expansion curves indicate a crystal structure change. The stabilized cubic structure is free of discontinuities. The bend strength of zirconia is very

sensitive to the quantity and type of the stabilizing agent present.

Addition of 10 mole percent of either CaO or MgO is best for obtaining maximum strength, whereas with yttria-stabilized zirconia lesser mole percent produces maximum strength. As with all other ceramics, the density and porosity effect the bend strength, compressive strength, tensile strength and the modulus.

- Yttria- stabilized bend strength at 500°C is 14×10^7 Pa and at 1000°C is 119×10^6 Pa.
- MgO stabilized compressive strength are 1576×10^6 Pa and 1197×10^6 Pa at 500°C and 1000°C, respectively.
- Sintered MgO-stabilized zirconia with 5.2g/cc density and 5% porosity at 25°C showed tensile strength of 147×10^6 Pa. and at 1200°C it showed 84×10^6 Pa.
- The room temperature bulk modulus of calcia- stabilized 5.15g/cc zirconia is 98×10^9 Pa
- Poisson's ratios of 0.23 to 0.32 were reported for various oxide- stabilized zirconia.
- The Young's modulus and the shear modulus are graphically shown in Figure 14 [12].
- The thermal stress resistance of zirconia depends on the degree of stabilization.

Zirconia is stable in both oxidizing and moderately reducing atmospheres. At 2200°C zirconia decomposes to form carbide, nitride or hydride in the presence of carbon, nitrogen or hydrogen, respectively. Lithium vapor can cause corrosion at about the same temperature and a low pressure of 0.1 to 1mm of mercury. Zirconia reacts rapidly with hydrochloric and nitric acid. It is nonreactive with most heat resistant metals, carbon and

silicon up to 1400°C and it begins to react with refractory carbides at about 2000°C. At about 2000°C the stabilized zirconia starts vaporizing.

The properties of zirconia indicate that unstabilized zirconia would not be suitable as a coating material, because its structure changes at 950°C. At temperatures around 857°C, it will have to be experimentally verified whether unstabilized zirconia can serve as a reliable protective layer. Among the three stabilizers, yttria stabilized zirconia should be chemically more inert because of the stability of yttria.

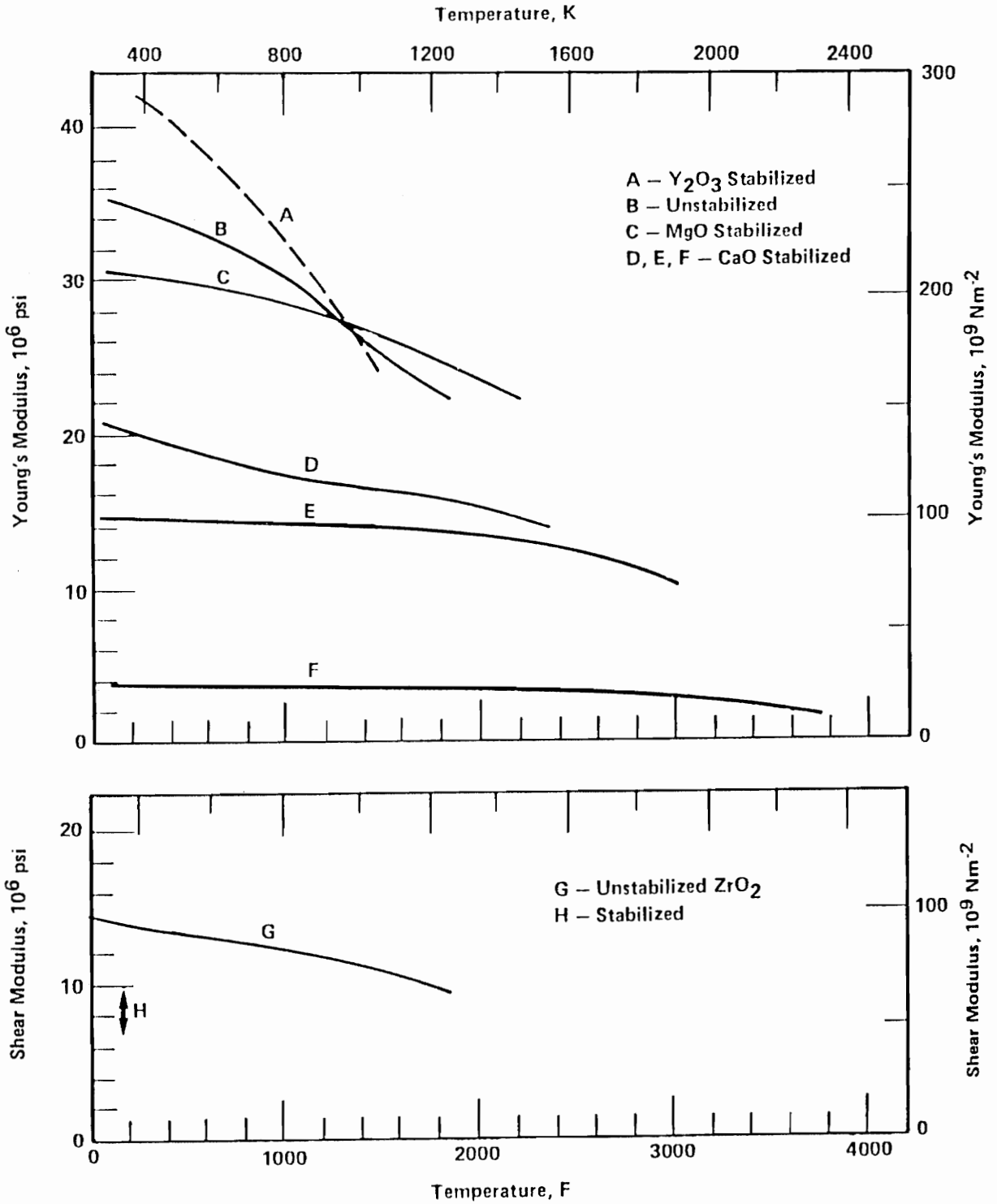


Figure 2.14 Young's and shear moduli of Zirconia [12]

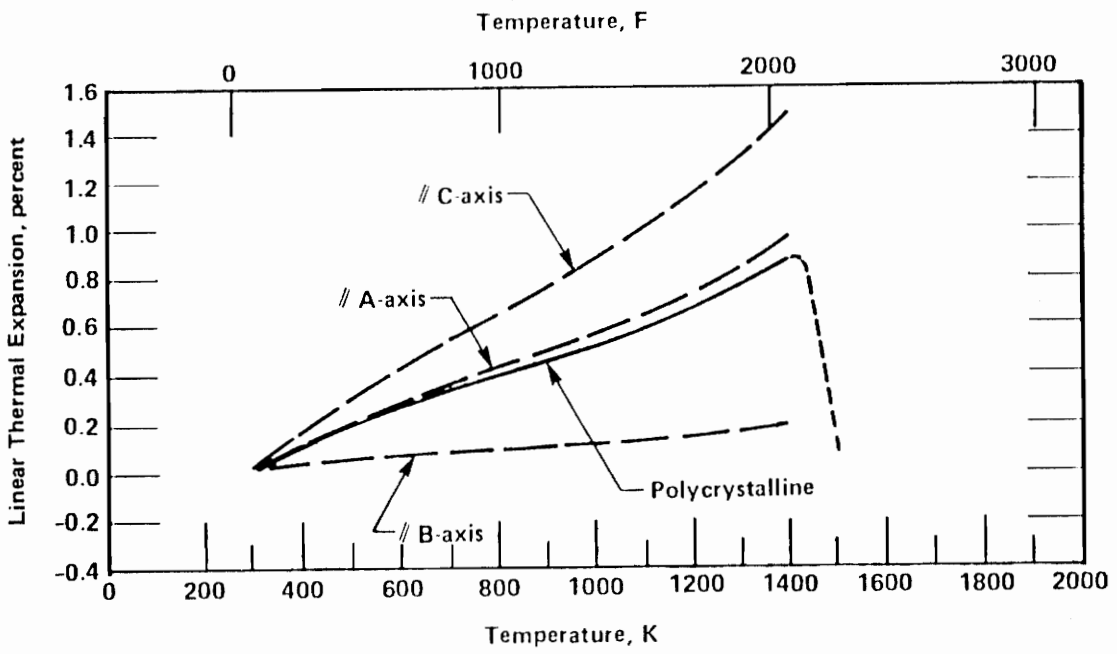


Figure 2.15 Linear thermal expansion of single-crystal zirconia as compared to unstabilized polycrystalline zirconia [12]

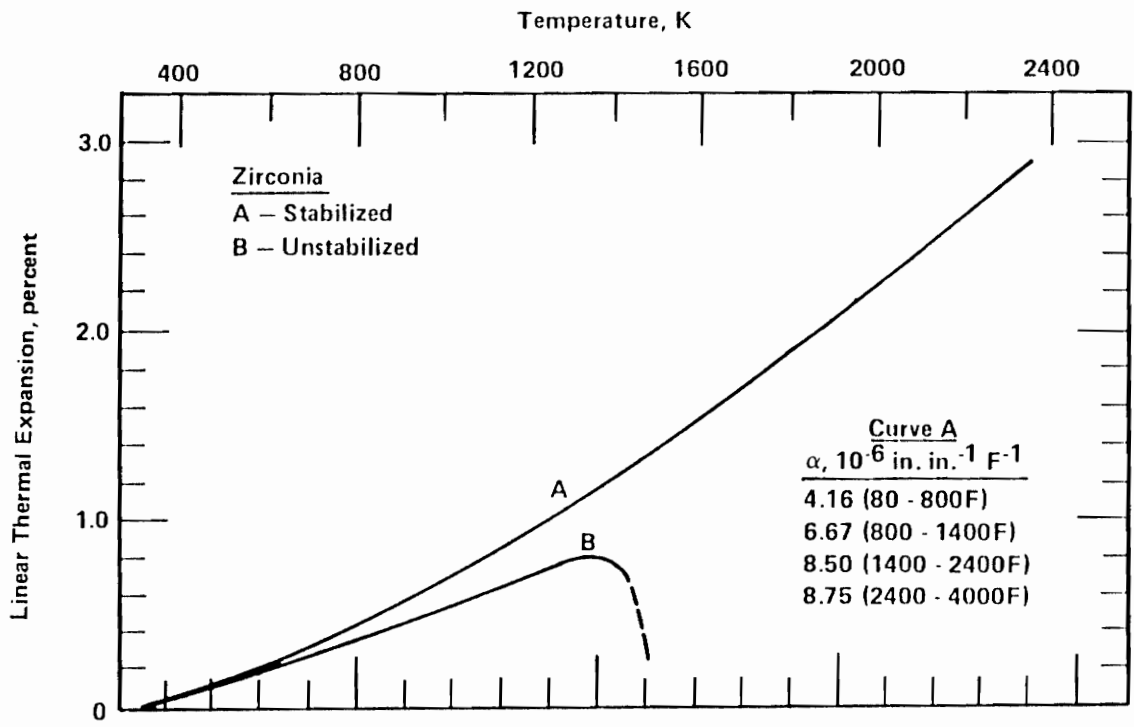


Figure 2.16 Linear thermal expansion of Zirconia

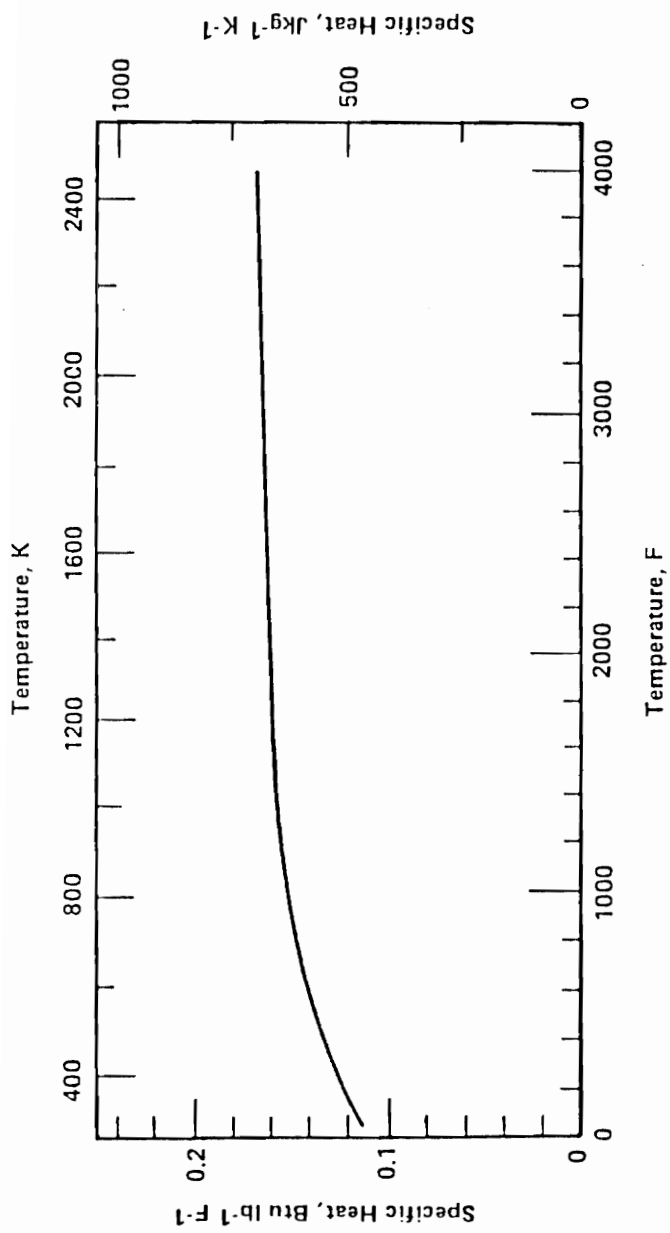


Figure 2.17 Specific heat of Zirconia [12]

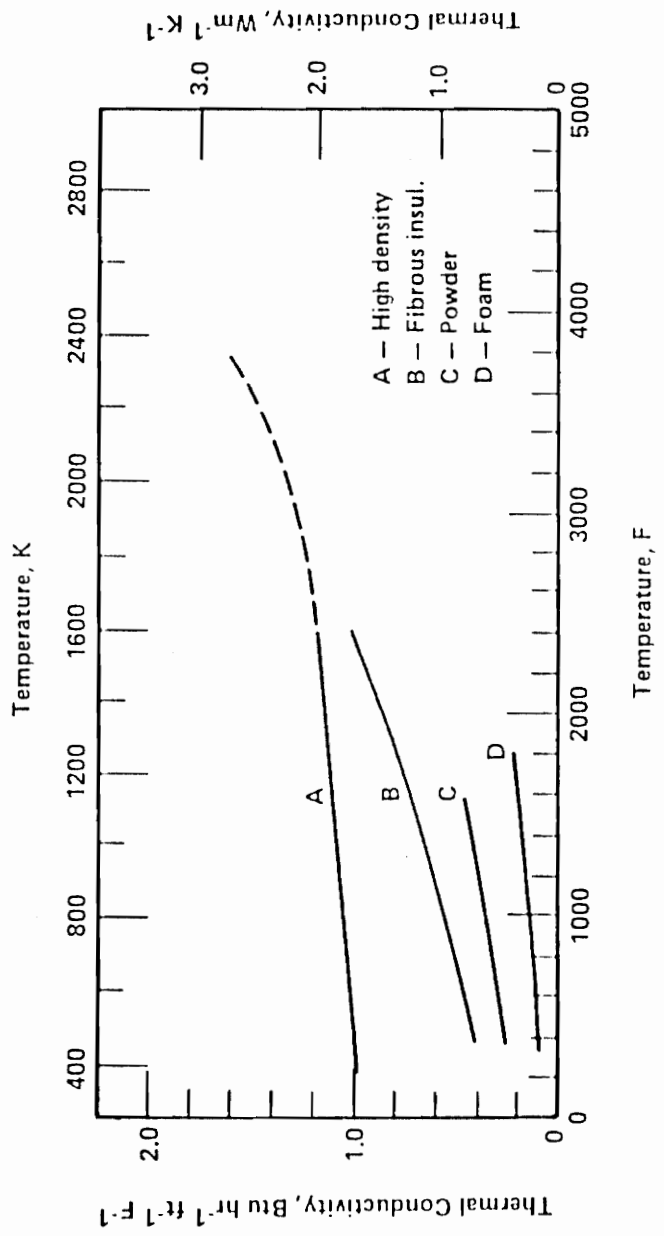


Figure 2.18 Thermal conductivity of zirconia as a function of temperature [12]

2.4 Niobium

Niobium or columbium is a shiny, white, soft and ductile metal, which takes on a bluish cast when exposed to air at room temperatures for a very long time. It has the following characteristics,

• crystal structure	bcc
• atomic weight	92.9064
• atomic number	4
• melting point	2468°C
• specific gravity	8.57 at 20°C
• thermal conductivity	0.125 cal/sq cm/°C
• specific heat at 25°C	0.065 cal/g
• linear coefficient of expansion	$7.1 \times 10^{-6}/^{\circ}\text{C}$
• tensile strength (annealed)	35×10^7 Pa

Niobium and PCA have matching thermal expansion coefficients and hence would be ideal for coating on sapphire. It is also resistant to sodium, mercury and other contaminants at high temperatures [9]. Hence it is used as a feed through in hps lamps. At temperatures above 1000°C and in the high sodium vapor atmosphere, the alumina to niobium seals react [11].

3.0 PHASE DIAGRAMS AND ANALYSES

3.1 Introduction

Most of the systems studied have been under mechanical, thermal or chemical equilibrium with their surroundings. Some interest in nonequilibrium states has developed during the last few decades. When there is no unbalanced force in the interior of a system, and also none between the system and its surroundings, the system is said to be in mechanical equilibrium. When these conditions are not satisfied, the system, or both the system and its surroundings, undergoes a change of state which ceases when the mechanical equilibrium is restored.

A system in mechanical equilibrium can undergo a spontaneous change of internal structure through chemical reaction, diffusion, dissolution, fission, fusion, etc. A system in chemical equilibrium does not undergo chemical reaction, diffusion or solution, however slowly. A system in thermal equilibrium has no temperature difference between parts of the system or between the system and its surroundings. When a system is in mechanical, chemical and thermal equilibrium the system is said to be in a state of thermodynamic equilibrium [21].

Phase diagrams and phase rules apply only to systems under thermodynamic equilibrium. A phase of a system is a mechanically separable portion, bounded by a surface and physically homogeneous. A system may contain more than one phase. Phases are distinguished by their different physical characteristics. The solid, liquid and gaseous states of a system represent three different phases of that system. Gases are completely miscible at ordinary pressures and hence represent only one phase. Solids and liquids, on the other hand can have several phases. Silica, for example, can exist in

several different crystalline structures. Each structure is a distinct phase. Since phases differ in physical characteristics, different phases of a system can be distinguished by their density, structure and optical properties.

The phase rule defines the conditions of equilibrium in terms of the number of phases and components of the system. A component of a system is one of the smallest independent chemical constituents of the system. In the alumina - silica system, there are two components - alumina and silica. Al, Si and O are not the components because they do not exist independently in the system. The phase diagram shown in figure 3.1 is a direct consequence of Gibbs free energy relation ($G = H - TS$), stated in differential form as

$$\partial G = V \partial P - S \partial T,$$

where G is the Gibbs free energy, H is the enthalpy defined by

$$H = U + PV,$$

where T, V and P are the temperature, volume and pressure, respectively, and S is the entropy of the system.

On integrating, the free energy surface for constant pressure and for constant temperature can be constructed as a three - dimensional graph.

$$G(P_1, T_1) = G(P_0, T_0) + \int_{P_0}^{P_1} V(P, T_0) \partial P - \int_{T_0}^{T_1} S(P_0, T) \partial T$$

where the $G(P_0, T_0)$ is an arbitrary reference point of the free energy surface. The first integral can be easily determined experimentally, and the integral variation of V as a function of P is can be constructed graphically.

The second integral at constant pressure, can be evaluated from

$$\partial S = \left(\frac{C_p}{T} \right) \partial T ,$$

where C_p is the heat capacity of the material at constant pressure. Heat capacity increases with temperature and for most ceramic materials and metals it can be represented by the equation

$$C_p = a + bT + cT^2 .$$

Coefficients a , b and c are experimentally determined constants and will vary from one material to another.

Phase diagrams are constructed for systems under equilibrium. If sufficient thermodynamic data were available, equilibrium relations of phases could be calculated and phase diagrams could be constructed from Gibbs free energy equation. Figure 3.2 illustrates the P-T diagram of water at ordinary pressures. Most phase diagrams are determined by experiments, because of the great difficulties involved. Phase diagrams are not constructed as a function of time. This is because the 'time' parameter does not explicitly come into the definition of equilibrium. A change of state can attain equilibrium in a few seconds or in several hundred years, depending on the system under consideration. Repeated experiments alone can provide information on the time involved in the establishment of a phase of a system.

The phase rule defines the conditions of equilibrium in terms of the number of phases and the components of the system.

$F = C - P + 2$, where

F = number of degrees of freedom,
 C = the number of components, and
 P = the number of phases.

This rule defines the maximum number of phases that can coexist at equilibrium. The constant "2" comes from the two variables, temperature and pressure.

A system consisting of two components is called a binary system and can be represented on the phase diagram as a function of pressure, temperature and composition. The phase relation of great interest in this project is the phase variation of the binary system as a function of temperature. Three variables, in general, control a binary system.

$$F = C - P + 2 = 4 - P,$$

where $C = 2$ in a two component system. From the equation it can be seen that there can be four coexisting phases with zero variance, three coexisting phases with a single variance, two coexisting phases with bivariance or a single phase that is trivariant. More explicitly, this implies that an invariant system could commonly consist of vapor, liquid and two solid phases, or two liquid and two solid phases, and so on. If only a single phase exists, for example, a liquid or a solid phase, then three variables would be needed to completely define the system, ie. the pressure temperature and the composition. Figure 3.3 is a schematic representation of a three- dimensional binary system.

The vapor pressures of most ceramic liquid and solid phases are so negligible up to 1500°C - 2000°C that the phase relations established at

atmospheric pressure would suffice. This simplifies the phase rule relation to

$$F = C - P + 1 = 3 - P.$$

Temperature - composition two-dimensional diagrams are sufficient to represent most binary systems where the phases can exist as simple eutectics, intermediate compounds and solid solutions [22].

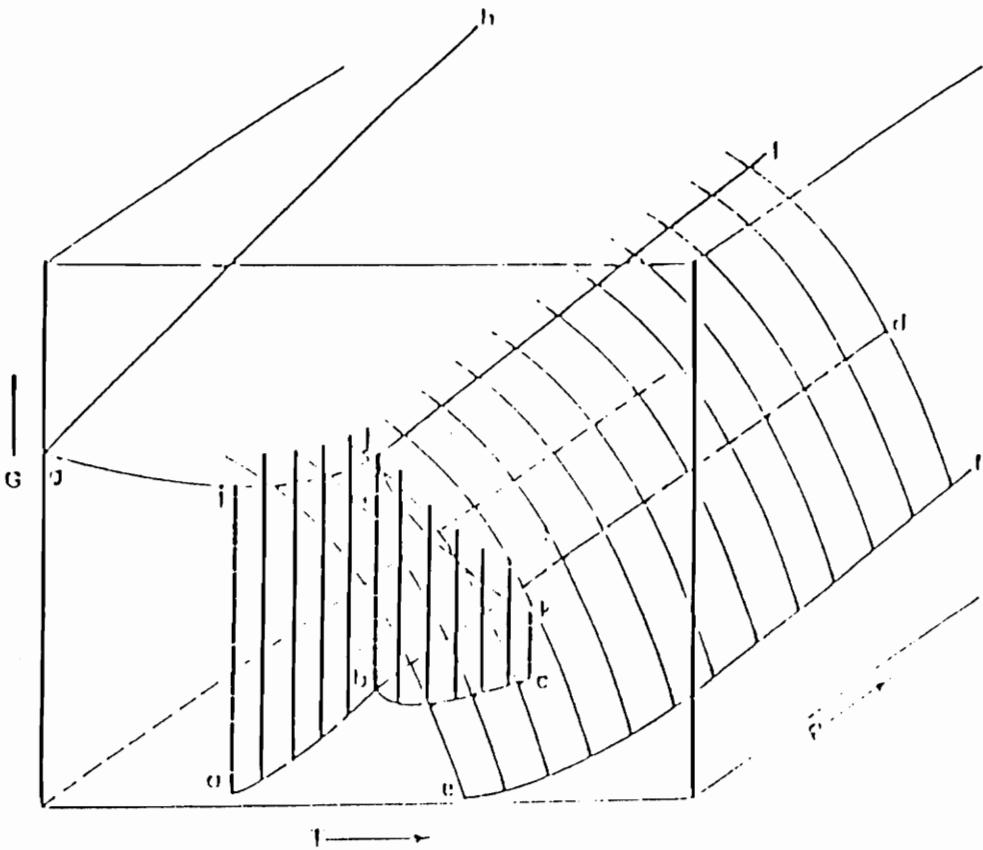


Figure 3.1 Schematic G-P-T diagram showing origin of P-T Diagram [22]

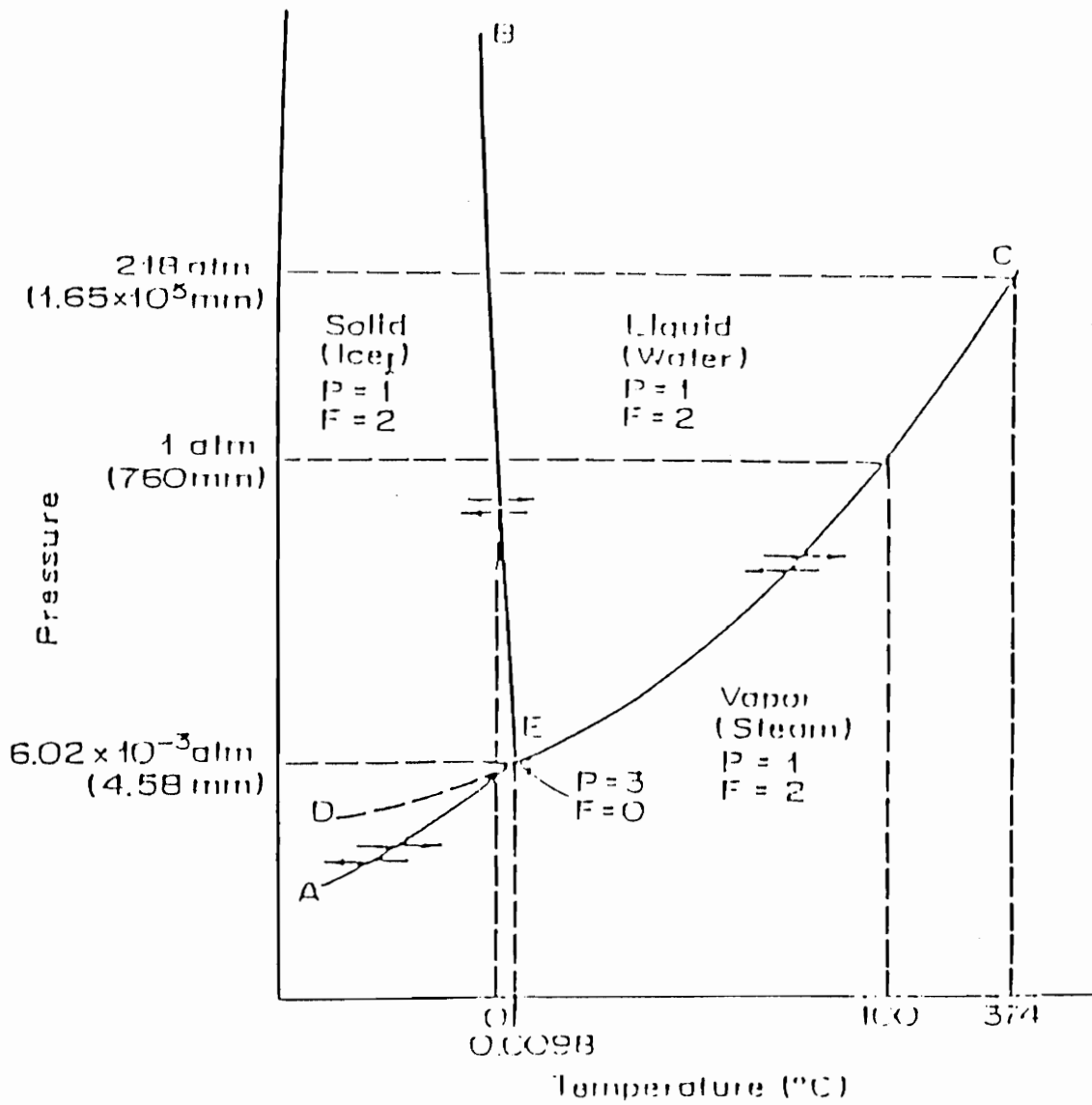


Figure 3.2 Schematic diagram of the System H₂O at ordinary pressures [22]

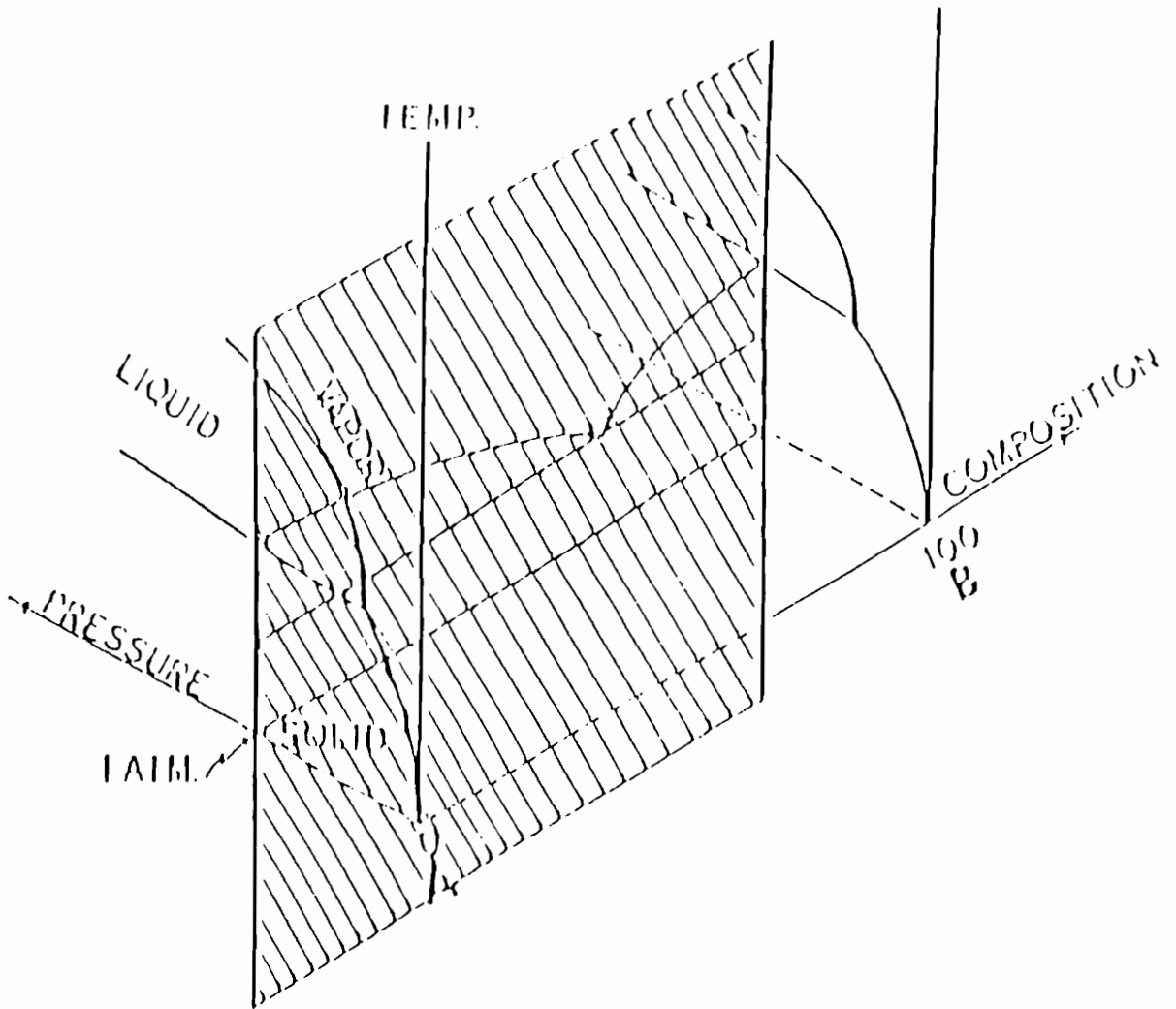


Figure 3.3 Intersection of Plane of Constant Pressure with Three Dimensional (P-T-X) Binary System [22]

3.2 Phases of selected ceramics

The phase diagrams of the selected ceramics and metal are analyzed in following diagrams [23]. These diagrams help to establish the relation between the types of the phases formed and the temperature involved. Again, since the phase relations do not consider the time factor, experimental confirmation is the only sure test of the nature of the thermodynamic relation between the optical waveguide substrate and the coating materials.

Figure 3.4 [23] describes the phase relation of alumina and silica for temperatures up to 2000°C. Samples studied were prepared from single crystal sapphire, mullite and fused silica, cristabolite, or 15% - 85% by weight of alumina and silica, respectively. The samples were then fired in air and in helium at 1550°C to 1800°C for varying times and then analyzed by an electron microprobe.

The two diagrams in Figure 3.5 [23] describe the alumina - zirconia phases. The distribution of the phases were found to be dependent on the composition and the cooling rate. The composition of alumina : zirconia (99 : 1) when fused in an arc furnace and quenched in water, yielded a new phase - ϵ alumina.

Figures 3.6 [23] illustrates the various phases of the silica - zirconia binary system. "C", "mon" and "tet" refer to cubic, monoclinic and tetragonal symmetry, respectively. Figures 3.7 [24] and 3.8 [24], respectively, indicate the reaction of metal niobium with oxygen and platinum. Niobium easily oxides in air and any coating with niobium has to be carried out in vacuum or under suitable inert gas atmosphere. Since niobium reacts with platinum, platinum containers cannot be used to conduct tests on niobium.

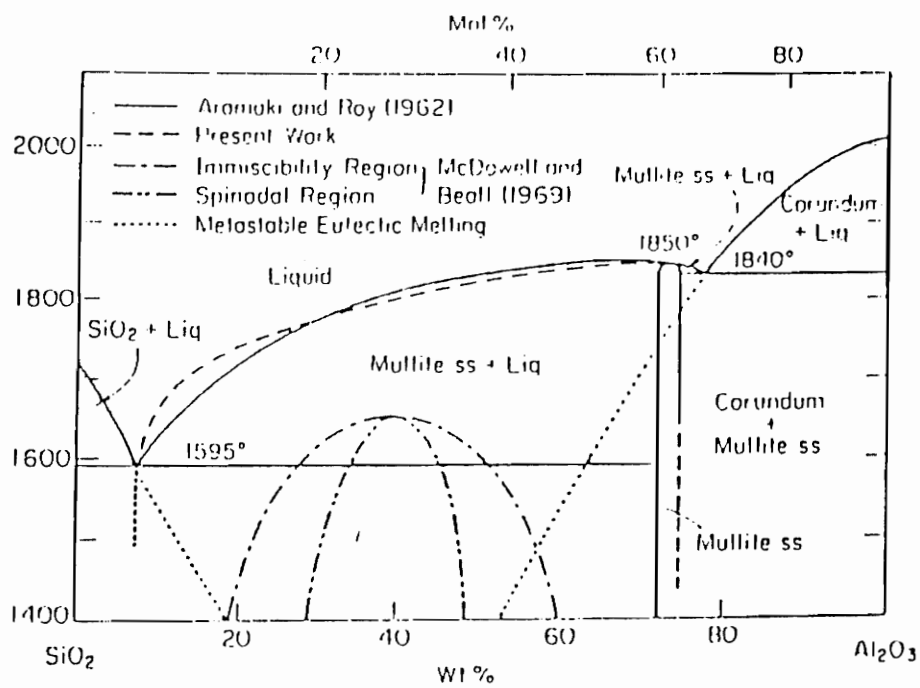


Figure 3.4 Al_2O_3 - SiO_2 System [23]

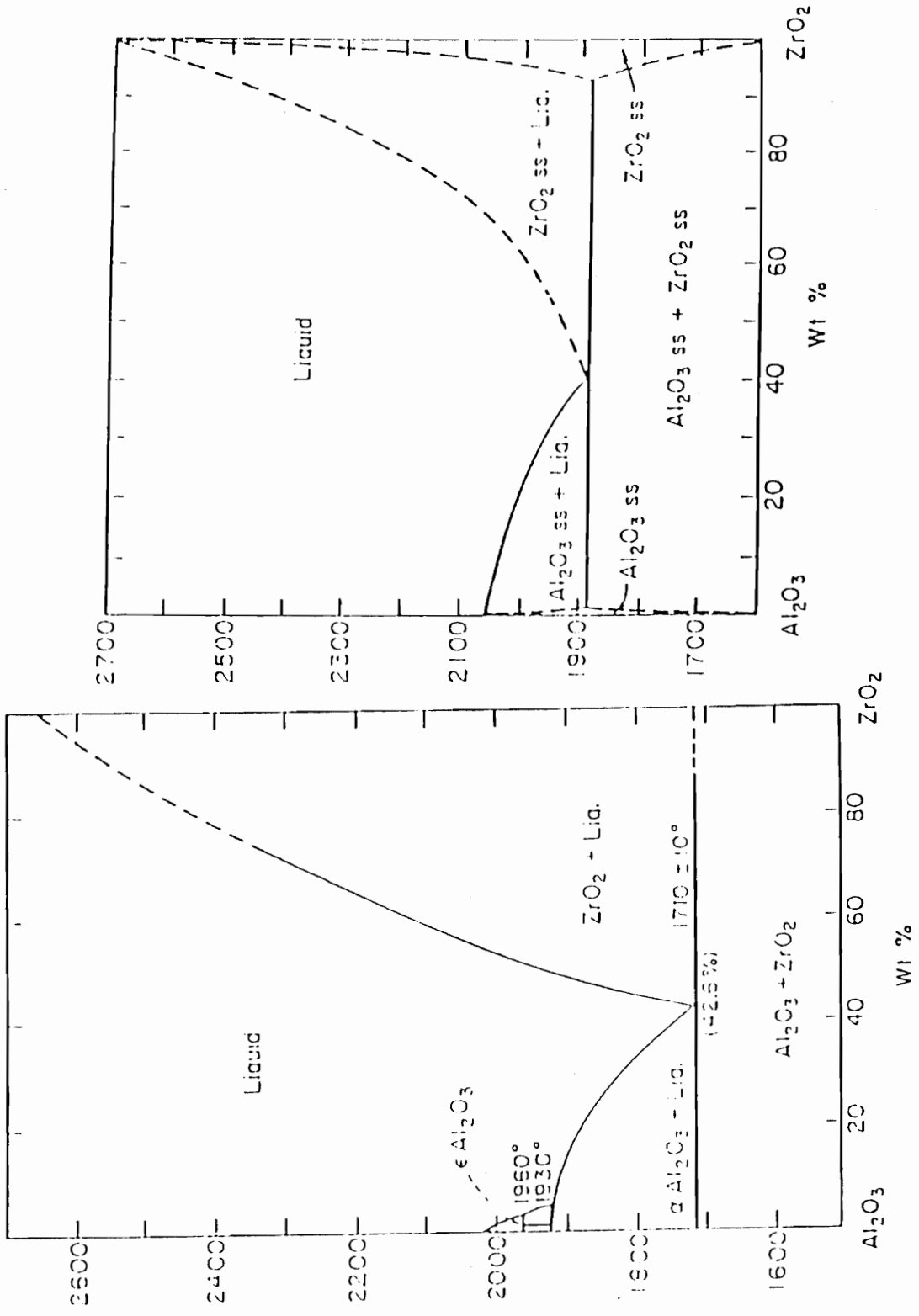


Figure 3.5 Al_2O_3 - ZrO_2 systems in air [23]

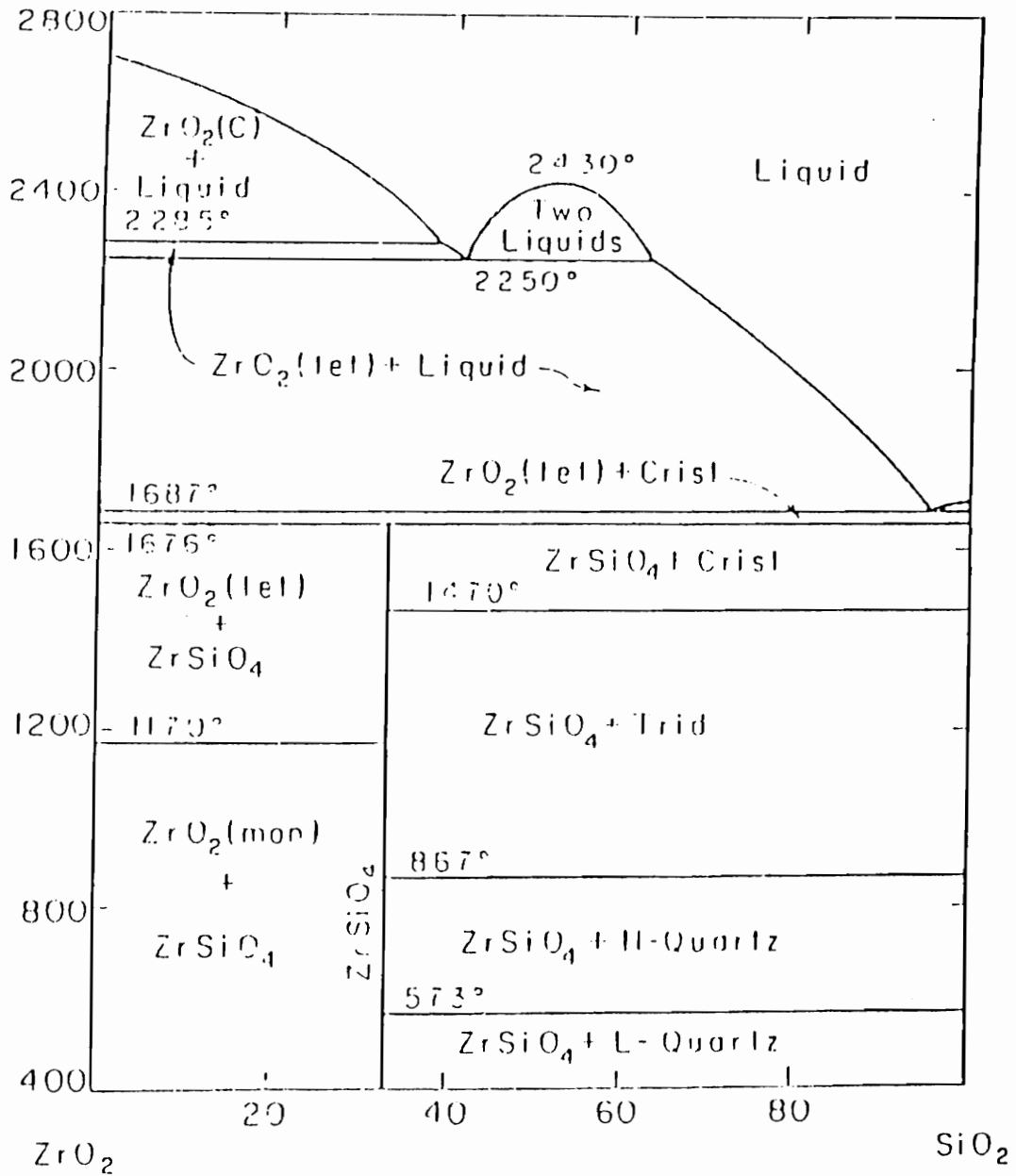


Figure 3.6 ZrO_2 - SiO_2 system [23]

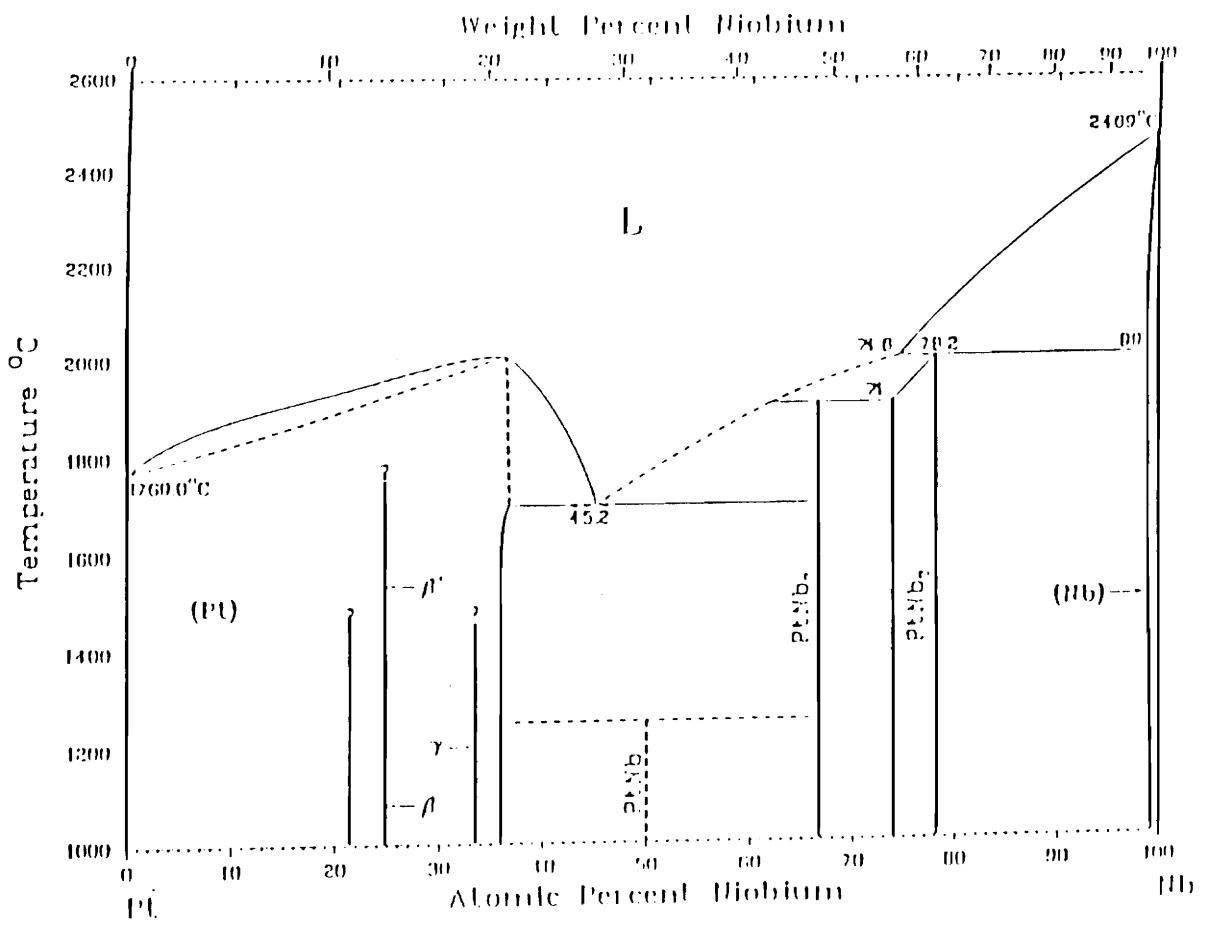


Figure 3.7 Pt - Nb phase diagram [24]

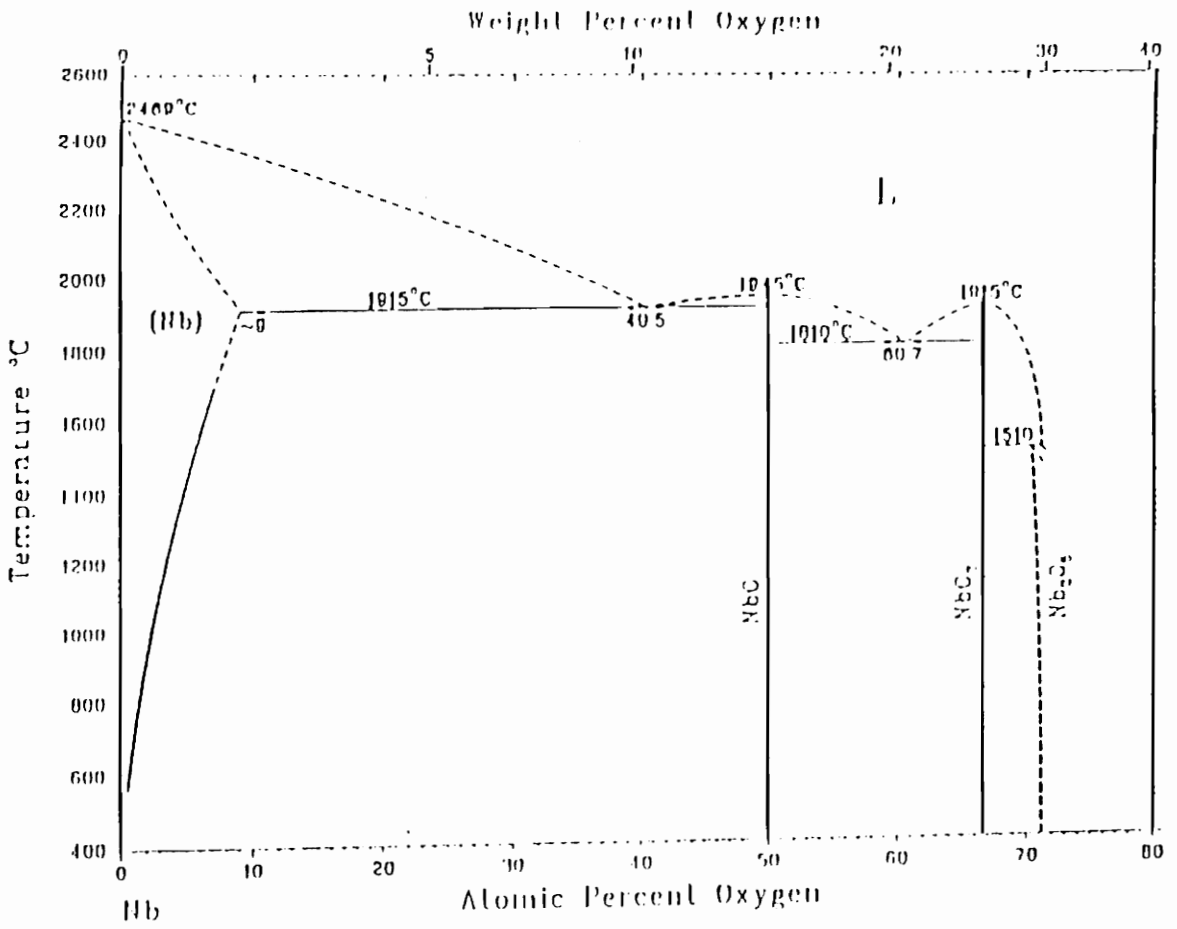


Figure 3.8 Nb - O Phase Diagram [24]

4.0 SILICA AND SAPPHIRE FIBERS

4.1 Silica

Optical waveguides are transmission lines at visible and infrared frequencies. Glass and sapphire are examples of two transmitting media transparent to the frequencies stated. Optical waveguides can be classified into single-mode and multimode, step index and graded index fibers, where a lower refractive index outer cladding region of the fiber minimizes transmission losses. Fused silica glass purified to a great degree can transmit light with very low losses in the near infrared region. Much literature is available concerning the optical aspect of glass. Since this paper is concerned with coating compatibility of materials, both glass and single crystal alumina are examined from the materials point of view.

Fused silica has high thermal stress resistance due to its exceptionally low thermal expansion coefficient. It has excellent resistance to most chemicals at ordinary temperatures and pressures. When exposed to hydrofluoric and phosphoric acids and to concentrated alkaline solutions, the rate of the chemical reaction becomes a function of temperature, pressure and concentration of the chemical reagent [12]. Fused silica is not attacked by dry molecular or atomic hydrogen up to 800°C. Bulk fused silica has a low permeability for all gases, but at high temperatures it is permeable to gases with low molecular weight.

Even though glass is intrinsically one of the strongest known materials, water can attack glass. Flaw free glass can withstand very high tensile loads but the presence of microcracks can severely retard the load-to-failure characteristics of glass. The rate of crack growth depends both on the chemical environment and the magnitude of the applied stress. In the absence of stress silica reacts very slowly with water. Water reacts with silica

by rupturing the silicon - oxygen bond at the crack site and gradually the crack advances.

The strength of optical waveguide fibers and the static fatigue failure of optical fibers due to bending have been studied [25 - 31]. Flaws in the fiber lead to fatigue. The three most contributing factors are moisture, strain and crack or flaw. If one of the factors is absent fatigue will not occur. Fused silica fiber has relatively high tensile strength in inert gas or vacuum when compared to its tensile strength in room atmosphere. This is due to the presence of moisture. Coated silica fibers are protected from moisture. Bending techniques are a useful for providing additional information on the strength of a fiber.

Figures 4.1 to 4.6 provide graphical analyses of thermal expansion, Young's modulus, velocity of crack propagation and thermal conductivity.

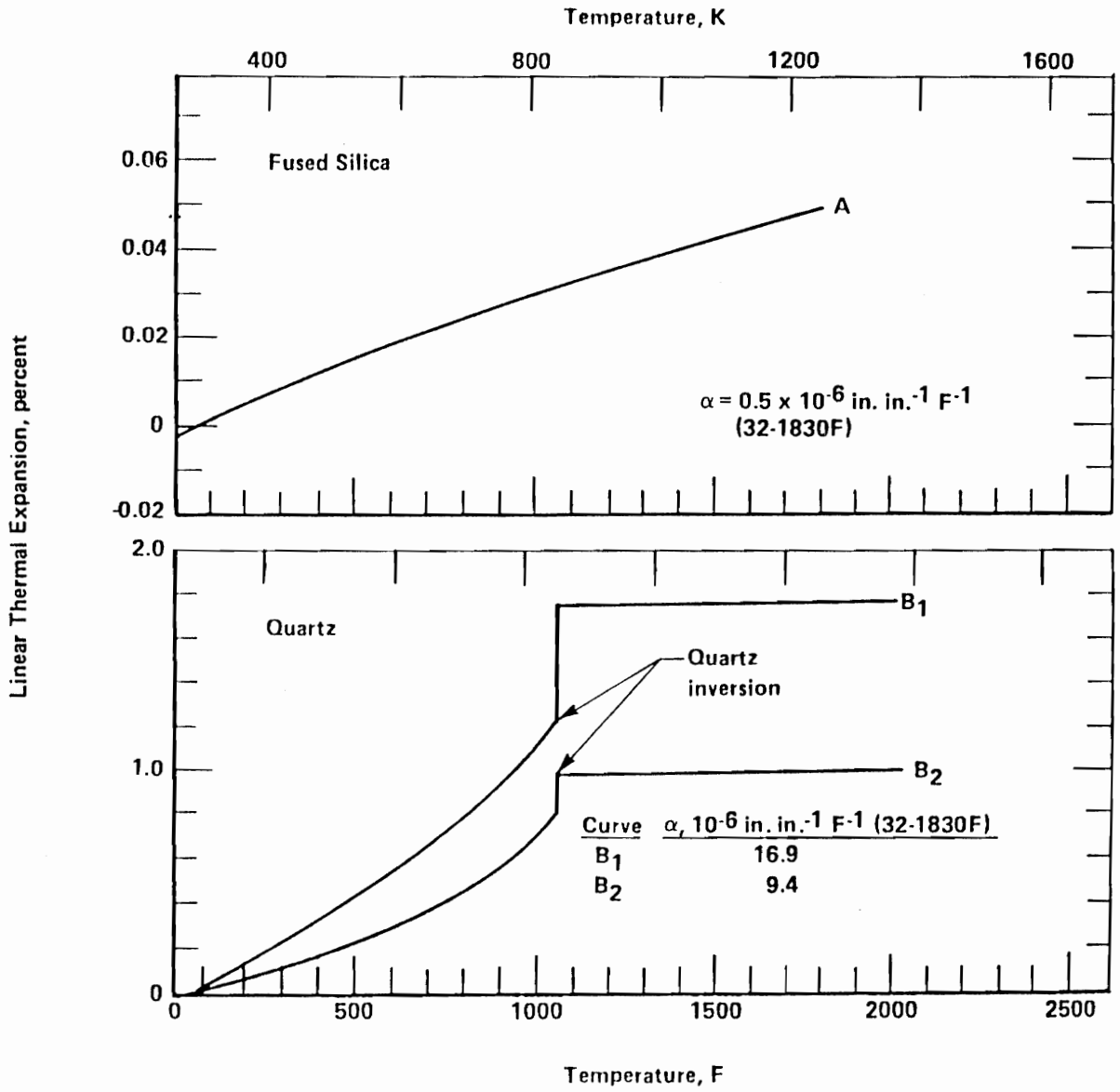


Figure 4.1 Linear Thermal Expansion of fused Silica and Quartz [12]

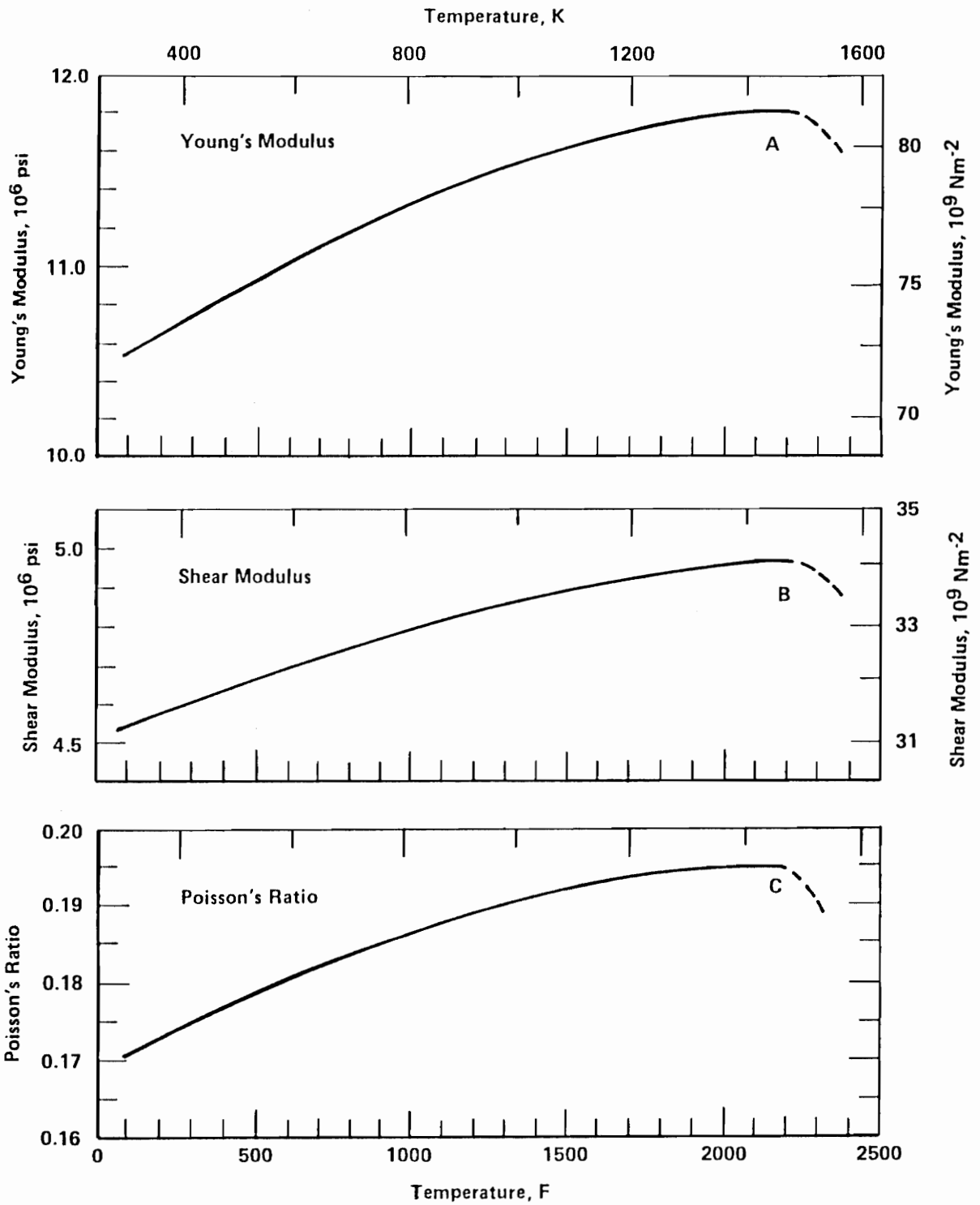


Figure 4.2 Young's modulus, shear modulus and Poisson's ratio of bulk fused silica [12]

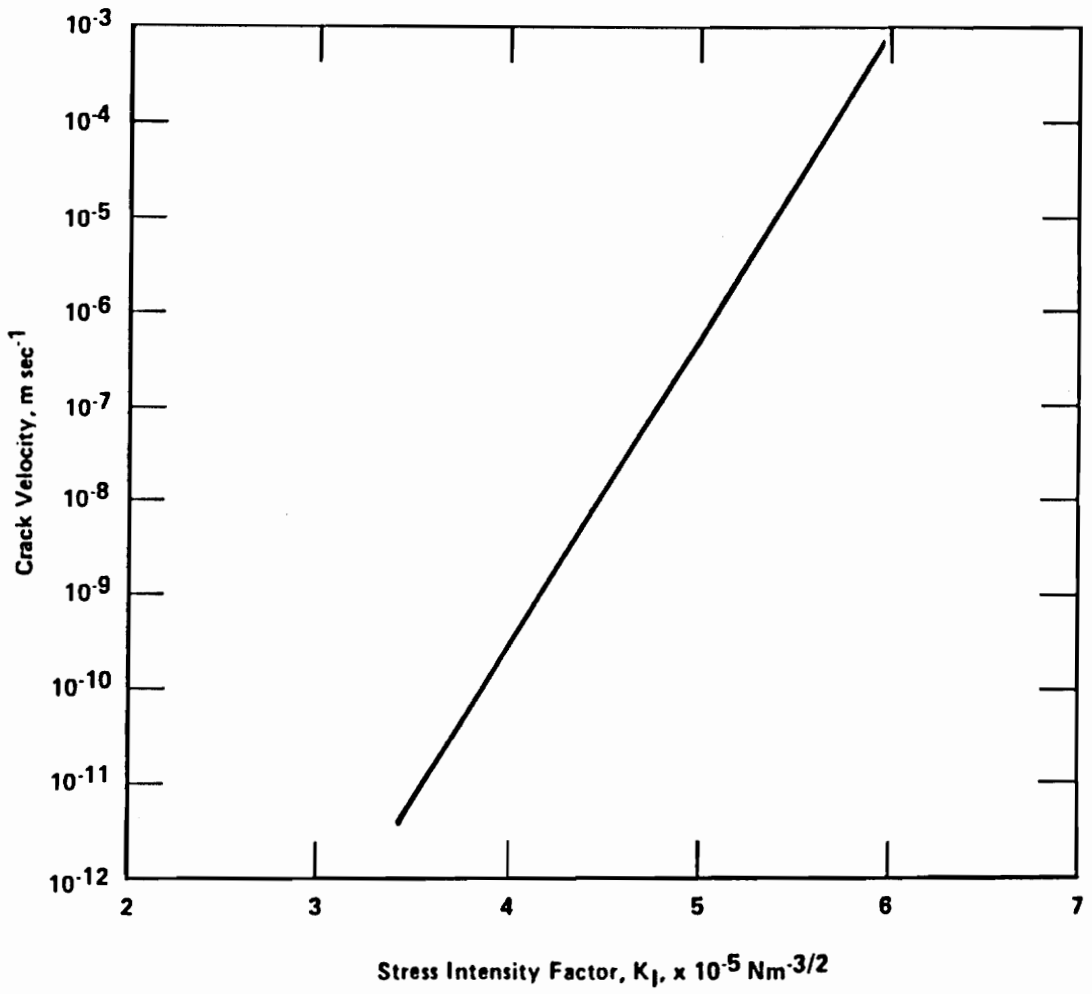


Figure 4.3 Crack propagation velocity in water saturated air as a function of stress intensity factor for fused silica [12]

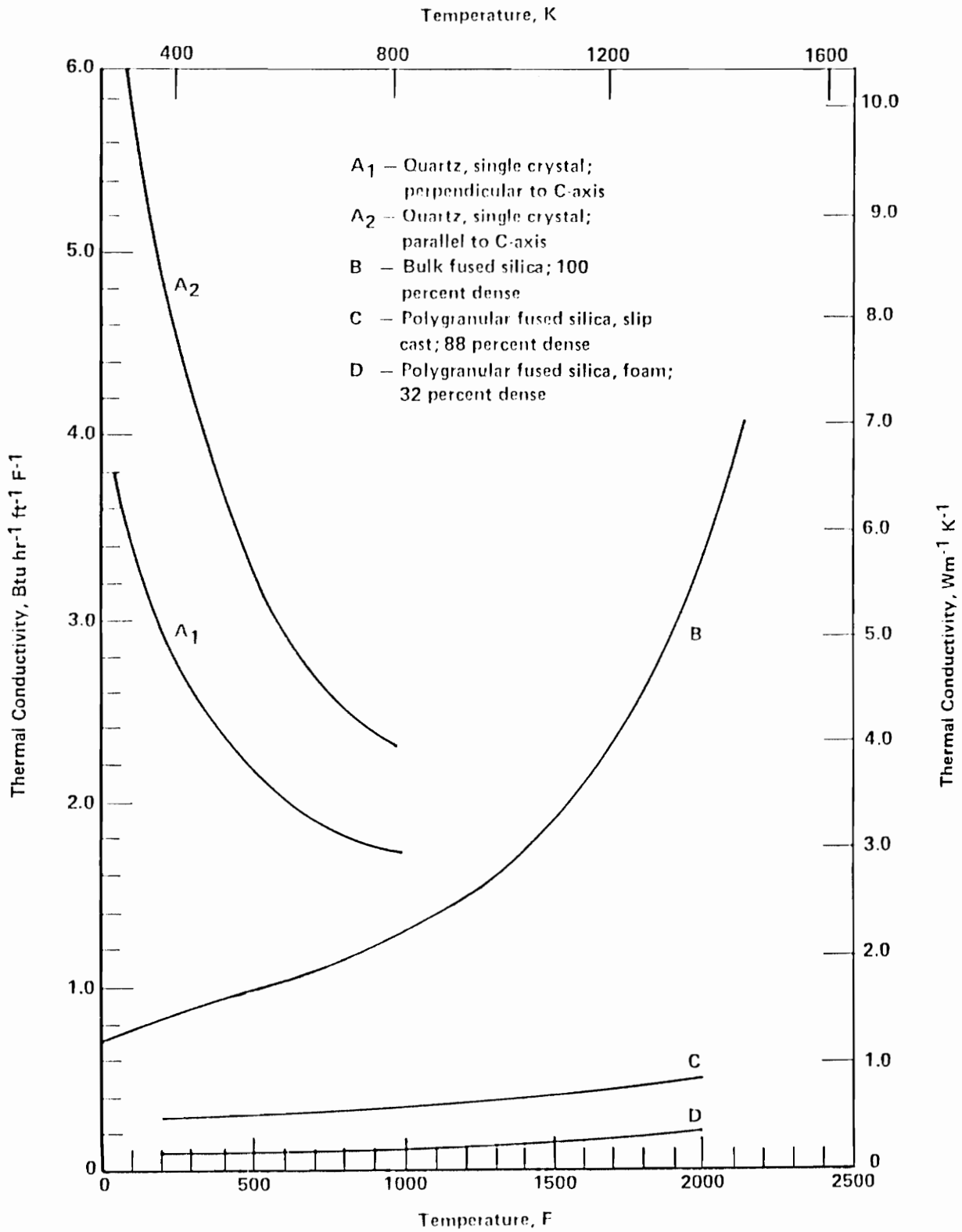


Figure 4.4 Thermal conductivity of quartz and fused silica [12]

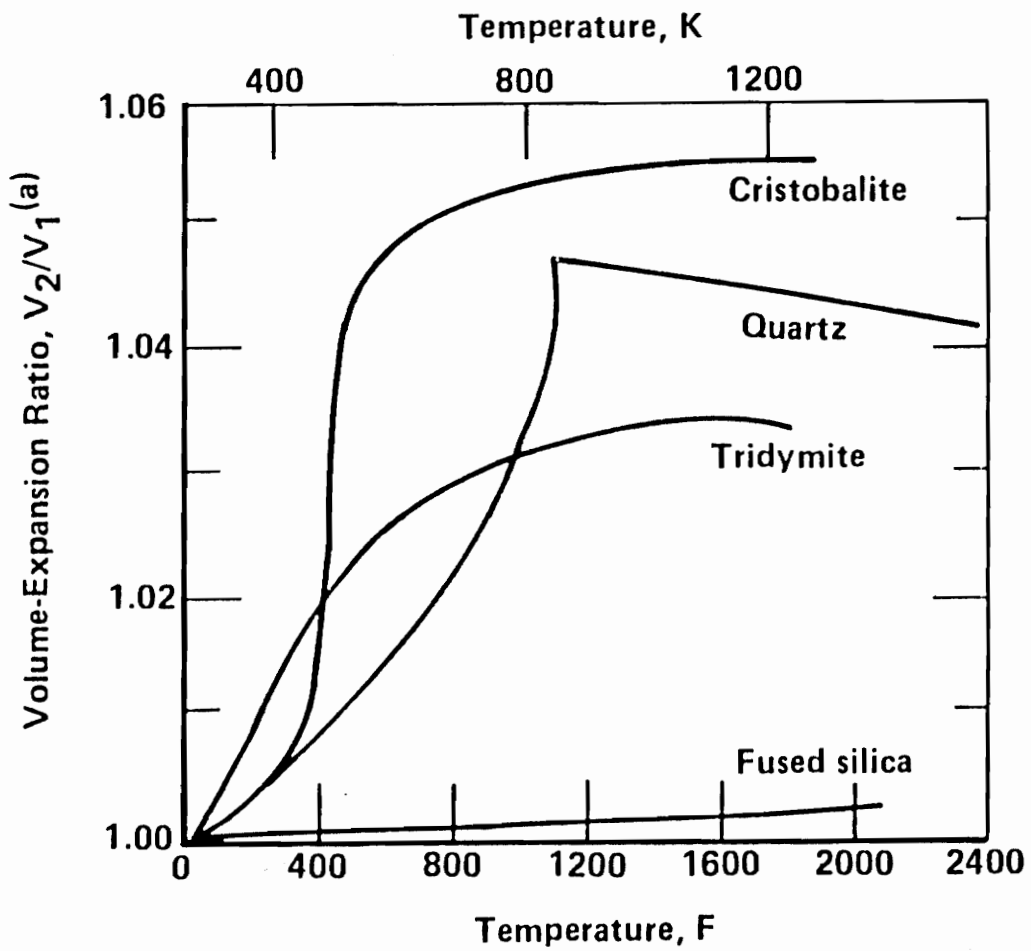


Figure 4.5 Relative volume expansions of crystalline and amorphous phases of silica [12]

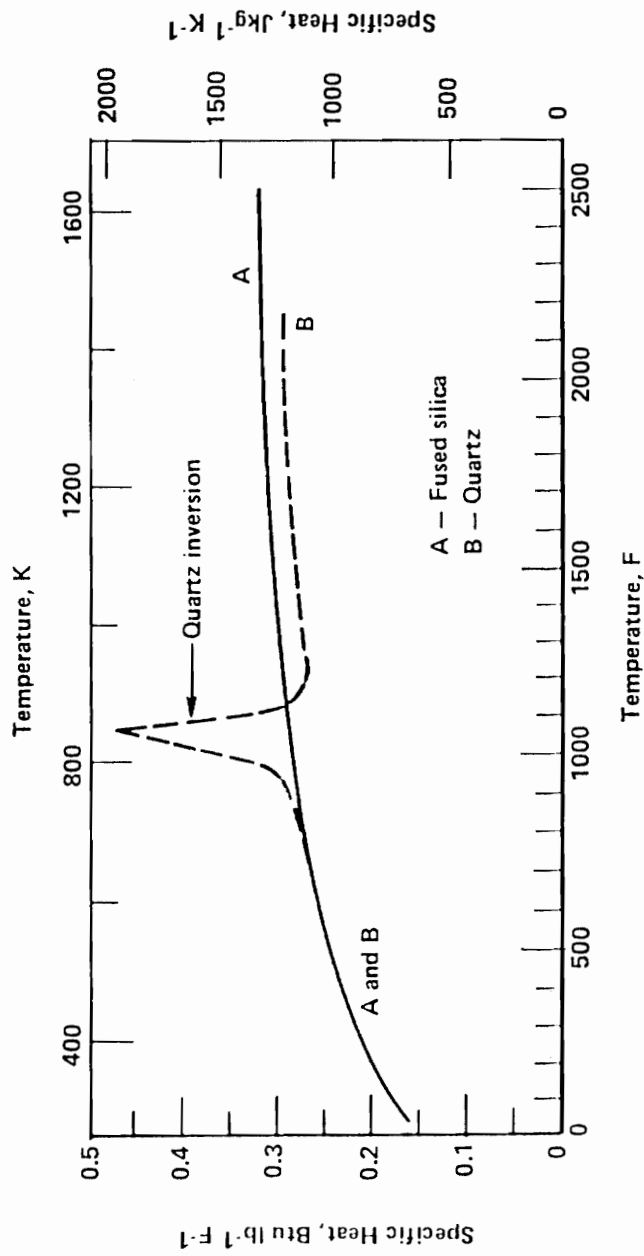


Figure 4.6 Specific heats for quartz and fused silica [12]

4.2 Sapphire

Sapphire is monocrystalline alumina and hence most of the physical and chemical properties applicable to bulk alumina apply to sapphire. It is anisotropic in characteristics because of its rhombohedral crystal structure. The compressive strength of C - axis oriented sapphire is 21×10^8 to 42×10^8 Pa (300,000 to 600,000 psi). The tensile strength of sapphire fibers is inversely proportional to the cross sectional area [12] and is very high. Sapphire is thermodynamically stable in many metals and alloys. Discharge tubes for hps lamps have been made from sapphire [7] and in this application it is more efficient than PCA since it is more resistant to alkali attack and can operate at a higher temperature. The disadvantages are that its anisotropic nature can lead to stress related cracks and leakages, and the high price.

Some papers are available on sapphire filament growth [17] and the mechanical and structural characterization [18]. Pure nickel reacts with sapphire in an oxidizing or inert atmosphere above 1050°C [19]. Sapphire whiskers and filaments have been embedded in aluminum and titanium matrices and this may be especially useful in high temperature composites and in highly corrosive environments. Research on the strength of the c-axis sapphire filament for composite application [20] indicates that surface defects play a major role in filament strength. Hence the fiber manufacturing technique is an important consideration in the lifetime and the strength of embedded sapphire.

Typical properties of sapphire as provided by Saphikon (manufacturers of synthetic sapphire) are listed below.

- | | |
|---------------------|-------------------------|
| • chemical formula | Al_2O_3 |
| • crystal structure | rhombohedral |
| • melting point | 2053°C |

• orientations	R - plane (1102) A - plane (1010) C - plane (0001)
• density	3.97g/cc
• Poisson's ratio	0.28 - 0.33
• max operating temperature	2000°C

Sapphire with its desirable optical, electrical, chemical and mechanical properties is an ideal medium as an optical waveguide. In the embedded form it may be used in smart skins and structures in a wide range of matrices, because it is chemically highly stable.

Figures 4.7 to 4.11 indicate the thermal and optical properties of sapphire. Some of the mechanical properties of sapphire are shown in the diagrams on alumina. Crystals grown along the A - axis have mechanical properties different from those grown along the C - axis as indicated. In Figure 31, letters A, B, D, and E represent C -axis grown filaments of different diameters, C represents A - axis grown filament and F represents A -axis grown whiskers.

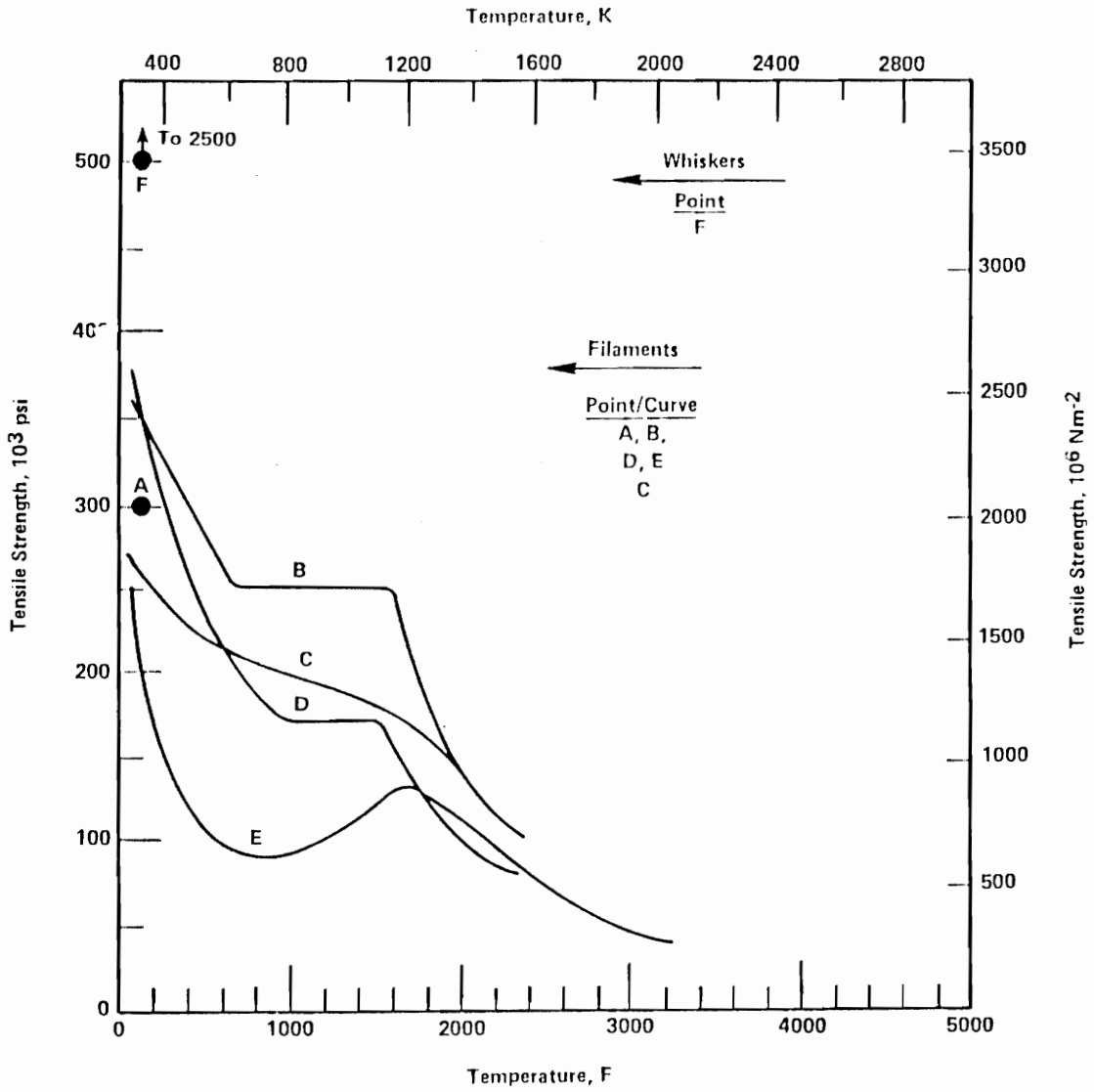


Figure 4.7 Tensile strength of sapphire filaments and whiskers as affected by temperature [12]

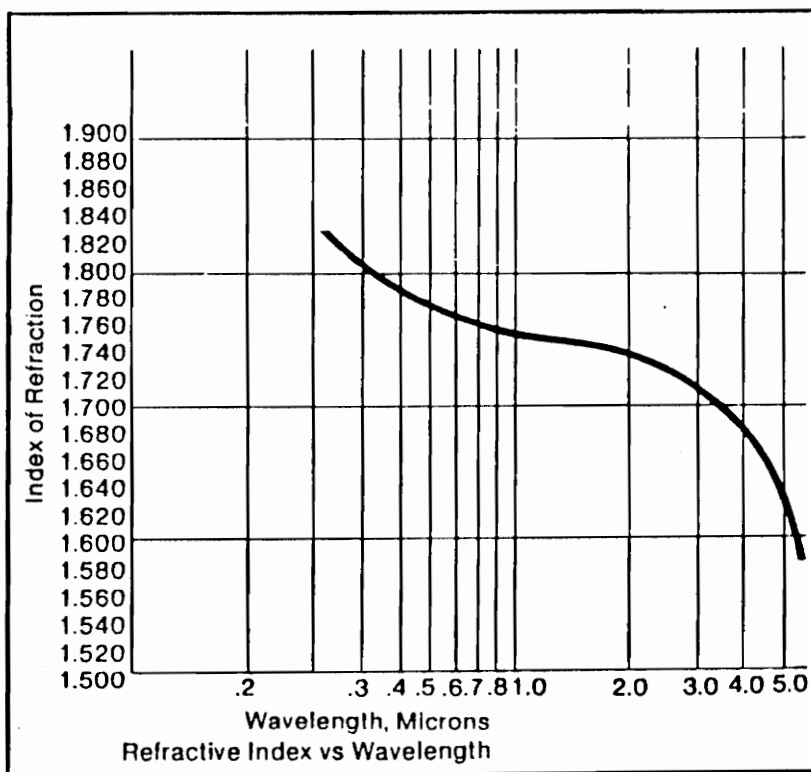


Figure 4.8 Sapphire - Refractive index vs wavelength [33]

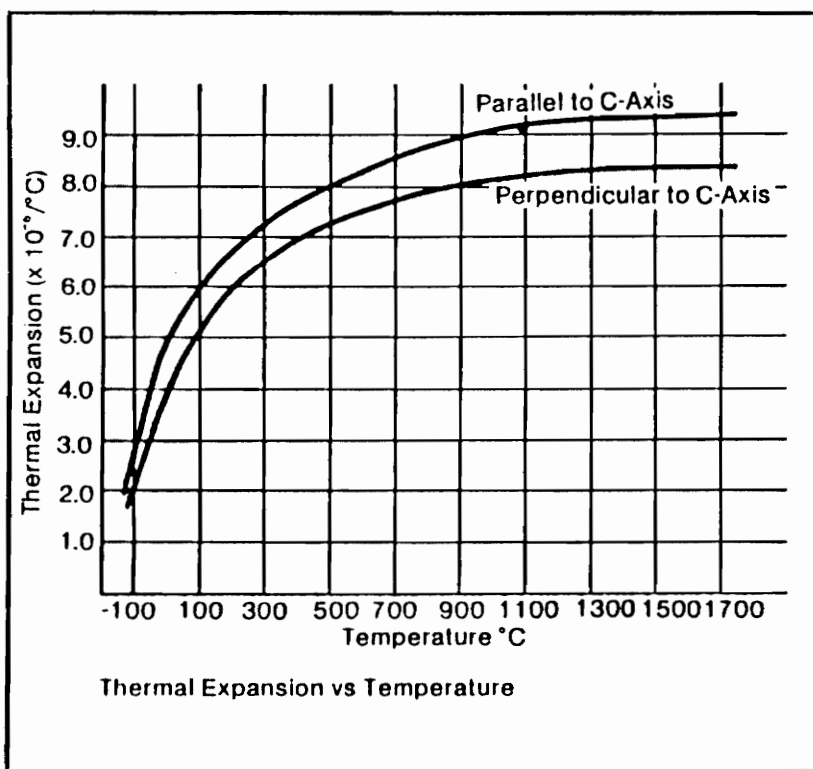


Figure 4.9 Sapphire Thermal Expansion vs temperature [33]

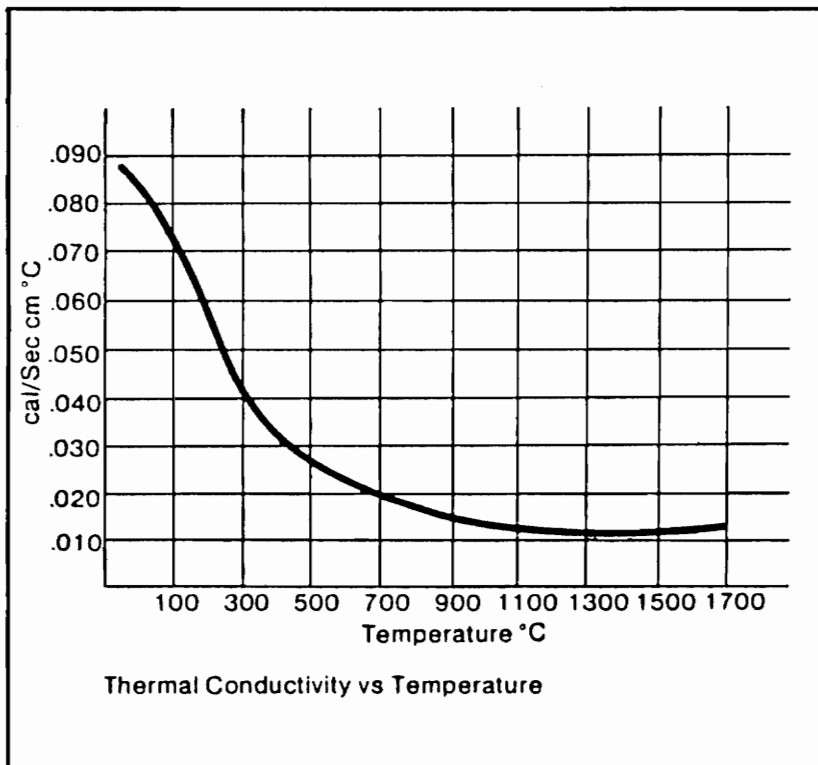


Figure 4.10 Sapphire - Thermal conductivity vs temperature [33]

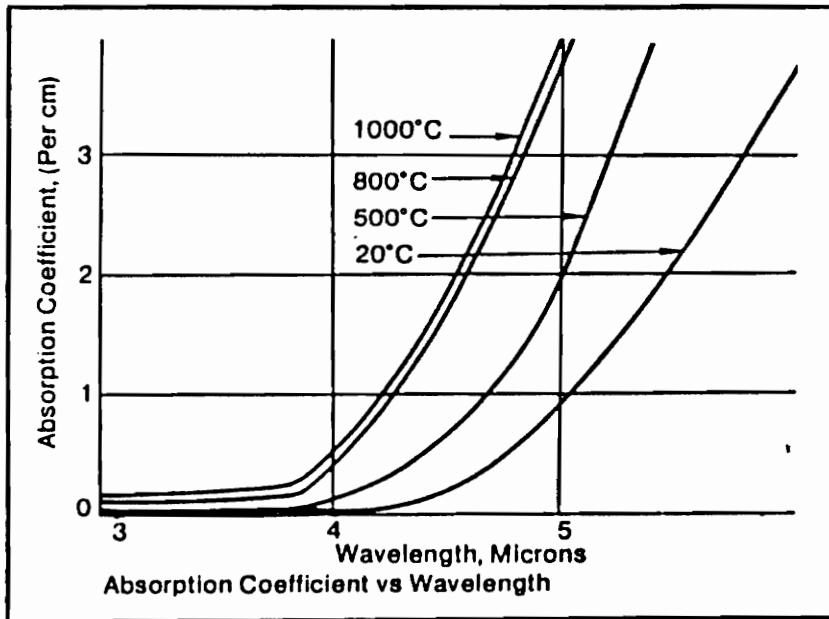


Figure 4.11 Sapphire - Absorption coefficient vs wavelength [33]

4.3 Fiber embedding

As indicated above, in order to use optical waveguides in embedded form or otherwise, for sensing or for communication, the fiber has to be suitably coated to prevent surface damaged and hence transmission losses. The fiber surface characteristics can be preserved for a long time if ideal coating materials are available. Practically, coatings which would minimize surface chemical interaction and at the same time form a protective layer between the fiber and the environment would suffice for small temperature ranges. When large thermal variation also is required the thermal shock resistance as well as matching the thermal expansion coefficient with the fiber becomes an equally important factor.

In the embedded form these considerations have to be extended to that of the matrix material as well so there is strong bonding between the matrix and the coating material, minimum chemical interaction and matching thermal expansion coefficient between the fiber coating and the matrix. The optical waveguides in embedded form is only an extension of the composite structure.

Optical fibers can be coated in several different ways. Chemical coating, chemical vapor deposition, plasma spraying and electrochemical plating are some of the commonly used techniques. Chemical coating is employed where the metal to be coated is available in an aqueous solution of the metal salt. A displacing agent added to the solution causes the metal to be displaced onto the substrate. If a uniform concentration can be maintained, uniform coating thickness can be obtained. The adhesion is strong and no electric current is needed. Metals like copper, nickel and cobalt can be coated using this method. Mg, Al, Zn or Fe can be used as a displacing agent [32].

Chemical vapor deposition is a slow process and it is difficult to obtain

coatings with uniform thickness. Physical vapor deposition can be done by evaporation, direct ion beam deposition and by sputtering. Plasma or thermal spraying is applicable to substrates which can withstand the high temperature of the molten ionized coating material. Electrochemical plating can produce firm and uniform coating with very good adherence. Besides these, coating can be done by painting on the material, or drawing the fiber through a paste of the material and then curing.

The process by which the fiber is embedded in the matrix depends on the fiber, coating material and the matrix. Diffusion bonding, cold isostatic pressing, hot rolling, extrusion and drawing, hot isostatic pressing, explosive welding, liquid matrix infiltration and investment or squeeze casting are some of the methods used to embed fiber. Many of these methods are employed in metal matrix composite fabrication. Ceramic matrices and resin matrices are also used in composite fabrication. Some of the available techniques can be used to embed silica and sapphire waveguides for "smart skin and structure" purposes.

5.0 EXPERIMENT

5.1 Description

The bulk chemical reactions of the silica and alumina substrate materials with each of the selected coating materials is of primary importance. Generally, any reaction will accelerate when the exposed surface area is increased. Hence powder samples of small particle dimensions and hence large surface area per unit volume are mixed together thoroughly. Samples of each of the coating materials and the substrates are then transferred to platinum tubing, evacuated, sealed, and the platinum tubes sealed in quartz tubing. The samples are then subjected to temperatures in the range of 860°C. Pictures of the prepared samples are provided in Appendix A. Since niobium reacts with platinum, silica holders were used to study niobium reactions. Samples heated for several hours, and from five days to fifteen days, were analyzed and the results recorded.

X-ray diffraction patterns of the mixture before and after the heat treatment provides information on the crystalline chemical reactions which have occurred, crystal phase changes and changes in lattice parameters. For any further information electron microprobe analysis has been used. The microprobe analysis provides the weight percentage of any phase transformation products.

Light microscope photographs of the fiber cross sections before and after the heat treatment provide visual evidence of changes in surface characteristics. Appendix B provides pictures of mounted fiber cross sections.

Samples found to be chemically inert can be studied in detail further for other thermodynamic compatibility. The suitable materials can then be coated on the fibers and exposed to harsh chemicals, like those present in the

coal gasification environment and analyzed for the extent and nature of the reaction as a function of the time involved.

Coated and embedded fibers also can be tested to detect signal variations which occur as a result of residual strain induced by the coating and the embedding. Experiments can be designed to sense various parameters, using the transmission of optical signals through these coated fibers. These studies and the instrumentation of these sensors form a separate, parallel area of research.

5.2 X-ray diffraction analyses

X-ray diffraction patterns of a crystalline solid provide information concerning the crystalline structure of the solid and thus can be used to analyze crystals. An electron in the path of an x-ray beam will oscillate in response to the changing electric field and, as a result, x-rays similar to the primary radiation are emitted in all directions,. An atom will scatter more x-rays than an electron due to its larger effective cross section and because its scattering power increases with its atomic number [34].

Bragg observed that the x-rays diffracted from a crystal could be likened to reflections from lattice planes. When an x-ray beam is incident on a crystal plane, reflection occurs only at certain angles of incidence of the beam. For a set of lattice planes the necessary condition for reflection to occur is that each reflected beam differ in phase by $n\lambda$. The condition can be stated as

$$2d\sin\theta = n\lambda$$

where d is the lattice spacing, n is the order of the spectrum, θ is the angle of the beam with the plane and λ is the wavelength of the incident beam.

The powder or Debye - Scherrer method is a powerful method of

identifying crystalline compounds. This method which uses the principles of Bragg reflection has been used in this experiment to look for changes in crystalline structure of the samples.

An approximate 50 - 50 volume mixture of half of the heat treated powder samples were each loaded into a sample holder and mounted onto an automated 25 cm vertical diffractometer (SCINTAG) equipped with a copper tube and a liquid nitrogen-cooled solid state detector (SCINTAG XDS 2000). Slit sizes used were 2° for divergence and 0.3 mm for receiving; the instrumental profile breadth was determined to be 0.030° 2 θ . Diffractometer alignment was checked with silicon at intervals. The sample was scanned between 20 and 80 2 θ with a chopper increment of 0.01 and a scan rate of 0.5 degrees per minute. The raw data was processed to remove background and $\kappa\alpha_2$ peaks and a peakfinder program used to locate diffraction maxima.

The following graphs (Figures 5.1 to 5.24) provide the diffraction patterns of the samples indicated. Powder mixture of the combinations

alumina - silica

alumina - silicon carbide

alumina - zirconia

silica - silicon carbide

silica - zirconia

silica - niobium

were each prepared in sets of threes and were heated to 857°C for 120 hours, 240 hours and 360 hours each.

FN: REFALOSIO.NI ID: ALUMINA SILICA REFERENCE SCENTAG/USA
 DATE: 11/28/89 TIME: 19: 0 PT: 1.200 STEP: 0.010 WL: 1.54059

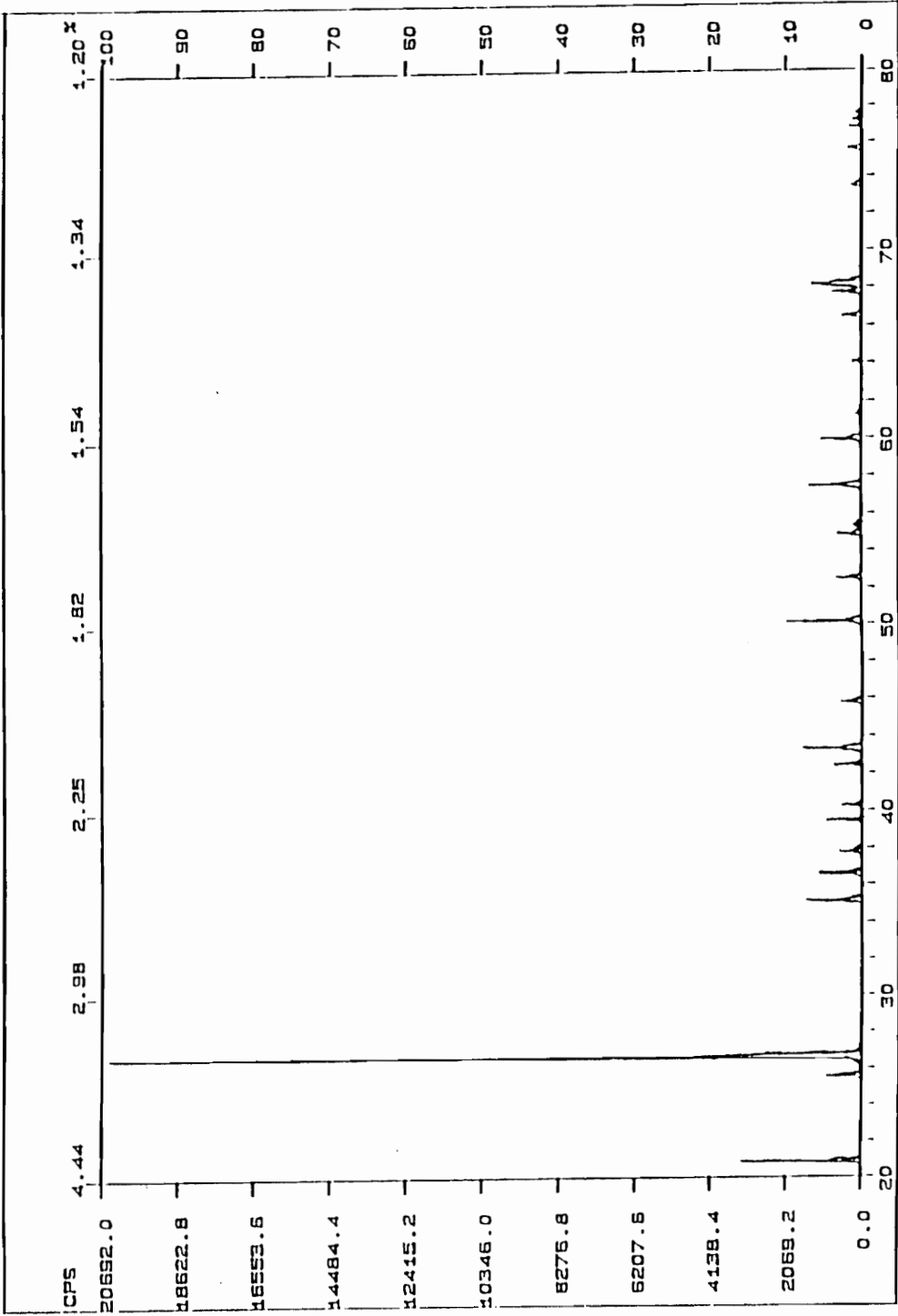


Figure 5.1 Alumina - Silica powder before heating

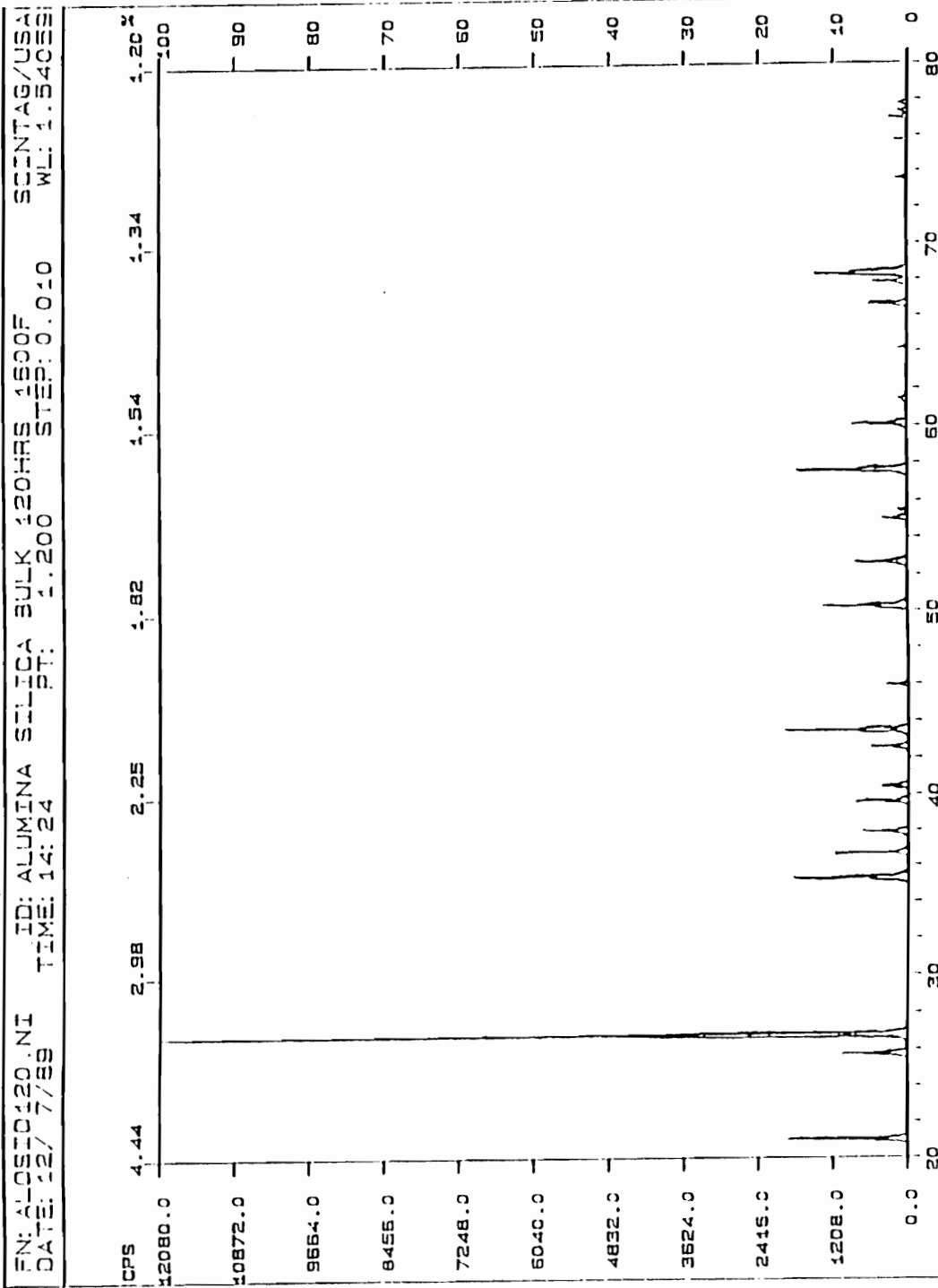


Figure 5.2 Alumina - Silica powder heated at 857 °C for 120 hours

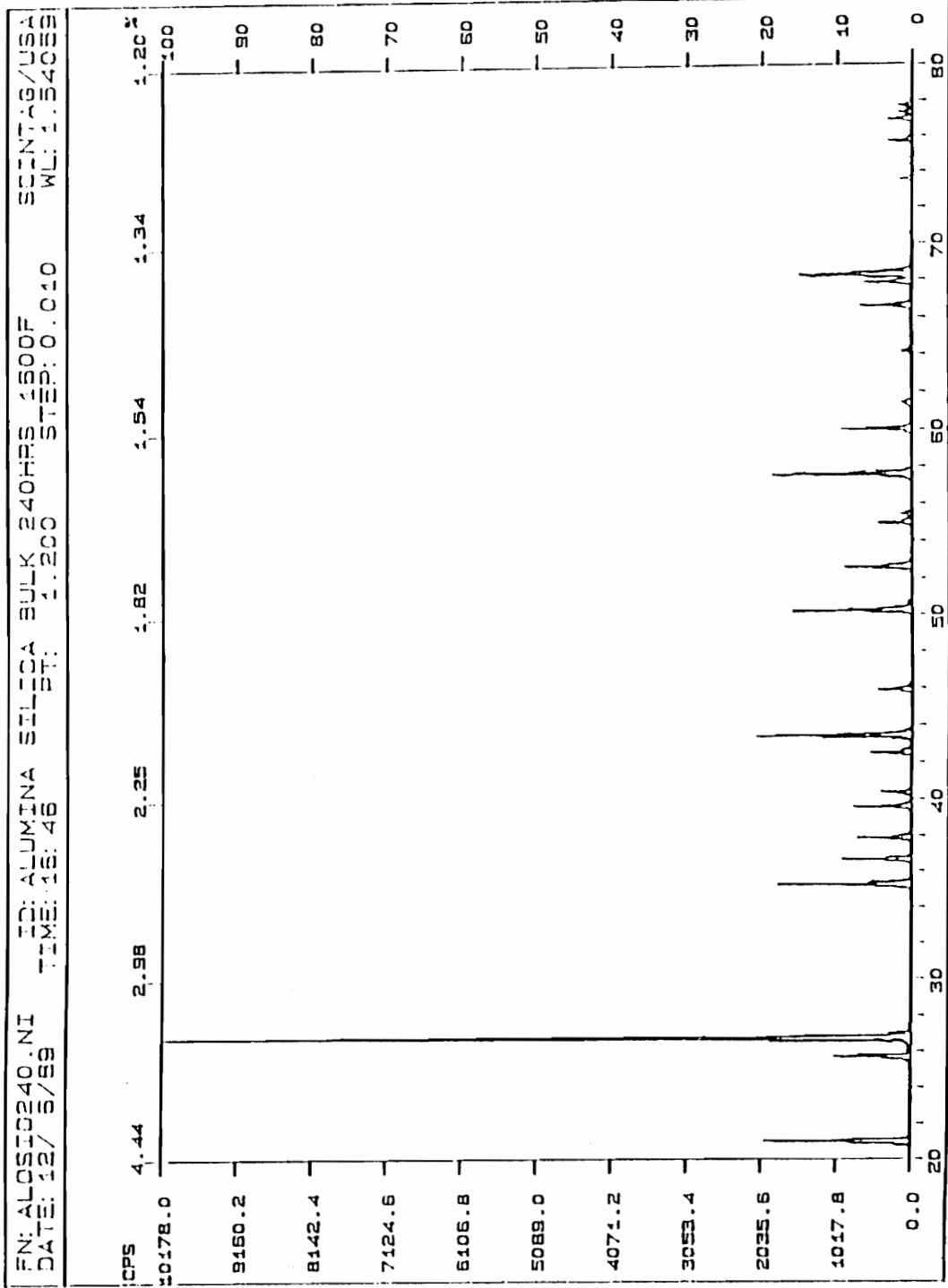


Figure 5.3 Alumina - Silica powder heated at 857 °C for 240 hours

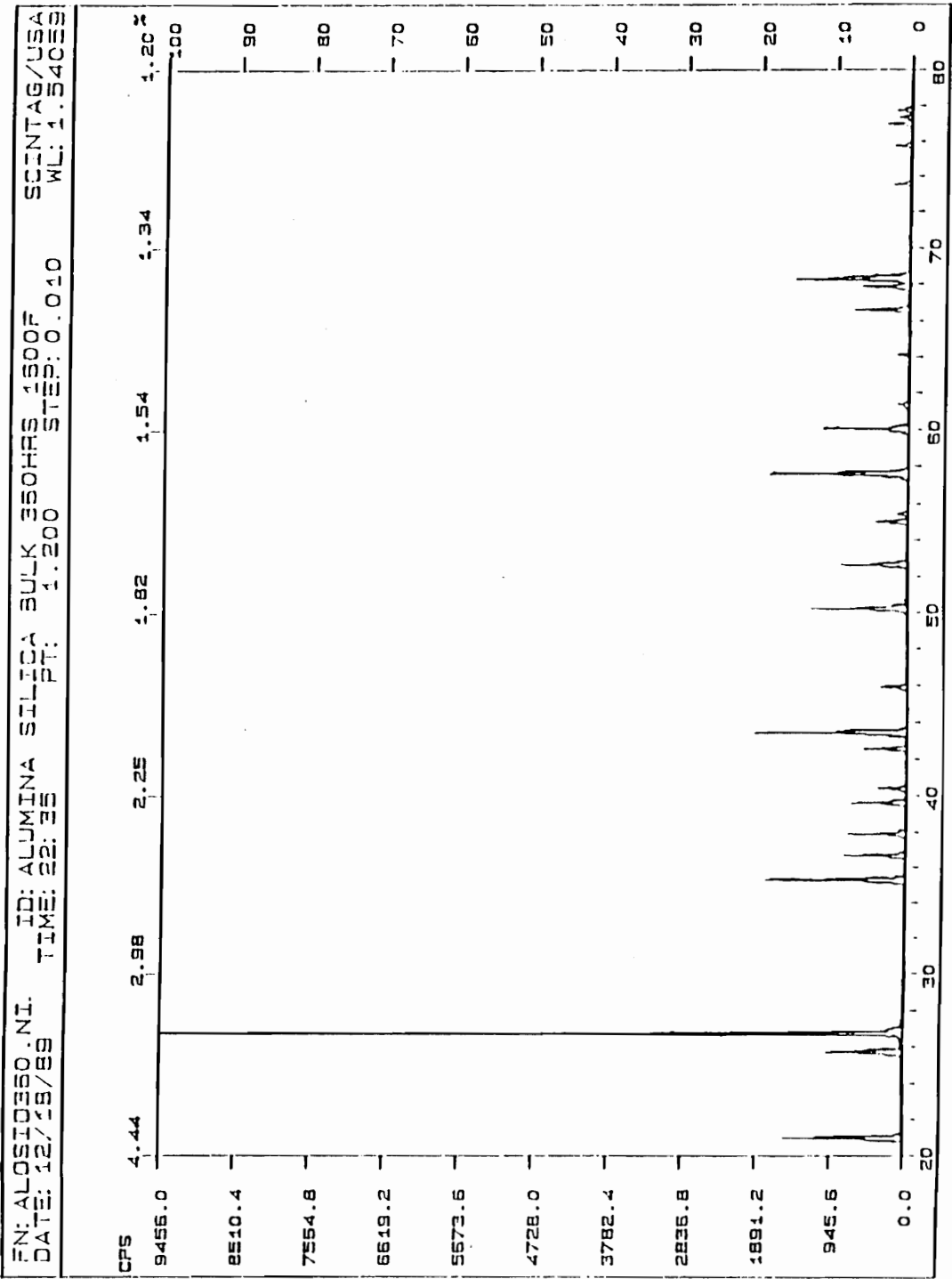


Figure 5.4 Alumina - Silica powder heated at 857 °C for 360 hours

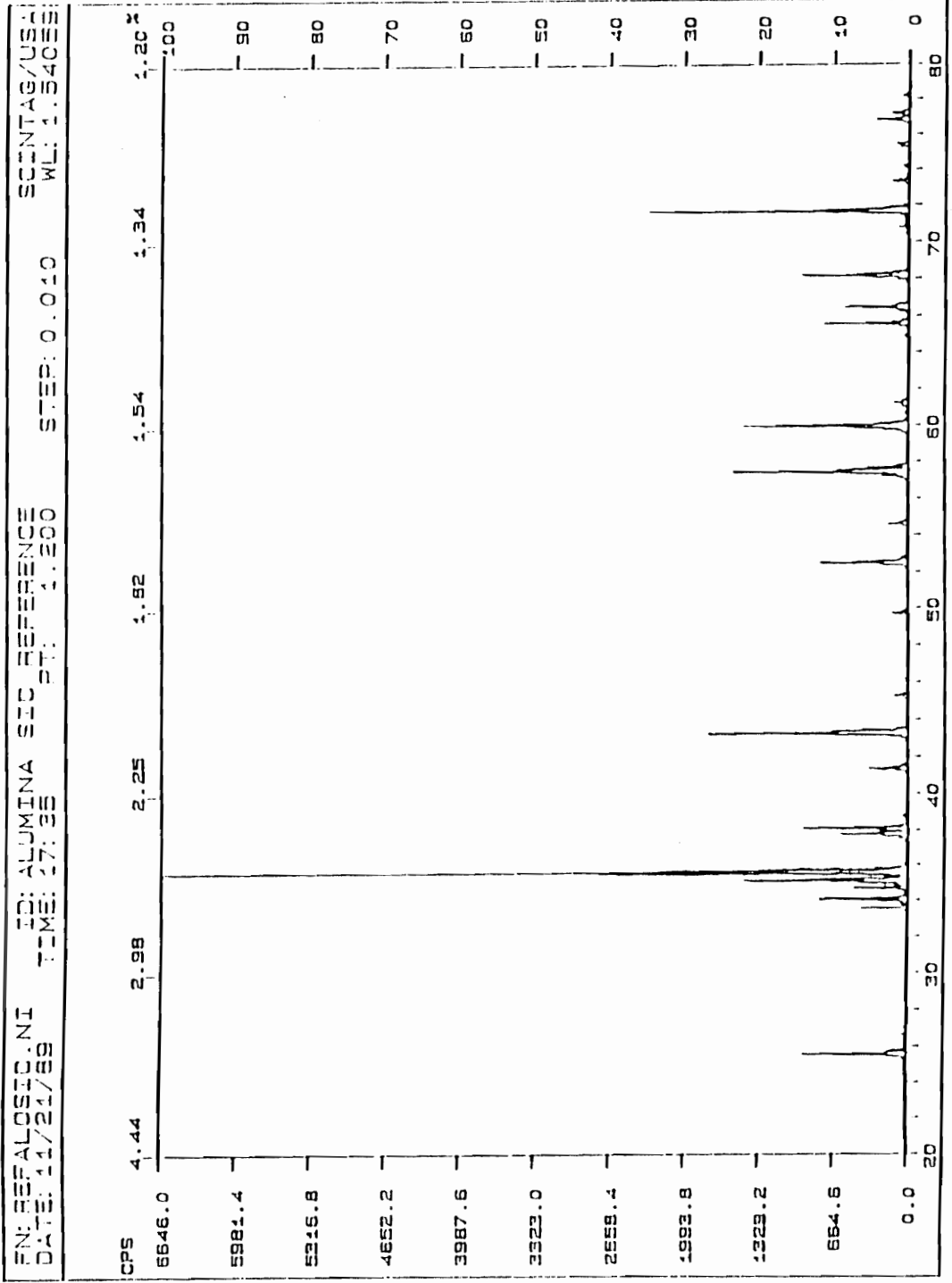


Figure 5.5 Alumina - Silicon carbide before heating

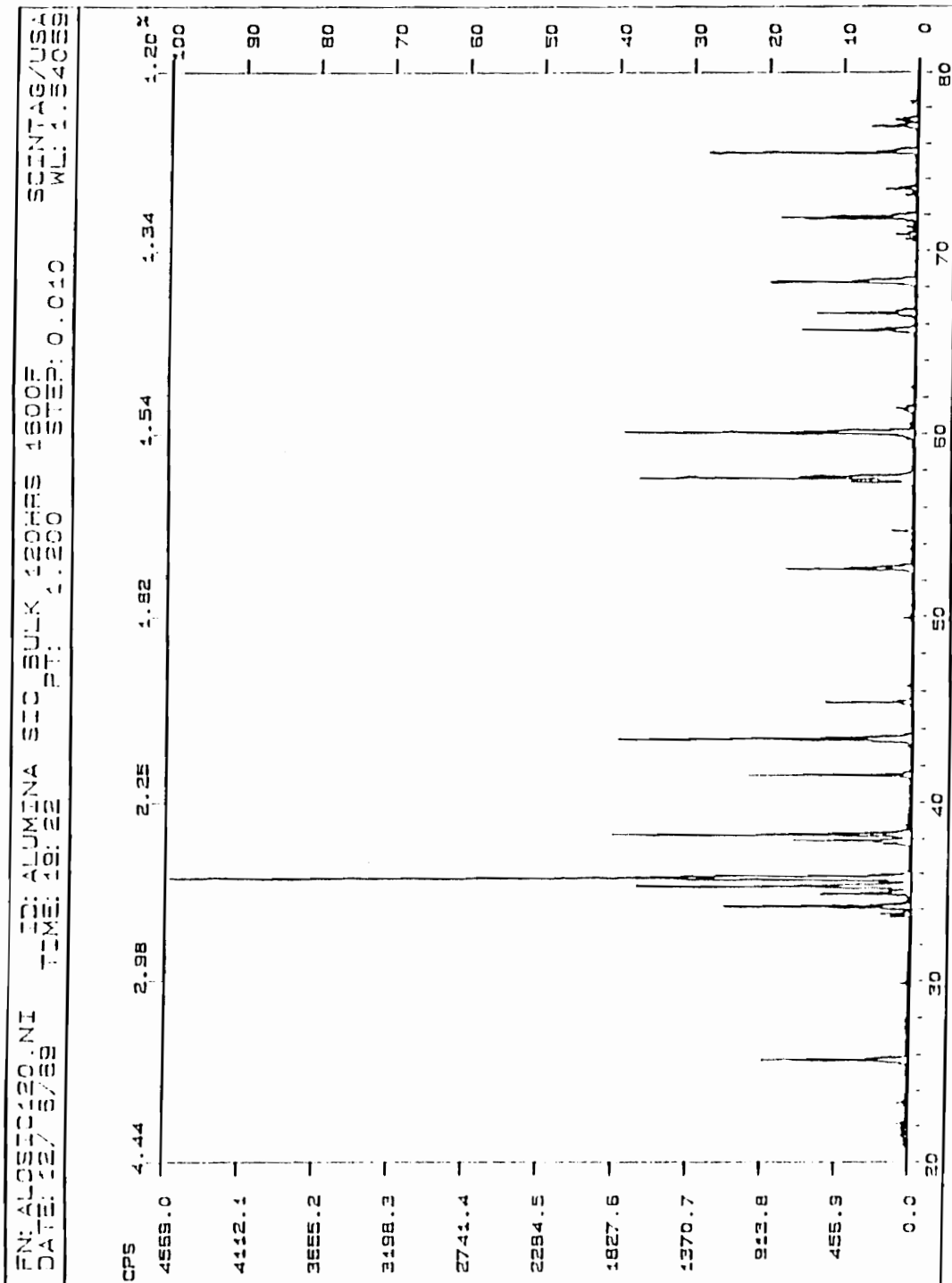


Figure 5.6 Alumina - Silicon carbide heated at 857 °C for 120 hours

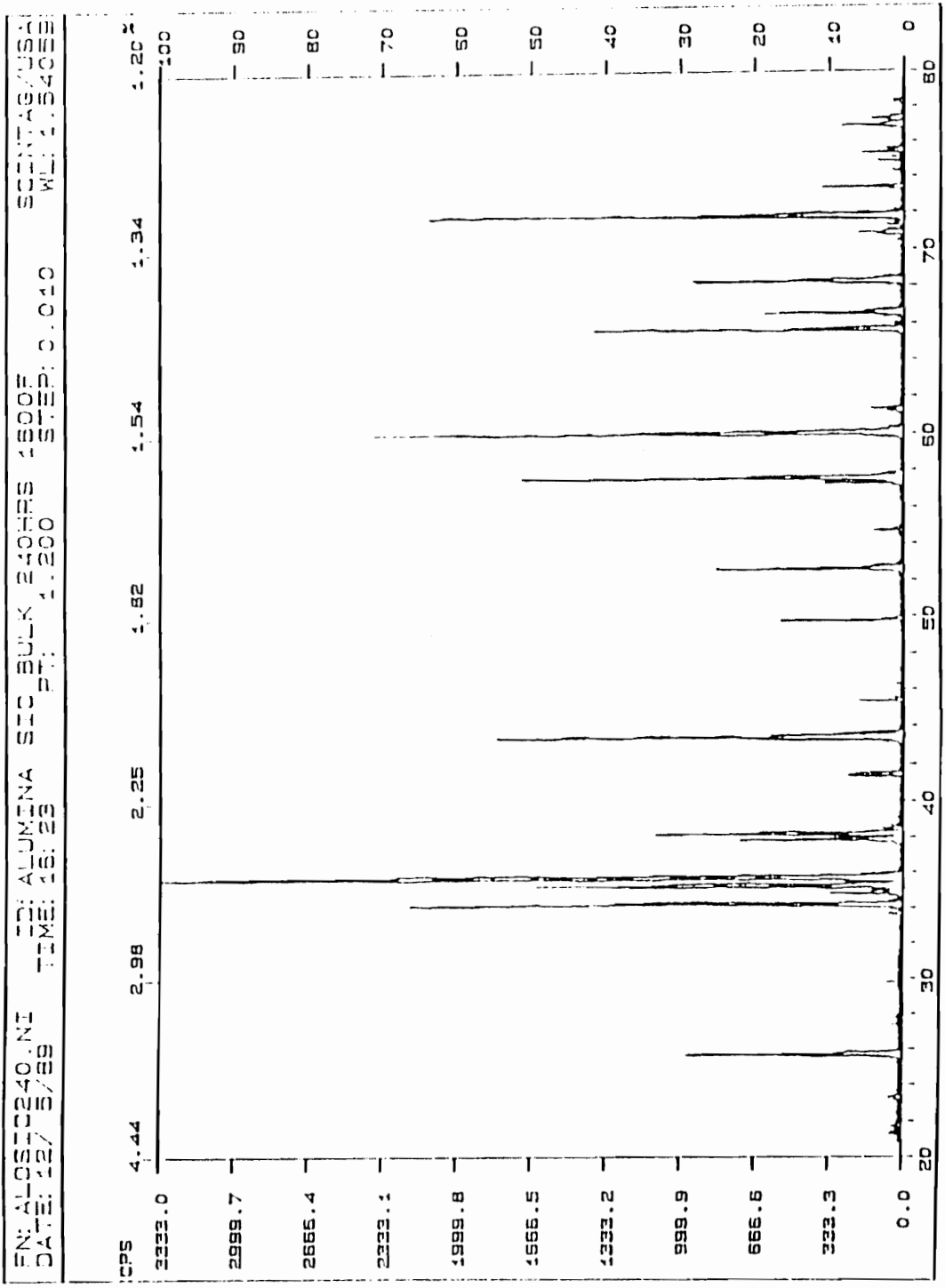


Figure 5.7 Alumina - Silicon carbide heated at 857 °C for 240 hours

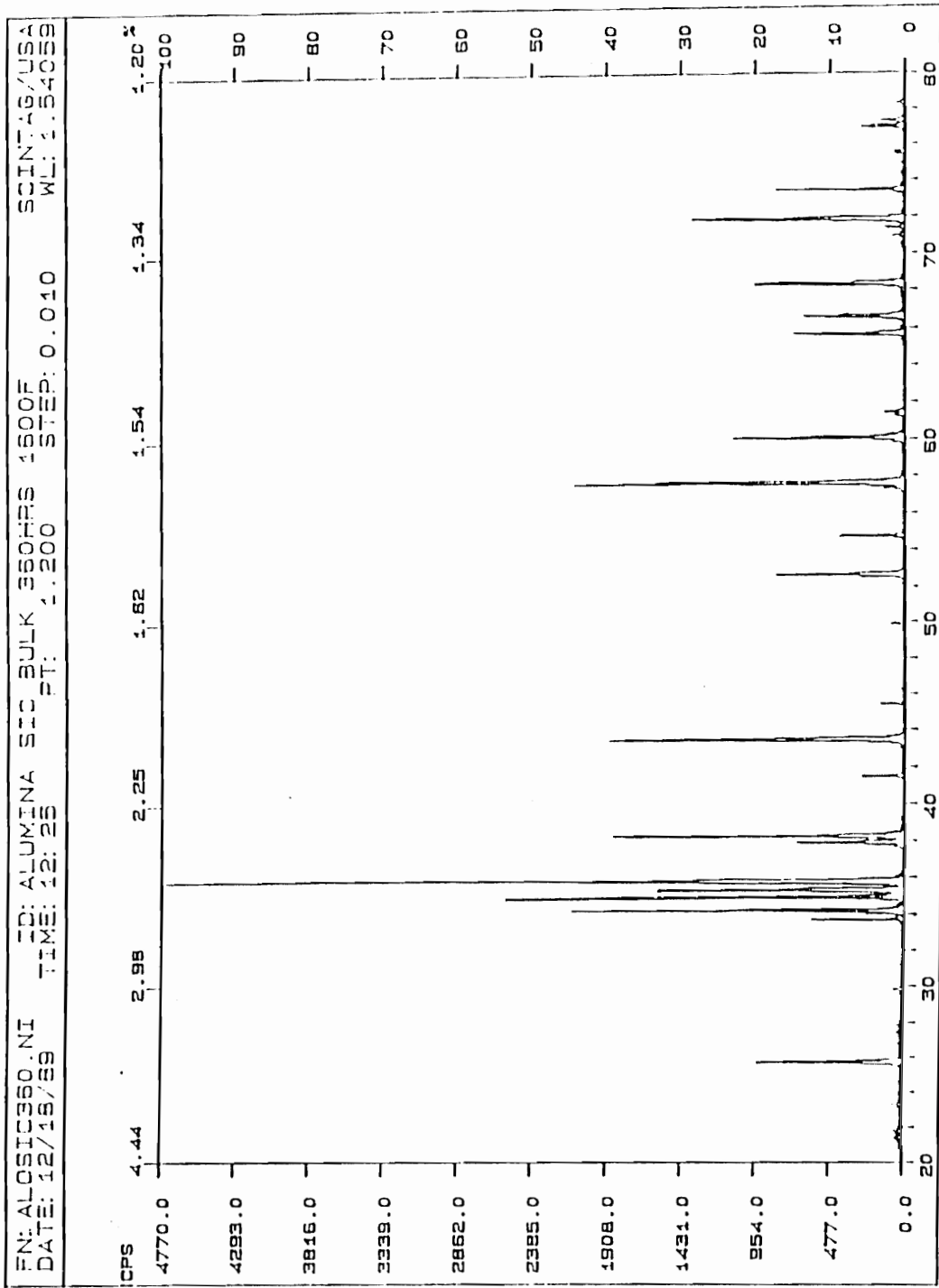


Figure 5.8 Alumina - Silicon carbide heated at 857 °C for 360 hours

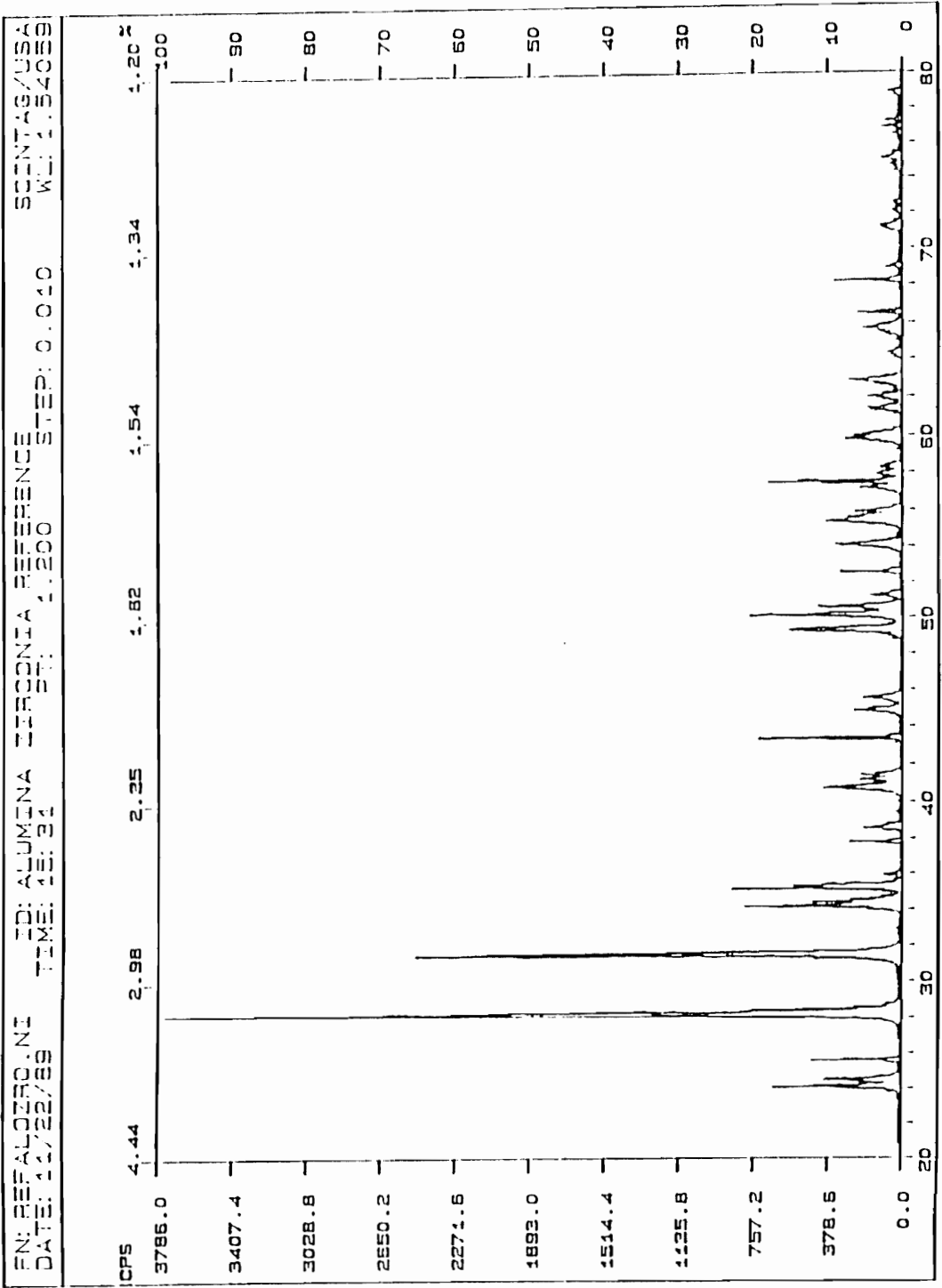


Figure 5.9 Alumina - Zirconia powder before heating

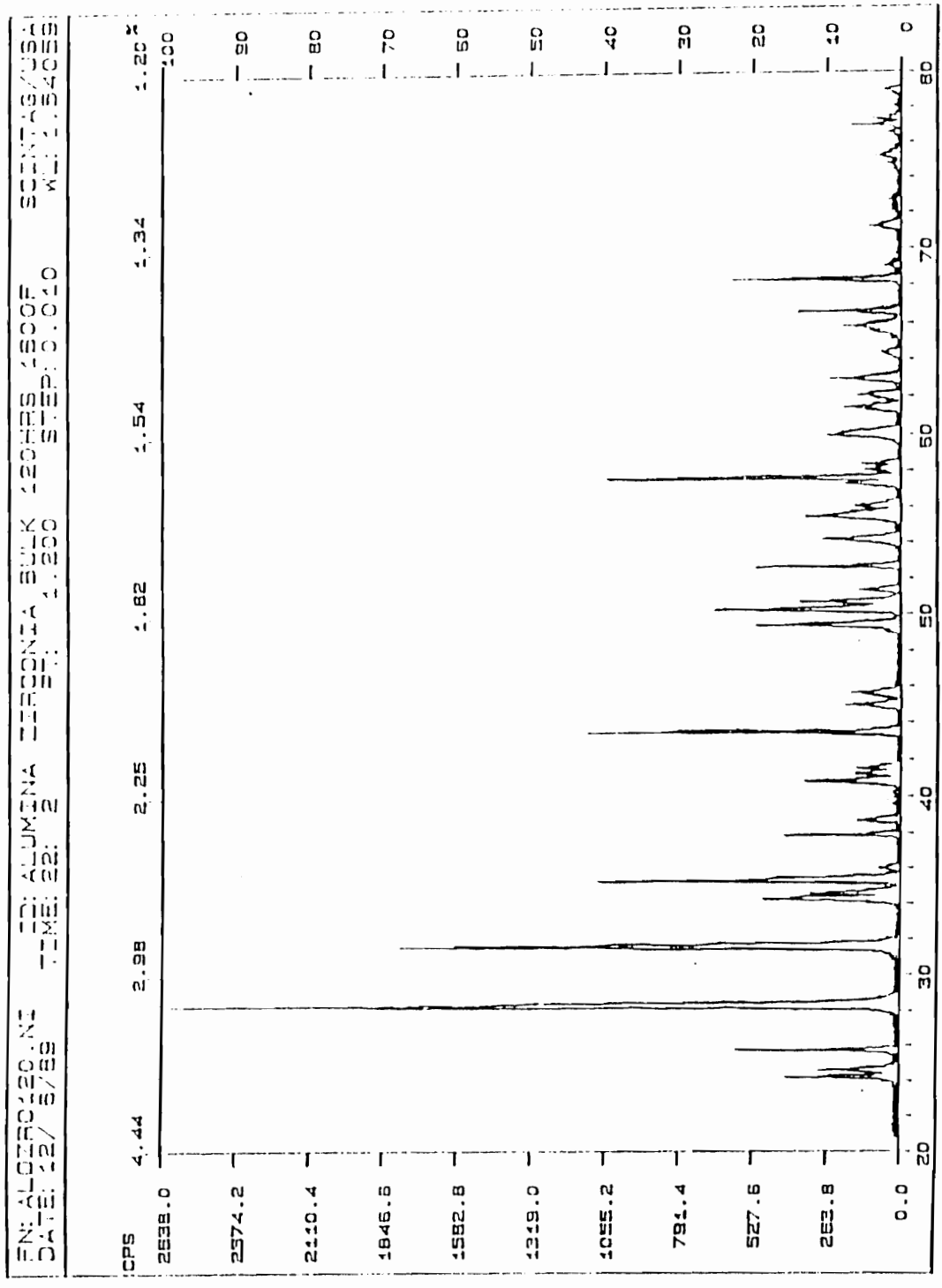


Figure 5.10 Alumina - Zirconia powder heated at 857 °C for 120 hours

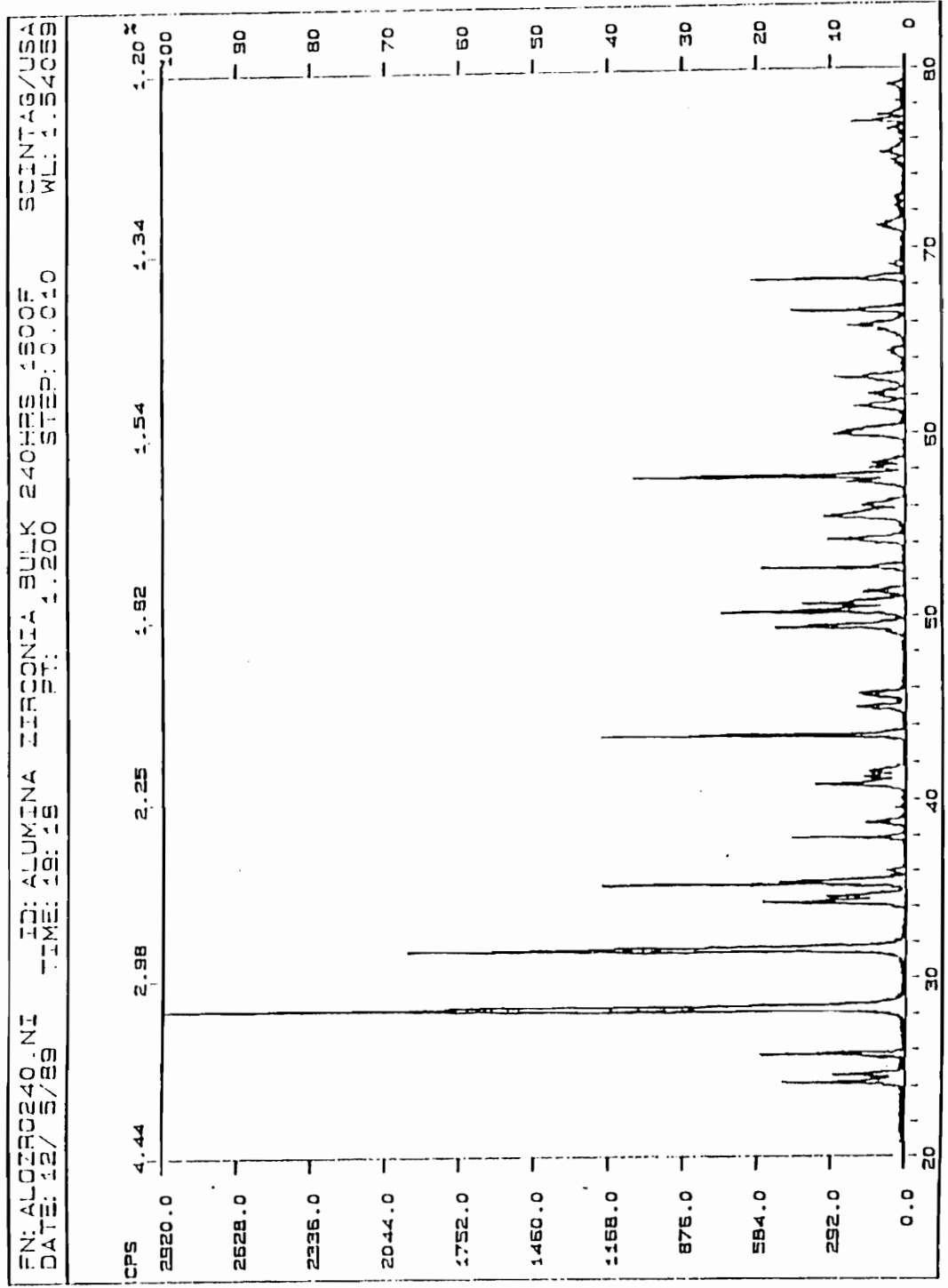


Figure 5.11 Alumina - Zirconia powder heated at 857 °C for 240 hours

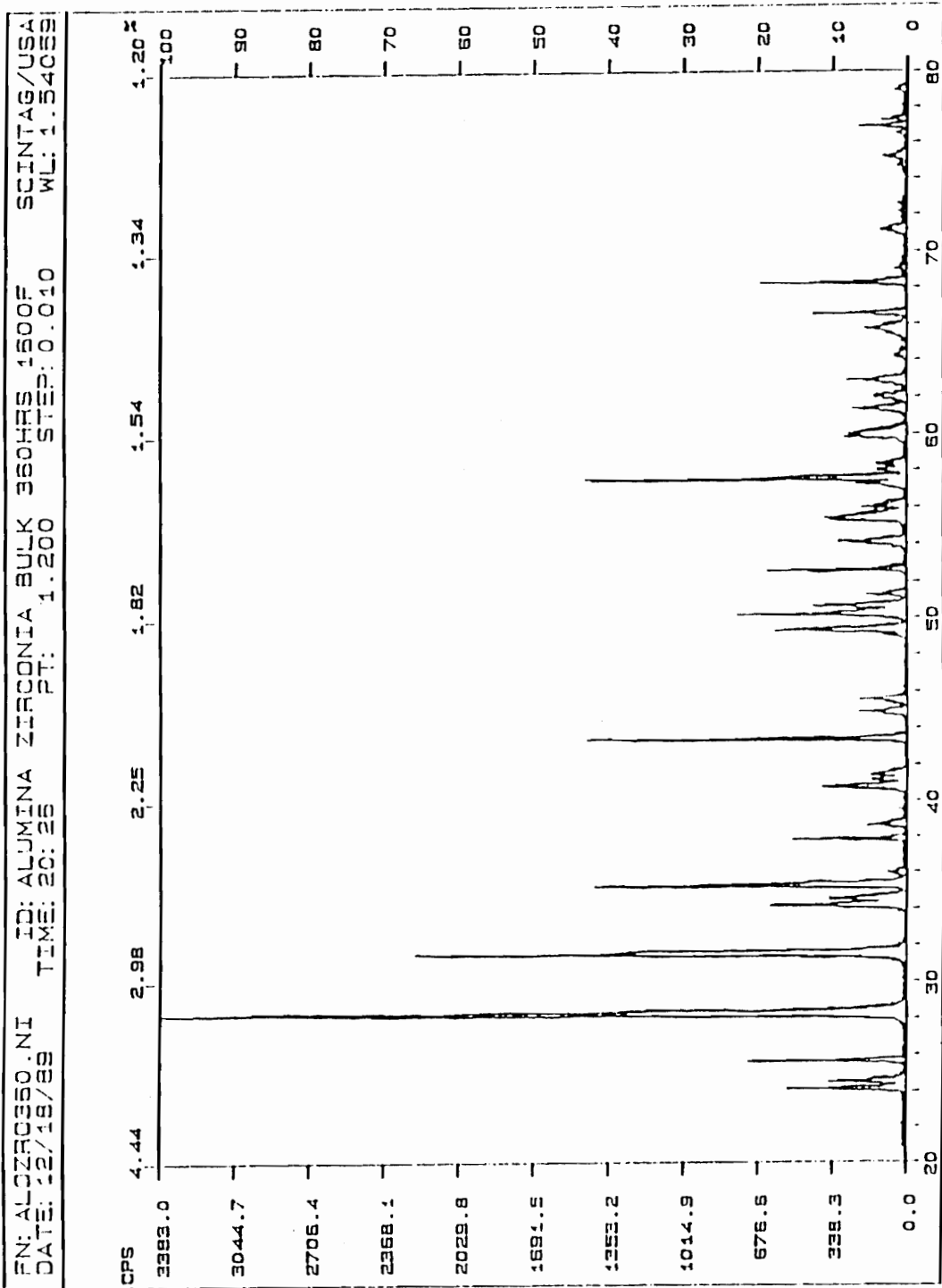


Figure 5.12 Alumina - Zirconia powder heated at 857 °C for 360 hours

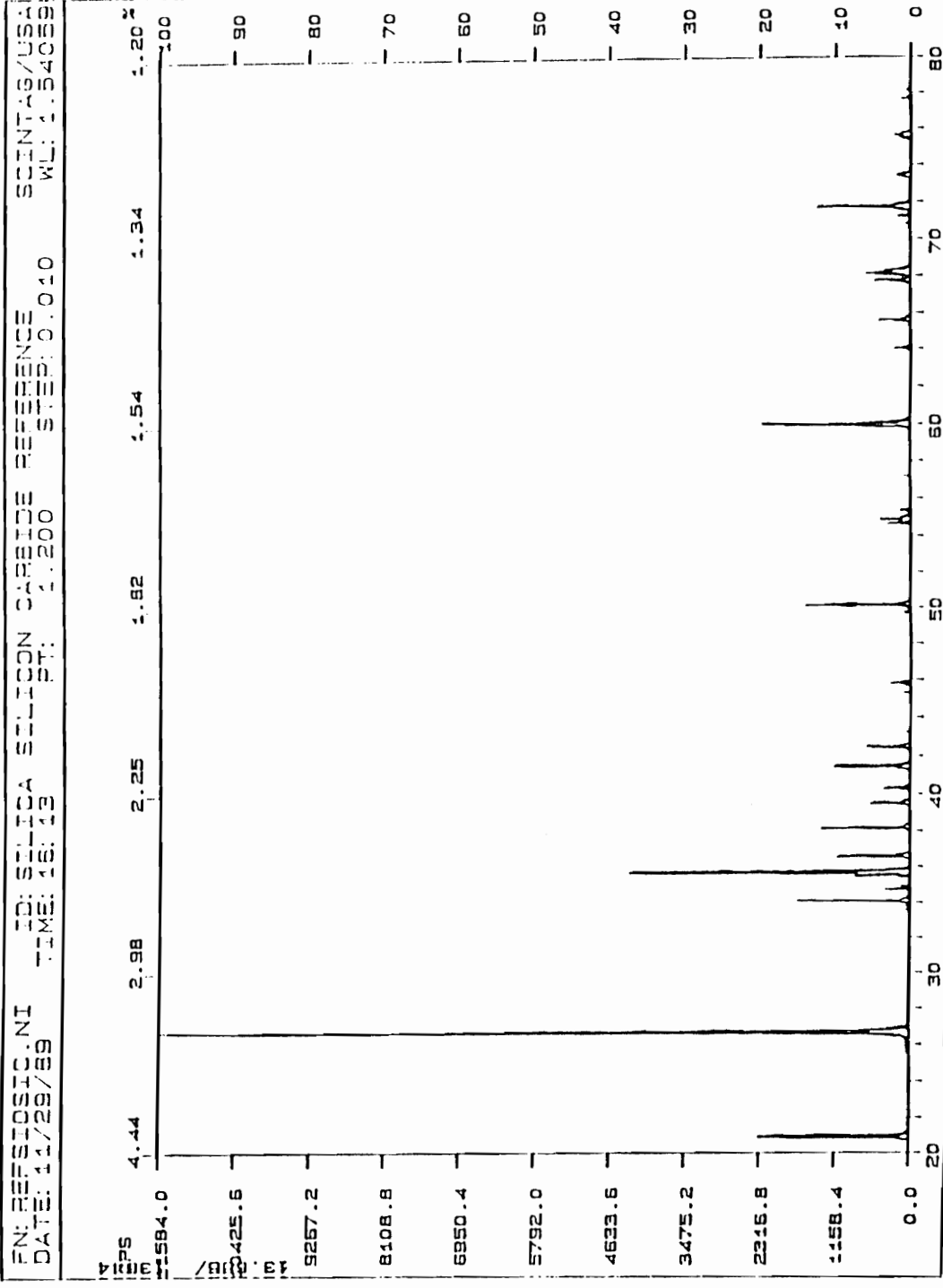


Figure 5.13 Silica - Silicon carbide before heating

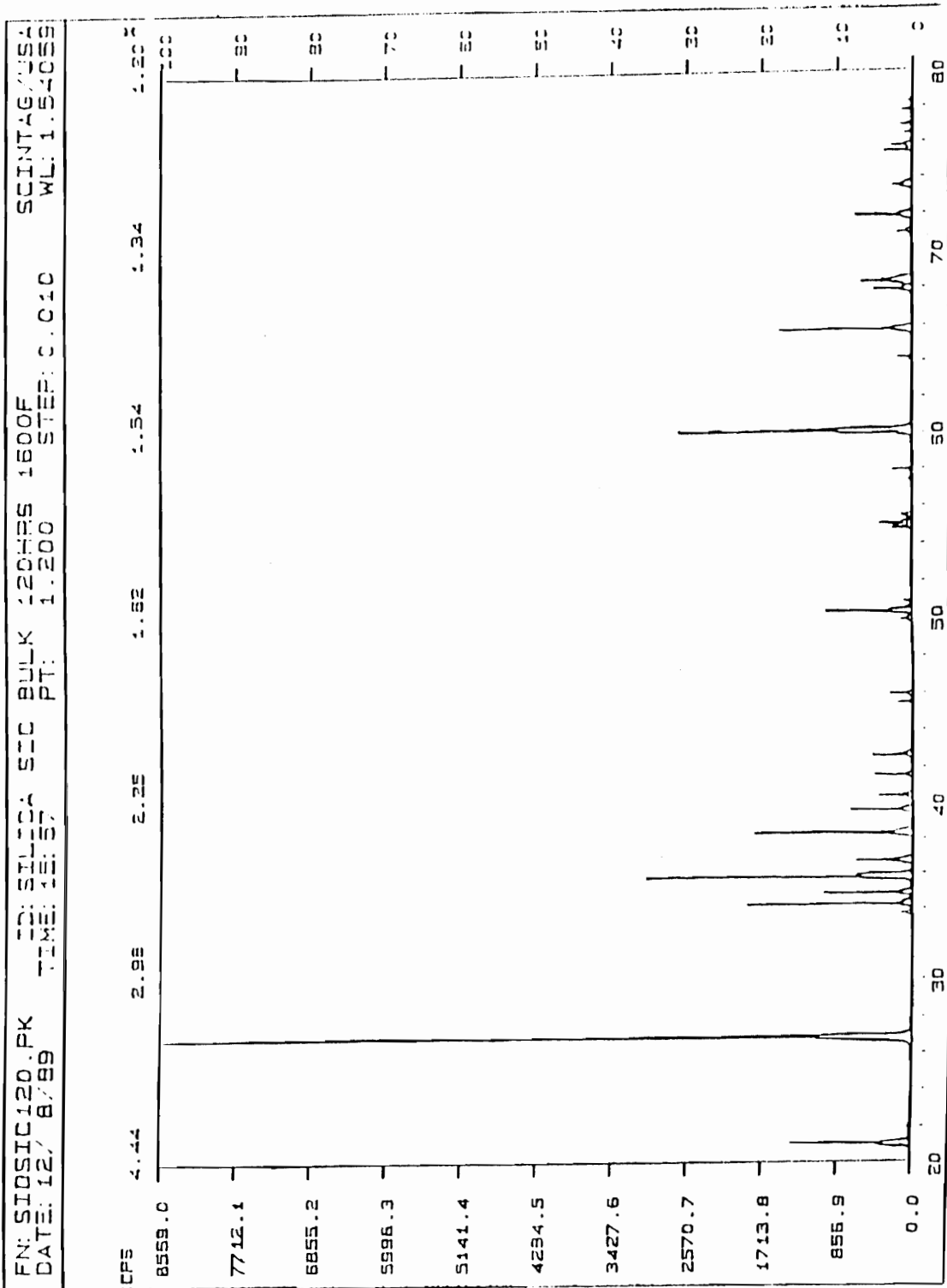


Figure 5.14 Silica - Silicon carbide heated at 557 °C for 120 hours

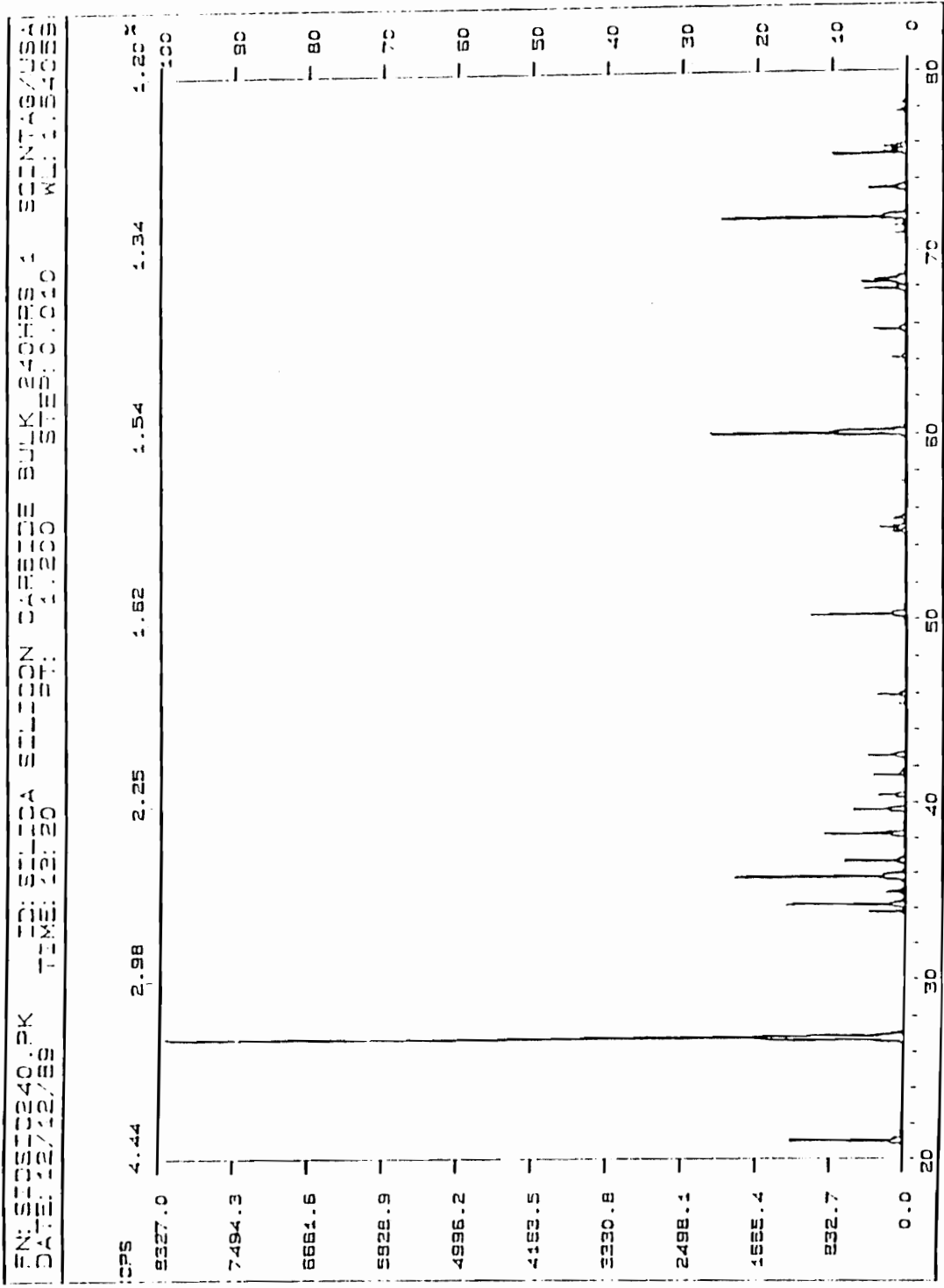


Figure 5.15 Silica - Silicon carbide heated at 857 °C for 240 hours

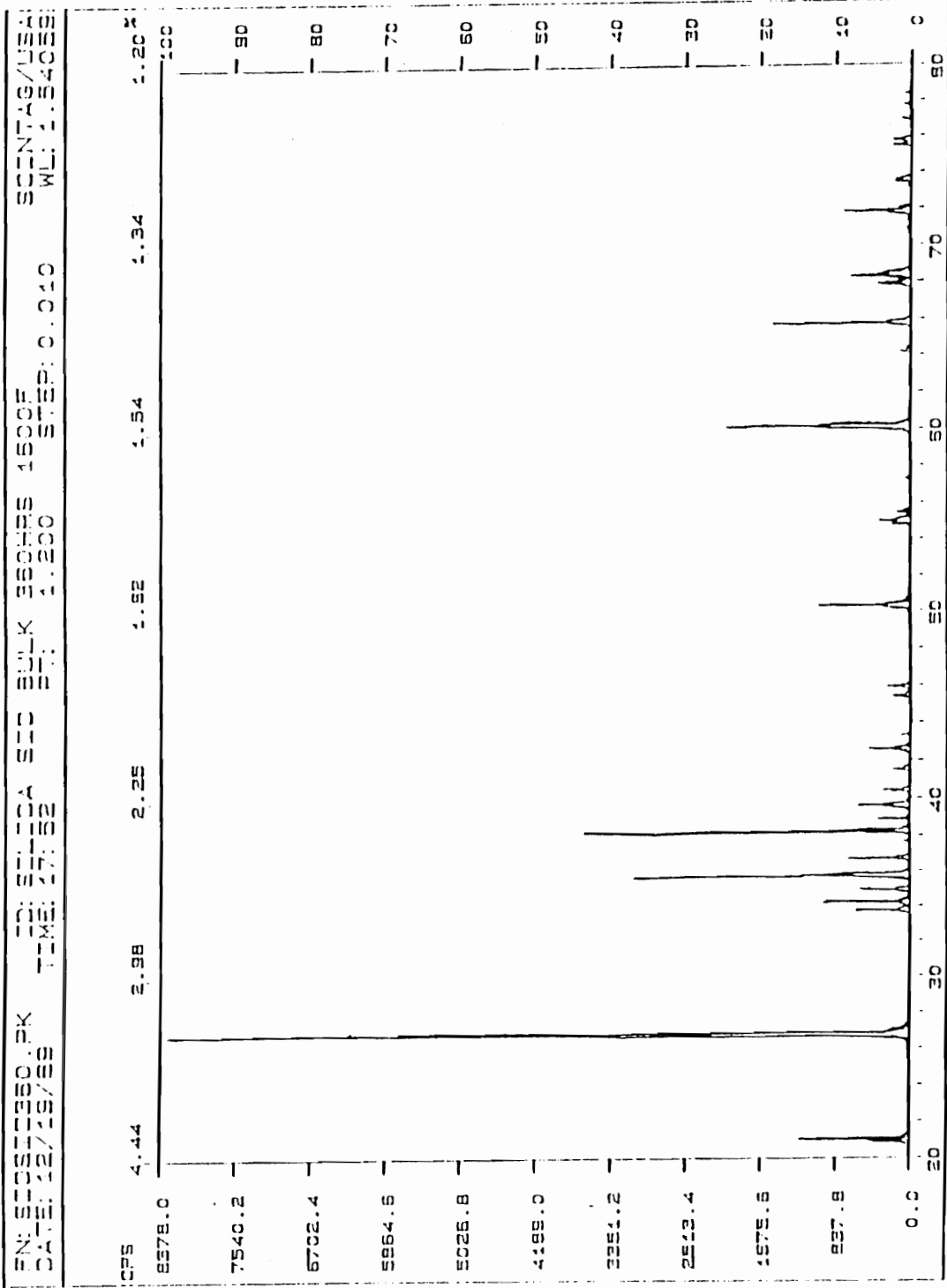


Figure 5.16 Silica - Silicon carbide heated at 857 °C for 360 hours

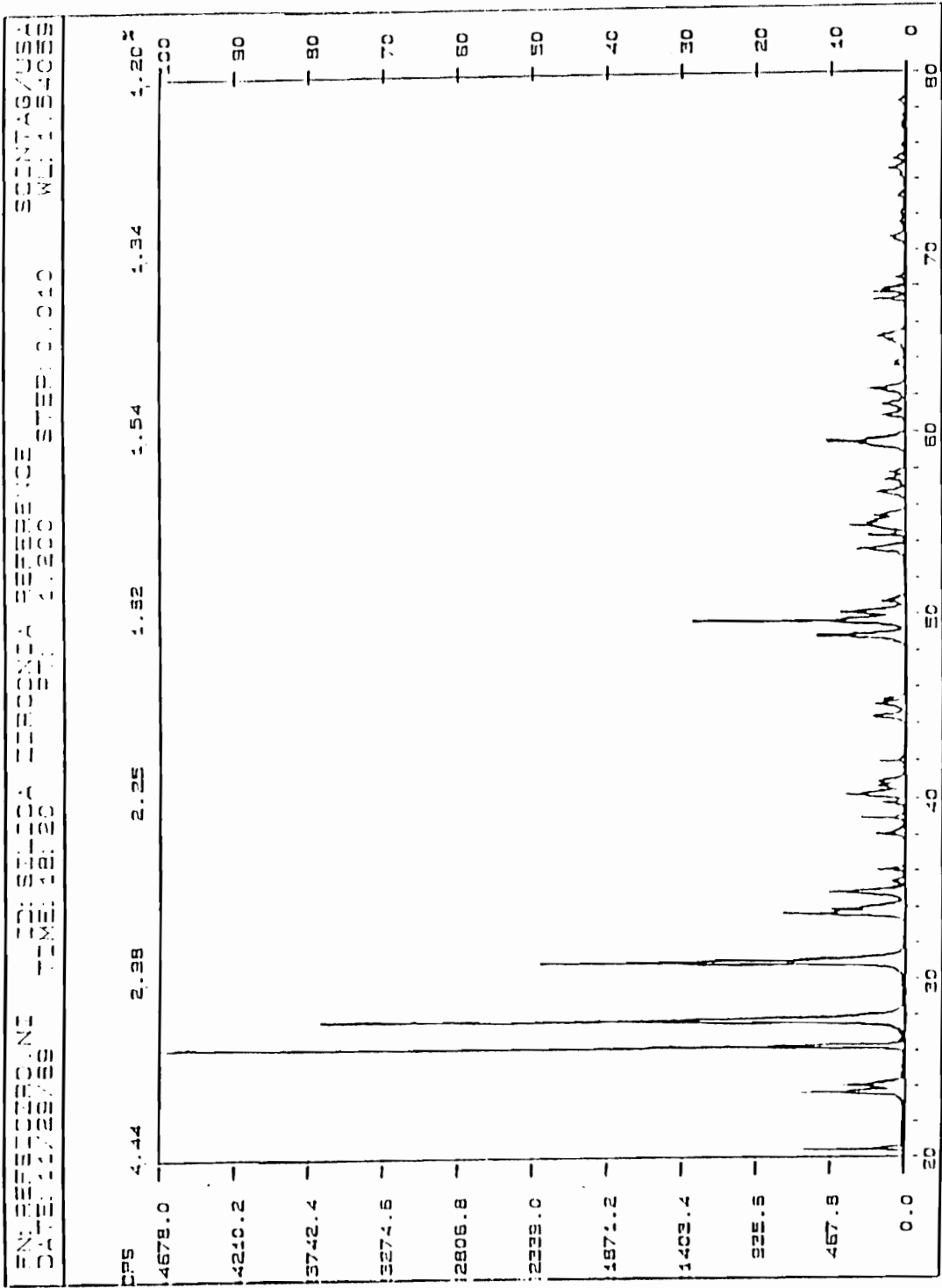


Figure 5.17 Silica - Zirconia powder: before heating

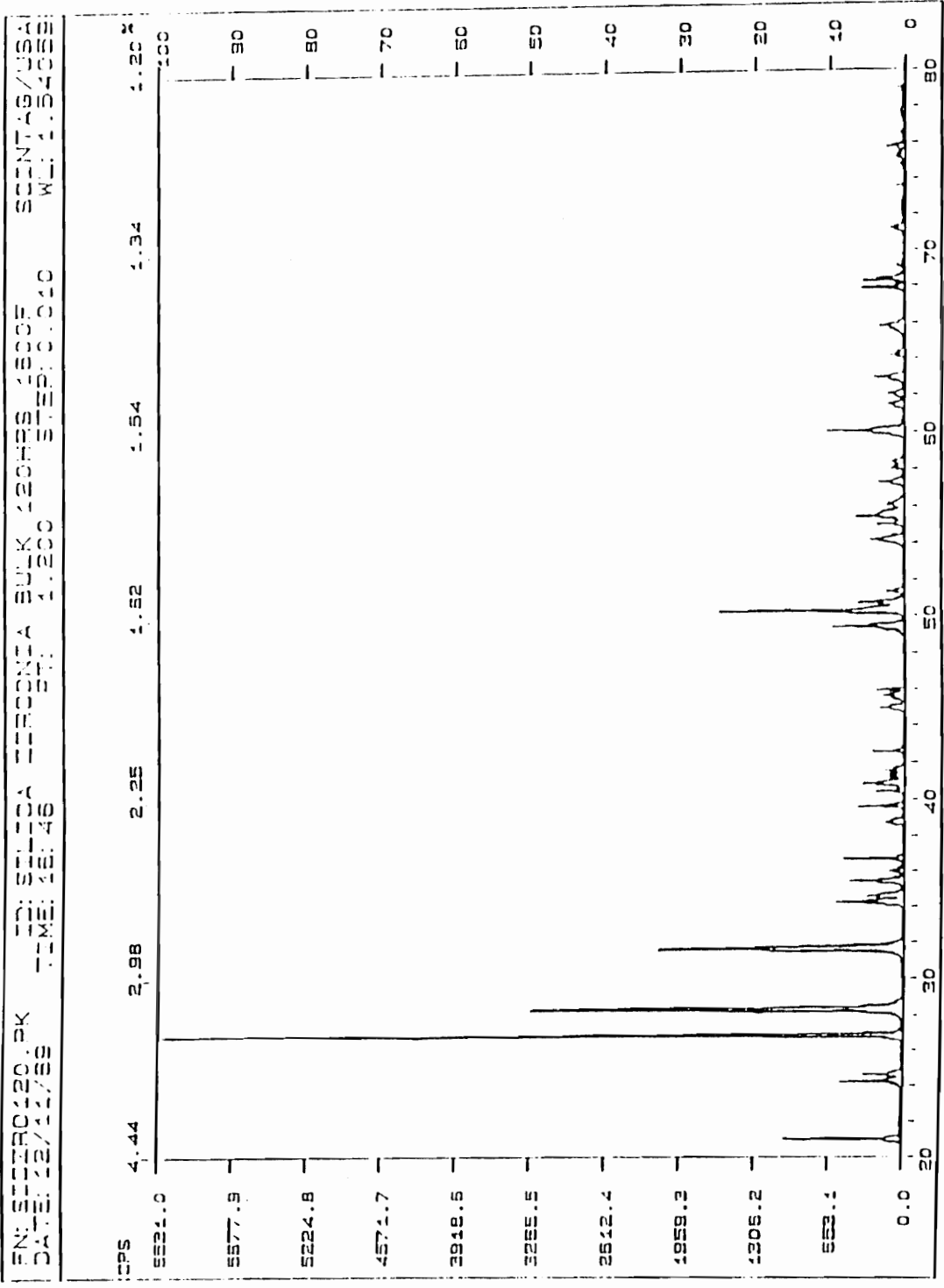


Figure 5.18 Silica - Zirconia powder heated at 857 °C for 120 hours

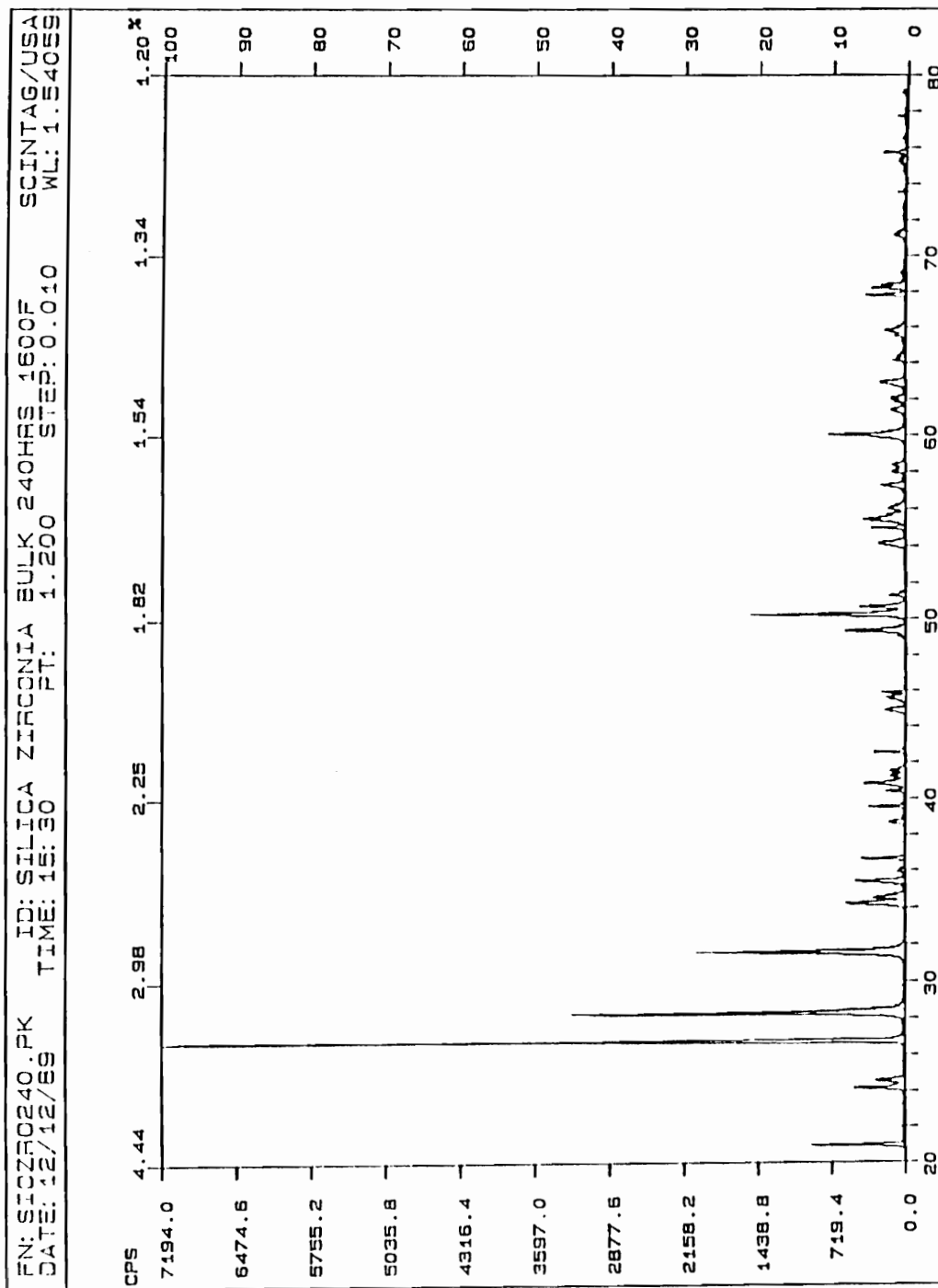


Figure 5.19 Silica - Zirconia powder heated at 557 °C for 240 hours

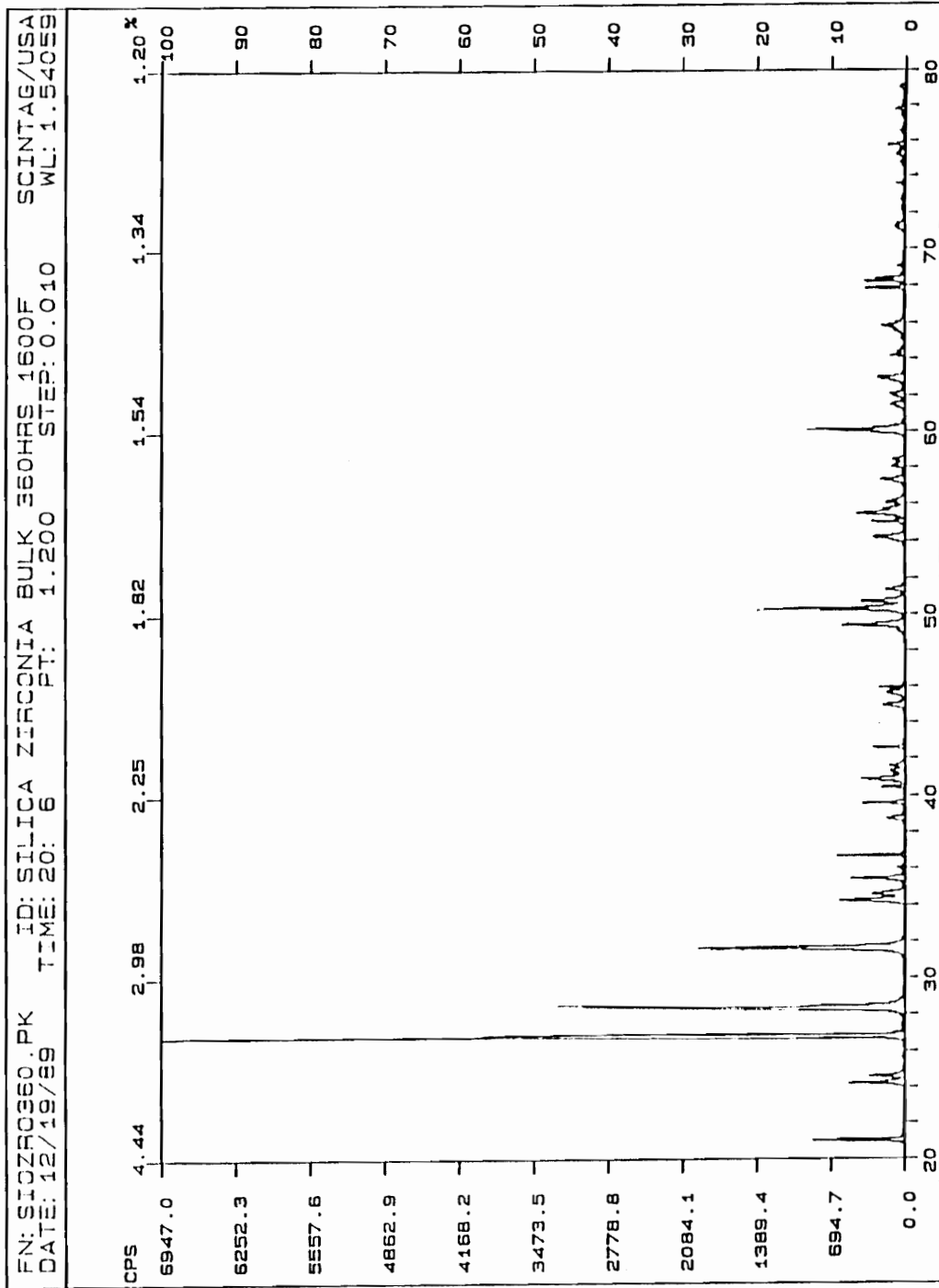


Figure 5.20 Silica - Zirconia powder heated at 857 °C for 360 hours

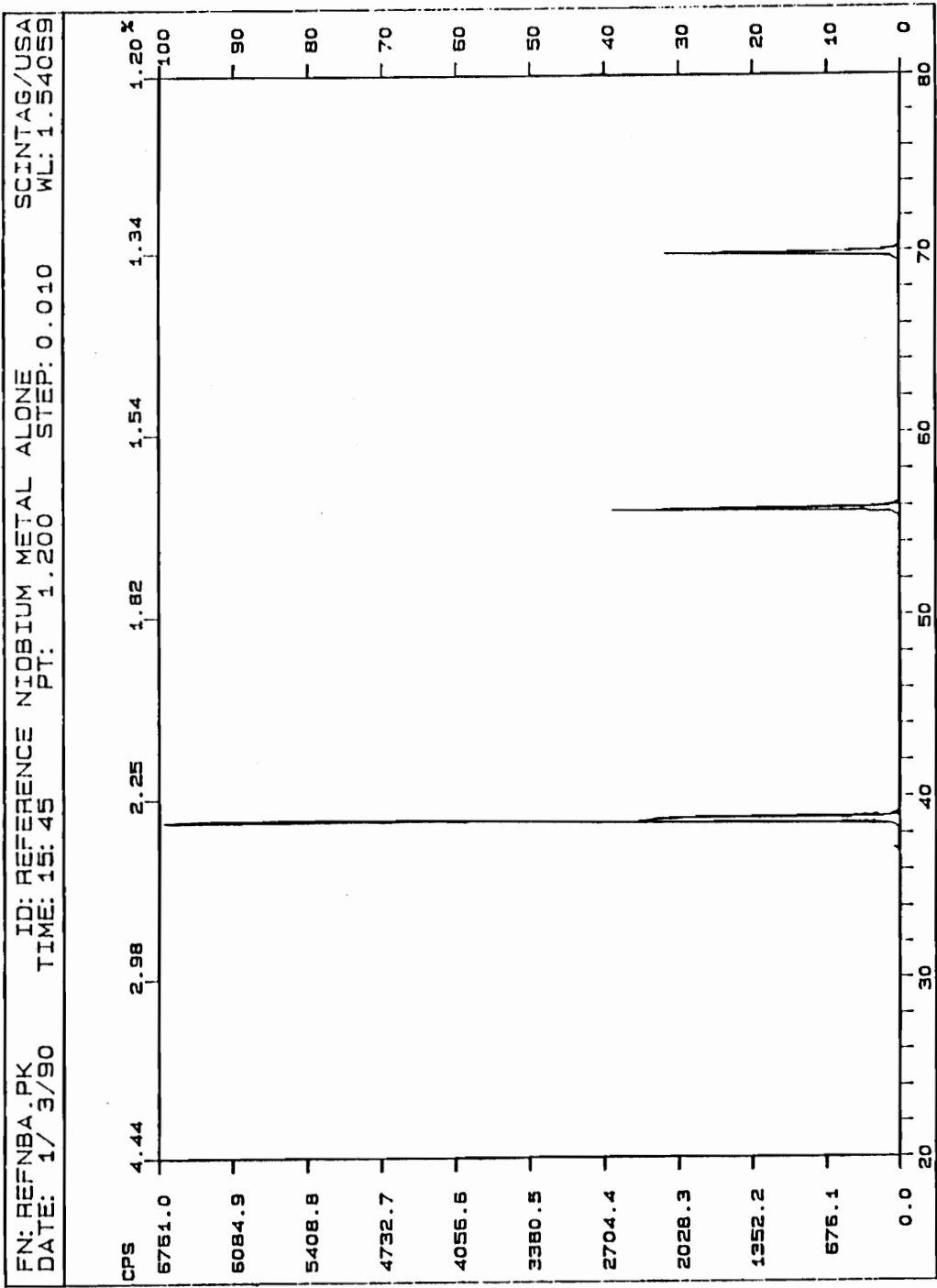


Figure 5.21 Silica - Niobium before heating

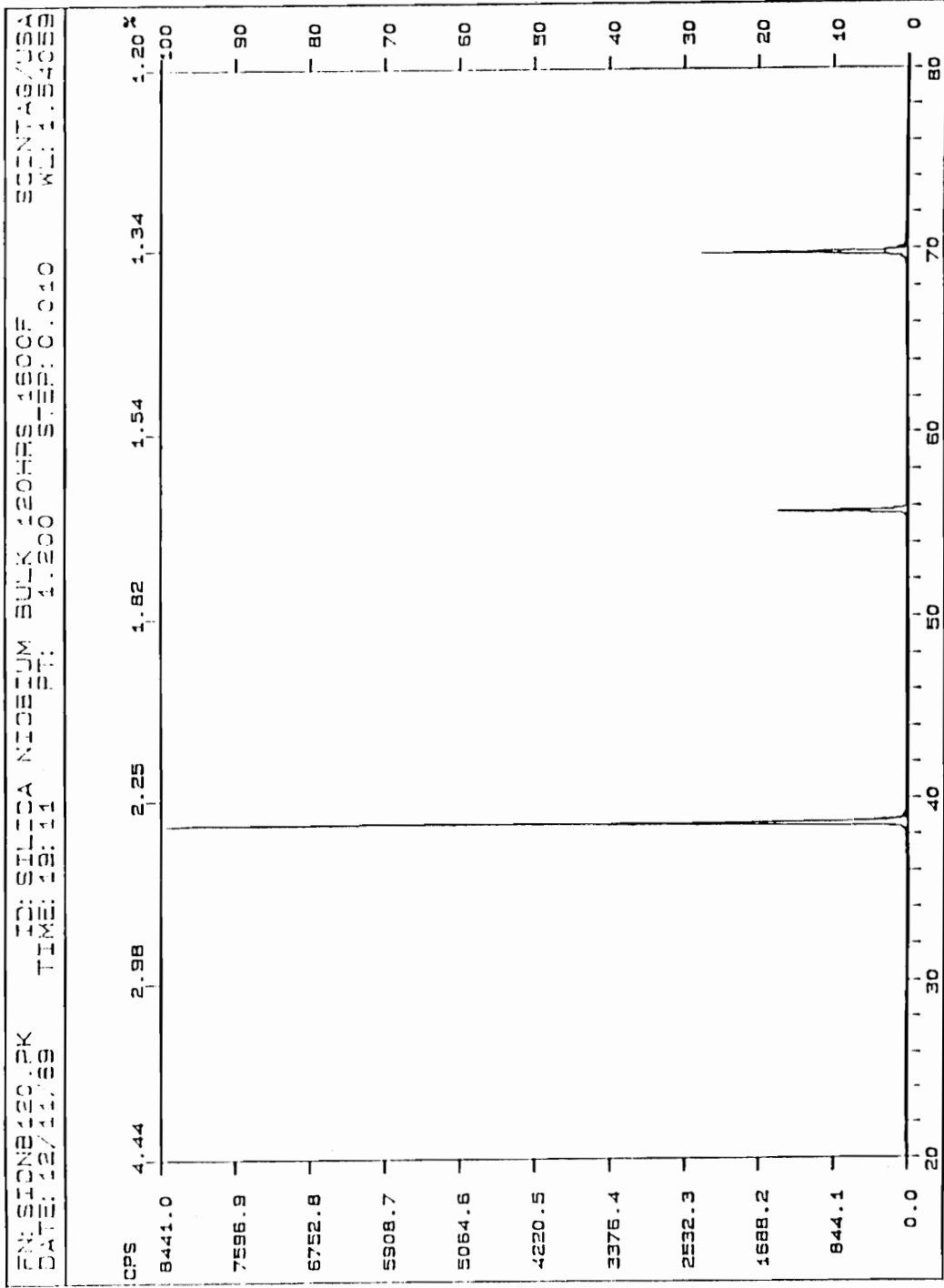


Figure 5.22 Silica - Niobium heated at 857 °C for 120 hours

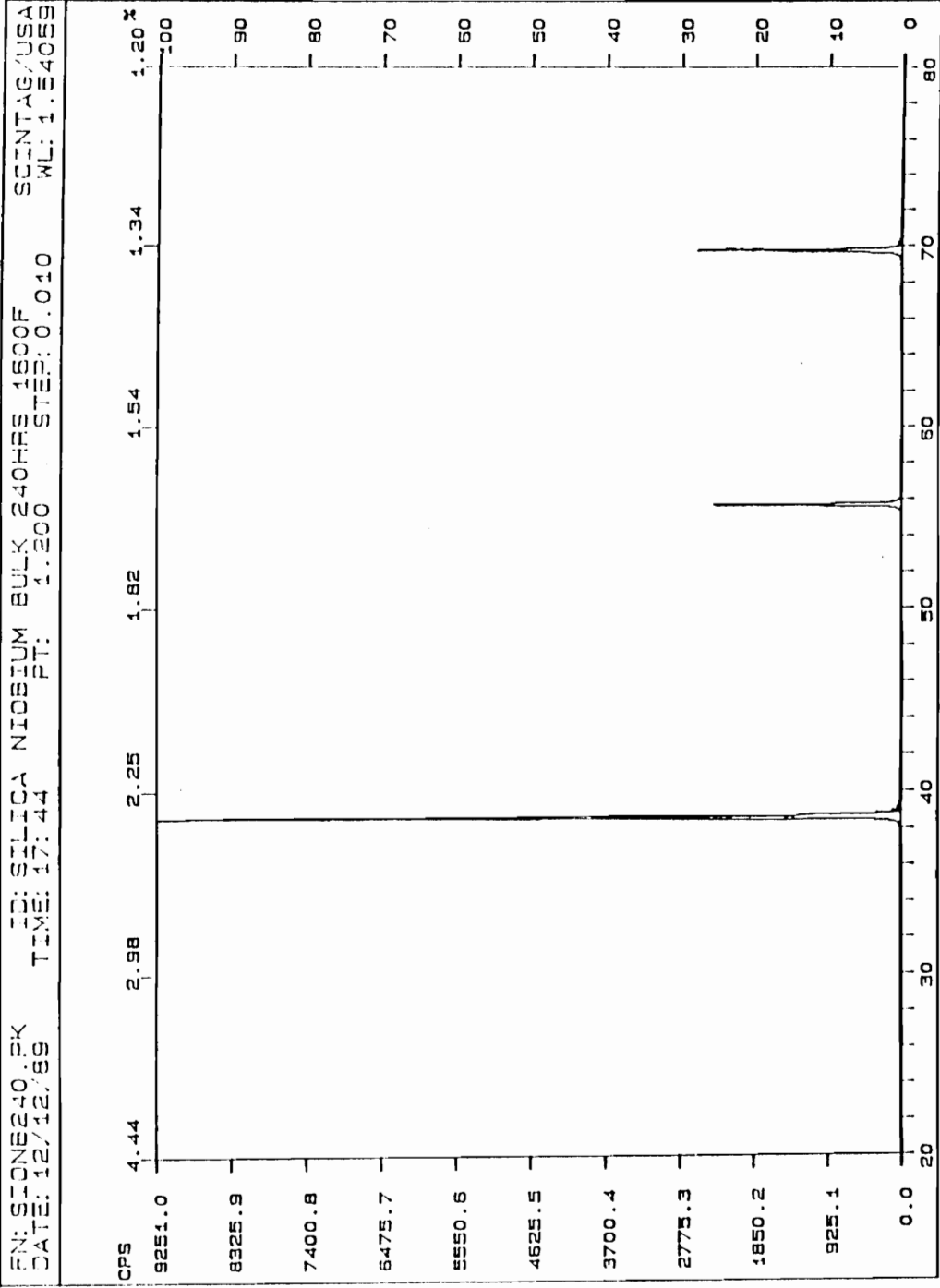


Figure 5.23 Silica - Niobium heated at 857 °C for 240 hours

FN: SION3360A.PK ID: SILICA NIOBIUM BULK 360HRS 1500F SCINTAG/USA
 DATE: 12/20/89 TIME: 16: 3 PT: 1.200 STEP: 0.010 WL: 1.54059

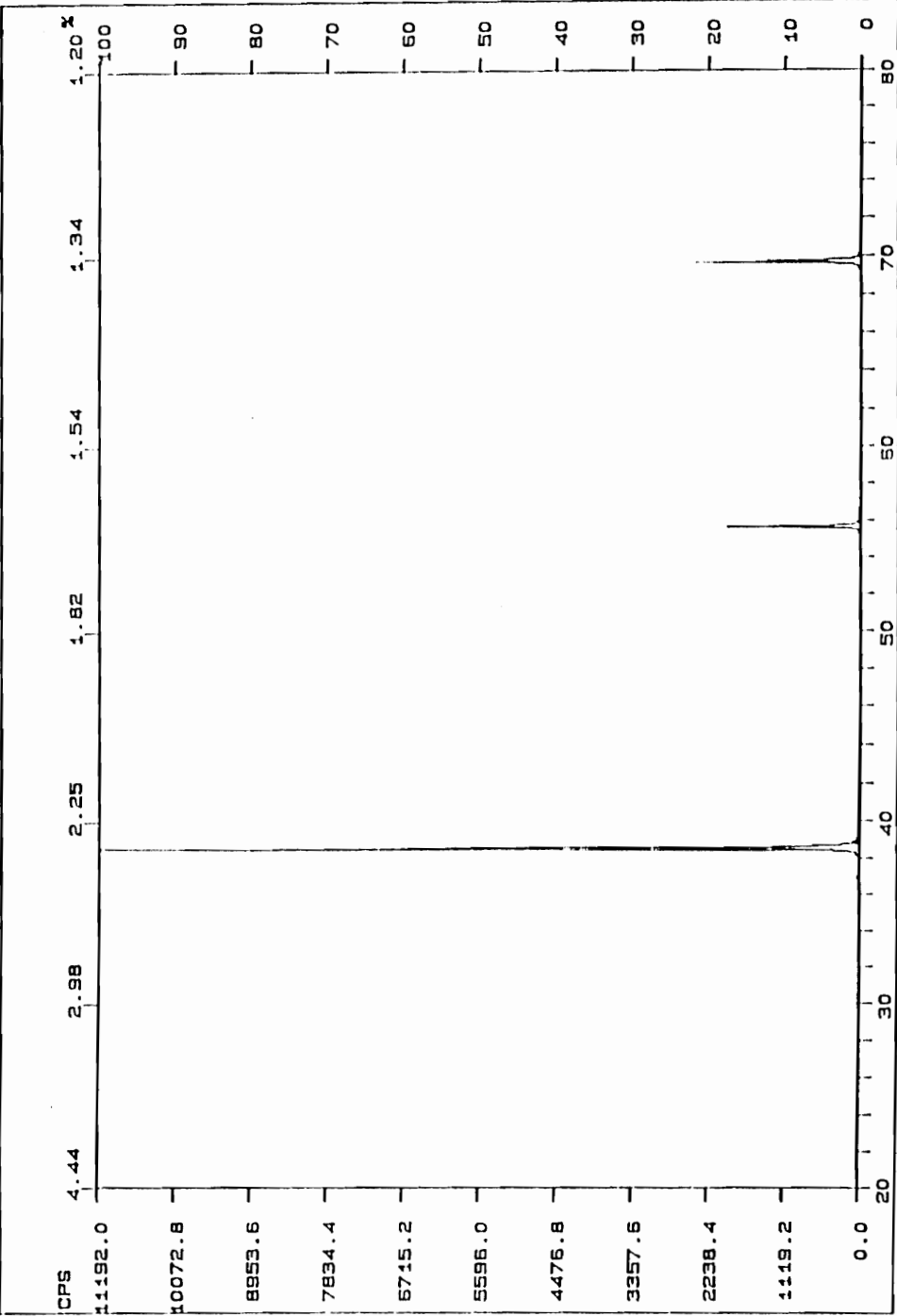


Figure 5.24 Silica - Niobium heated at 857 °C for 360 hours

5.3 The electron microprobe experiment

An electron microprobe analyzer employs a spectrochemical analysis of X-rays excited by electrons from a solid target. It can measure both qualitatively and semi-quantitatively the composition of grains as small as a few microns in size and for most practical purposes is a nondestructive method. The sample can be viewed during analysis and, most importantly, the grain can be studied in polished thin sections without disturbing it in its environment; hence it is particularly attractive to mineralogists.

A finely focused electron beam is directed onto the polished surface of the sample to be analyzed. The high energy electrons interact with the atoms of the elements present in the mineral and hence characteristic x-ray spectra of these elements originate. With the aid of X-ray spectrometers these spectra are then analyzed for wavelength and intensity. The wavelengths provide a qualitative analysis of the mineral and to a first approximation the intensity of a given characteristic X-ray peak is proportional to the concentration of the element in the mineral. Suitable standards have to be prepared and a proper correction procedure established for a large number of quantitative analysis [35].

5.3.1 Sample preparation

Electron microprobe analysis was done on the fiber in matrix samples prepared and the ones heated the longest were selected for analyses. The heat treated fibers were removed from the tubing and mounted with a small slope to the horizontal in cylindrical epoxy mounts. Epoxide resin and hardener made by Leco Corporation in the ratio 4:1 were mixed thoroughly and poured into molds and allowed to set overnight. In order to identify the samples an identification tag was placed in the mold before pouring the epoxy. Through the semitransparent mount, the tag could be detected and samples identified.

The mount was then removed from the mold and ground at some incline with the coarse grain grinding wheel. The mount was then reinserted into the original mold and the set of selected fibers were placed along the grooves created by the wheel and in a direction such that the fiber could be polished at an angle. More epoxy was poured over the fiber and allowed to set. When hardened the mount was ground down to the fine grain level and polished using alumina powder of 0.5 micron size in an ultrasonic vibrating tub. The sapphire fibers were again polished using 0.5 micron diamond paste and run for several hours before any reasonable polish could be obtained. Each sample was prepared in this manner. Extreme care was taken to avoid contaminant film build up during polishing and cleaning.

The electrically nonconducting samples were coated with a thin layer of (a few hundred microns thick) conducting material, ie. carbon, by vacuum deposition. The transparent carbon layer allows for the optical viewing of the fiber in the mount. A thin layer of carbon has an added advantage over metals namely that it does not absorb electrons nor X-rays of shorter wavelength. The carbon layer can be removed from the surface by rubbing it with acetone. Carbon painted along the sides of the mount touching the metal sample holder prevents charging and guarantees good electrical conductivity.

Figure 5.25 [35] shows a schematic diagram of the electron microprobe. The electron beam produced in the electron gun is demagnified to less than one micron in diameter and focussed onto the sample using two electromagnetic lenses. The X-ray spectrum produced is analyzed for wavelength and intensity.

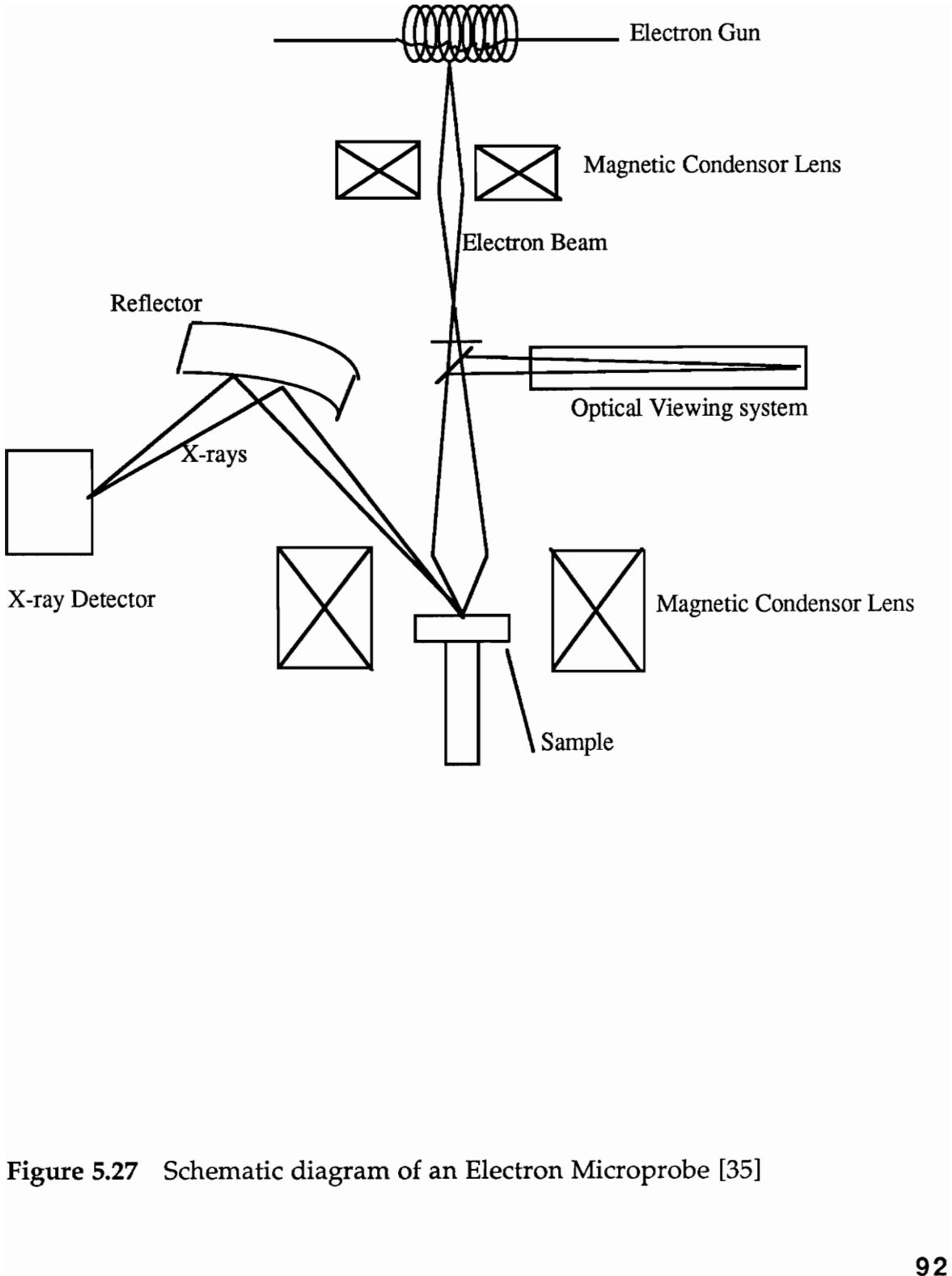


Figure 5.27 Schematic diagram of an Electron Microprobe [35]

The microprobe used for the qualitative analysis of the mounted fibers was the CAMEBAX SX 50, a product of Cameca. It is a highly automated and efficient analytical instrument and is controlled from a computer keyboard. It has a versatile specimen chamber and airlock for rapid change of specimen, many different configurations of X-ray spectrometers, a wide range of accessories for special applications and extensive software for automatic multi-point analysis and data manipulation.

Qualitative analysis with a static electron beam was used to establish which elements were present in the area along the edge of the fiber. The following samples were studied

Silica in alumina
Silica in zirconia
Sapphire in niobium

The selected samples were the ones heat treated for the longest period, 360 hour. The remaining samples

Silica in SiC
Sapphire in SiC
Silica in Niobium
Sapphire in Zirconia

had no particle adhering to it along the polished boundary and no surface reaction phases were observed. Figures 5.26 - 5.28 provide the plot of a static beam scan intensity versus the distance in microns.

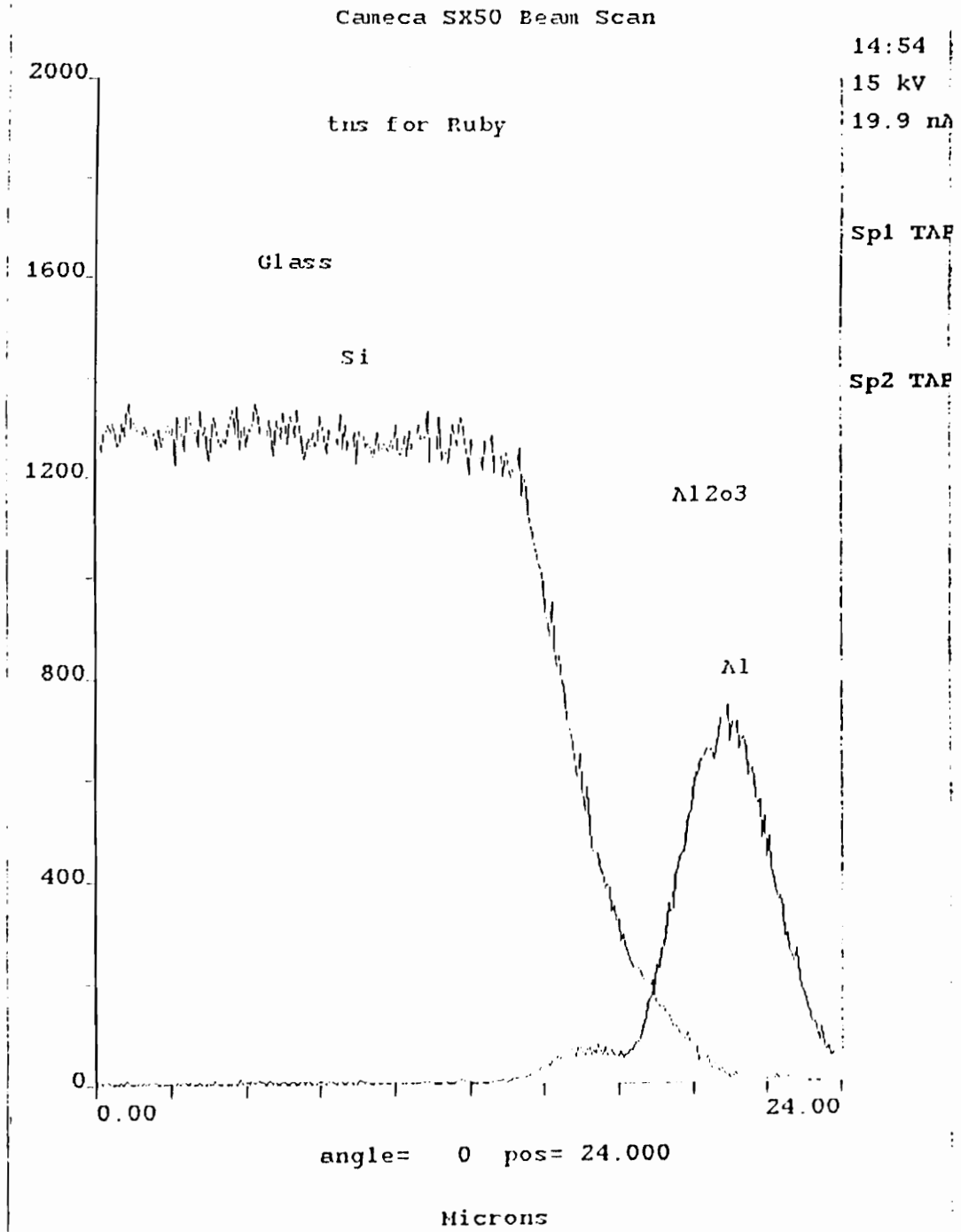


Figure 5.26

Silica fiber in Alumina heated for 360 hours at 857 °C

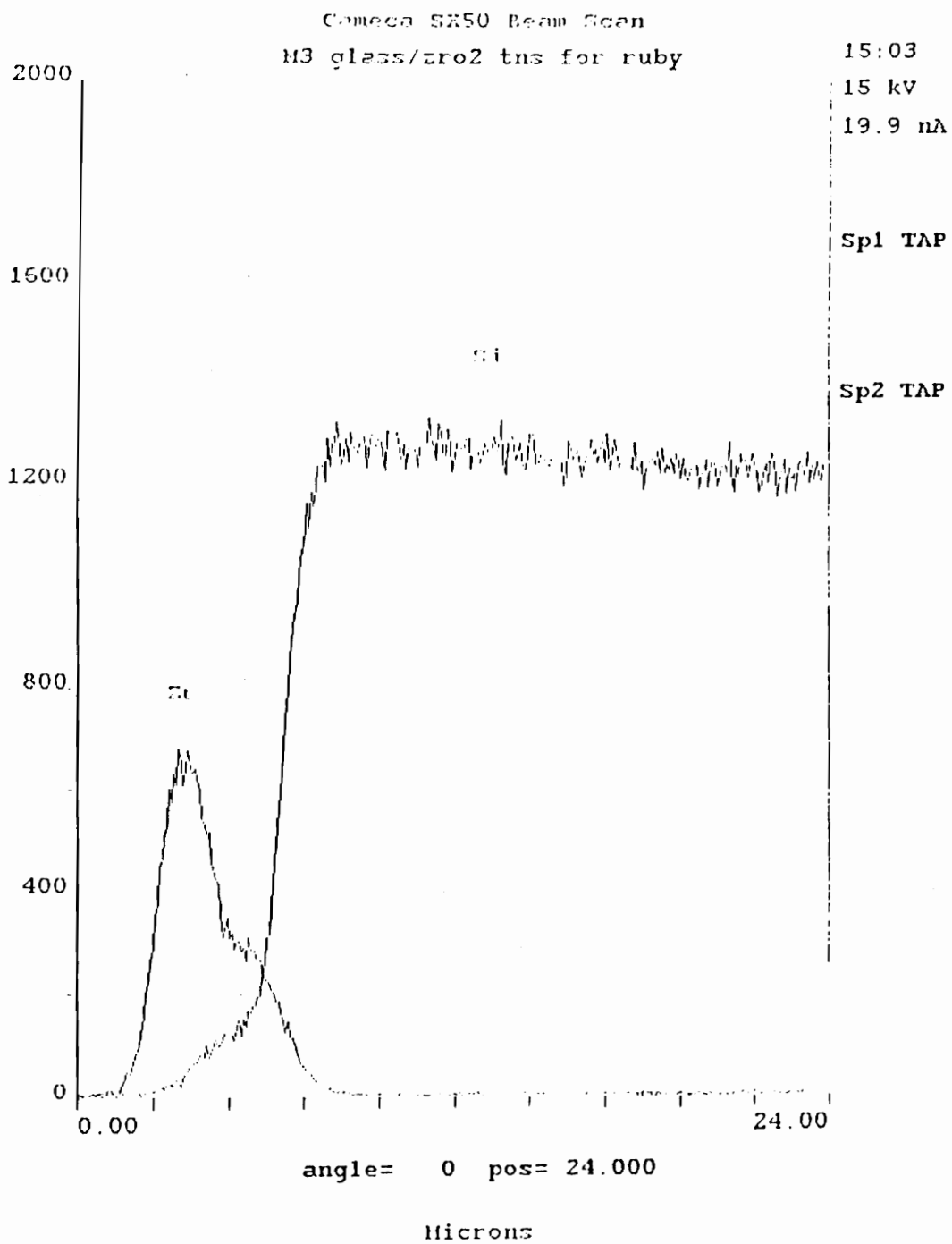


Figure 5.27

Silica fiber in Zirconia heated for 360 hours at 857 °C

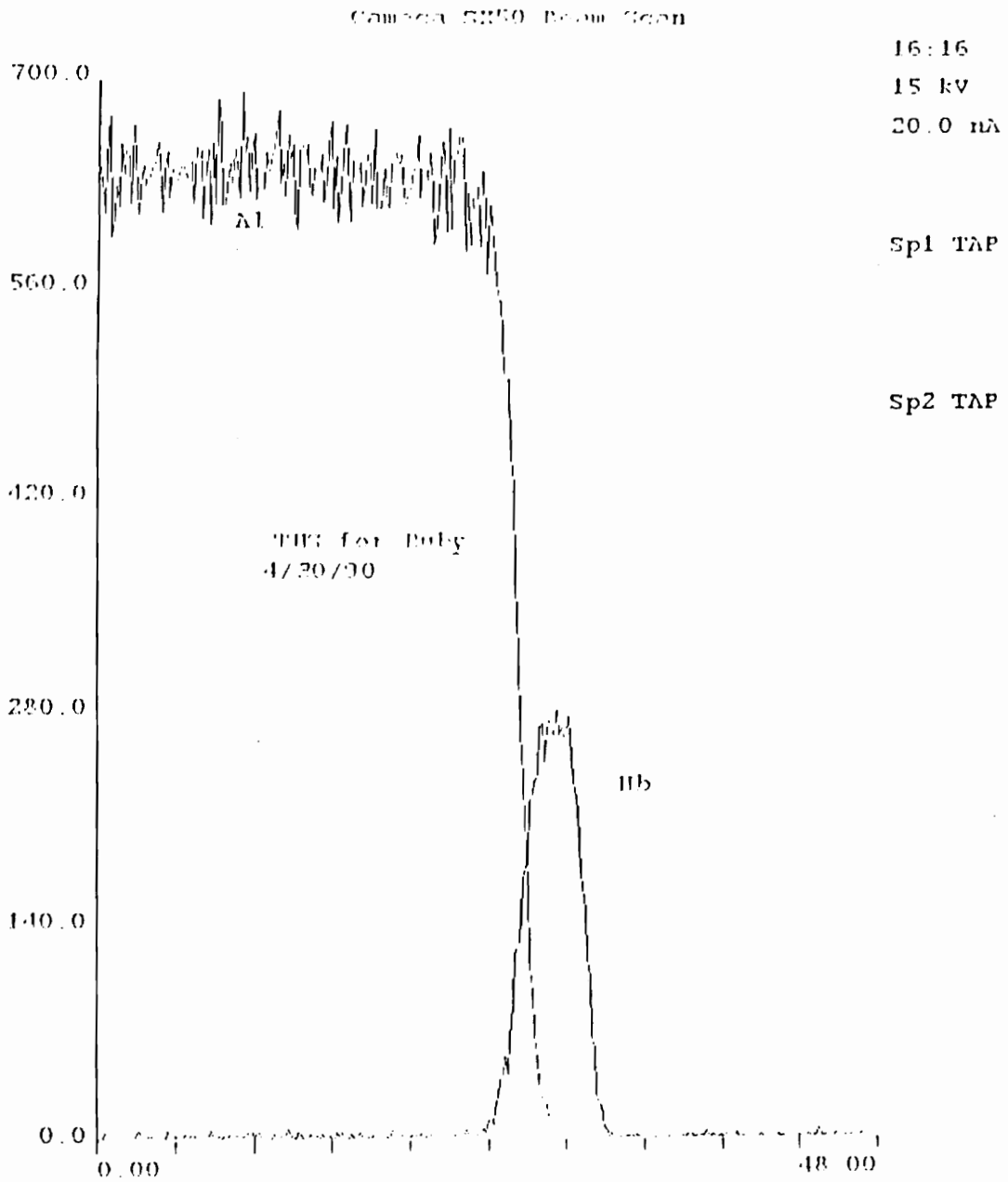


Figure 5.28

Sapphire fiber in niobium heated for 360 hours at 857 °C

5.4 Light microscope analysis

The fiber in matrix samples were examined under a light microscope to identify possible macroscopic changes in fiber structure as an added adjunct to the two major analyses conducted. Samples of the fiber in matrix were photographed using Polaroid films and are shown in the Appendix B. A Zeiss microscope was used to examine the samples and an attached Polaroid camera was used to take the pictures.

6.0 RESULTS AND CONCLUSIONS

6.1 Results of X-ray diffraction analyses

The bulk interaction of the encapsulated samples were analyzed for crystalline phases. X-ray diffraction patterns of the samples provide qualitative and comparative peaks of the mixture before heating and after heating for 5, 10 and 15 days, respectively. No bulk tests were made on niobium and alumina because their compatibility has been established due to their use in HPS lamps [8,10]. Figures 5.1 to 5.24 are the graphs of the sample mixtures analyzed. The graphs of the three heat treated sample mixtures were compared with the reference sample mixture and there was no indication of new crystalline phases. Figures 6.1 to 6.6 are the comparative diffraction patterns of the bulk mixture.

As can be seen from the graphs, there appears to be no evidence of new crystalline phases, even with the silica mixtures. This could be the result of the absence of chemical reaction or due to the absence of crystalline phases. The conclusion that there could have been no reaction can be substantiated by the fact that the experiments were conducted at temperatures far below the melting points of the components and also due to the fact that the heat treatment was carried out in a low oxygen atmosphere in which the samples had been evacuated and sealed. The only sure test of the nature of reactivity even under these conditions would be to take the temperature of the experiment to several hundreds of degrees above the range of interest and repeat the experiment and test for reactions. The absence of any reaction products at that temperature would be a fairly sure indication of the fact that under identical conditions the mixture would not react at the much lower temperature of interest.

6.2 Results of electron microprobe analysis

The plot of the static beam quantitative analyses using TAP crystals as standards indicated no new products. In fact; several microns separated the fiber and the particles. The irregularities present along the edge - the region of interest, produced irregularities in the plot. Otherwise it can be concluded that neither diffusion nor grain boundary phase changes were observed to be present.

6.3 Light microscope examination of fiber in powder

The mounted fibers were examined under a light microscope to identify any visible macroscopic changes in the fiber structure. Other than surface irregularities resulting from polishing, all the samples with the exception of 'silica fiber in silicon carbide' showed no visible structural changes.

The silica fiber in silicon carbide seemed to have undergone vitrification as seemed to be the case from the pattern observed throughout the cross section of the fiber. This could have been due to the fact that the fused silica fiber with the impurities present could not retain its structure under the environment it was exposed to. While detailed analysis of the fiber matrix reaction has to be conducted to explain the phenomenon, the carbide cannot be used as coating material on the fiber. The absence of any information on the x-ray chart could be due to the fact that commercial powder of silica was used and not the crushed fiber itself. Diffraction analyses of the crushed fiber material or the microprobe analyses with suitable standards would explain the phases present.

6.4 Conclusions

6.4.1 Niobium-Alumina coating on sapphire

Multilayer coatings on sapphire with metal niobium and alumina can be achieved in the following way. Niobium can be coated onto the fiber surface by the sputtering method where the unit can be adapted to feed continuous fiber. Since niobium oxidizes in air it should be coated soon after with alumina which can be done using CVD method. Aluminum isopropoxide, aluminum t-butoxide or aluminum sec-butoxide stearate solution can be used. Nitrogen gas bubbled through any one of the above solutions kept boiling will send vapor of the mixture into a connected high vacuum chamber heated to about 400°C and through which the fiber is drawn. Alumina will separate from the vapor and deposit uniformly on the fiber. A strong coating can be achieved this way.

6.4.2 Other coating materials

Since sapphire does not react with any of the selected materials it could be coated and definitely used in an identical environment for considerable length of time. Figure 6.7 provides a comparative chart of some of the physical properties of the materials analyzed. Fused silica thermal expansion coefficient differs considerably from that of sapphire. Depending on the temperature range it is to be exposed, it could still be used for coating sapphire. Sapphire could be coated with a single layer of alumina as it is a compatible and one of the toughest material selected. Silicon carbide and zirconia have both matching thermal expansion coefficient and from the available data, they could both be used as coating materials.

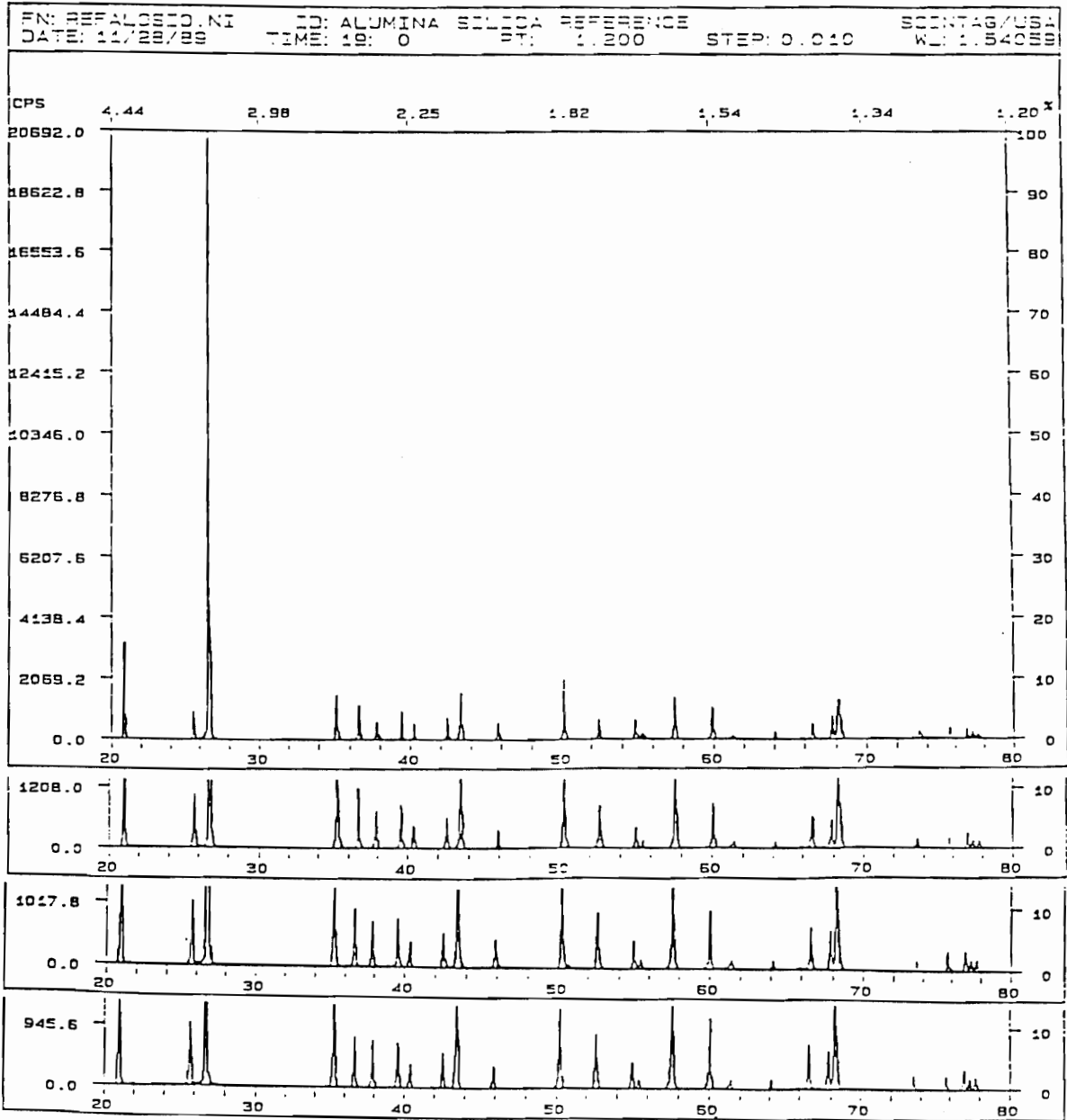


Figure 6.1 Alumina - Silica series

FN: REFALOSIC.NI ID: ALUMINA SIC REFERENCE SCINTAG/USA
DATE: 11/21/89 TIME: 17:35 PT: 1.200 STEP: 0.010 WL: 1.5403

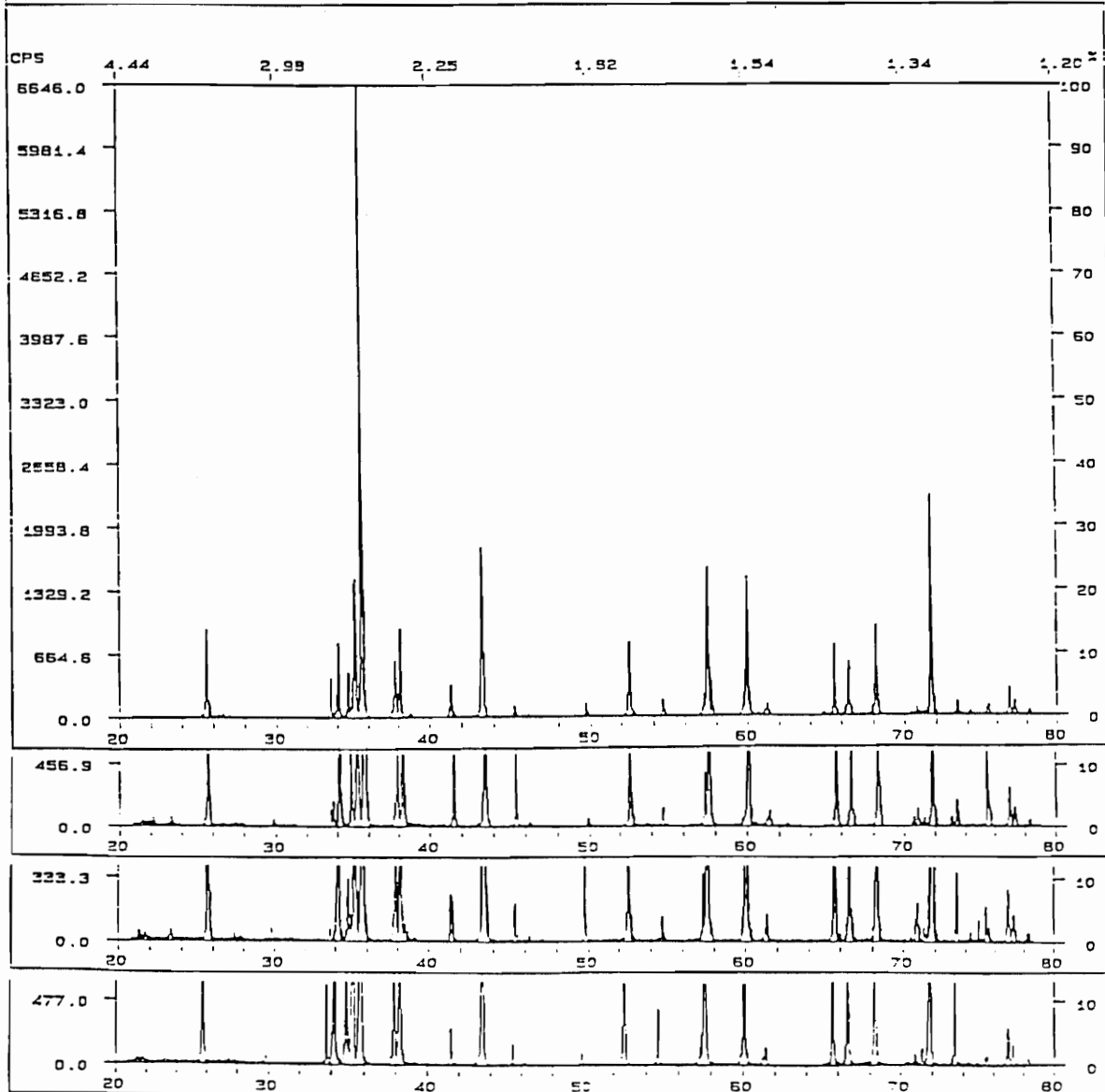


Figure 6.2

Alumina - Silicon carbide series

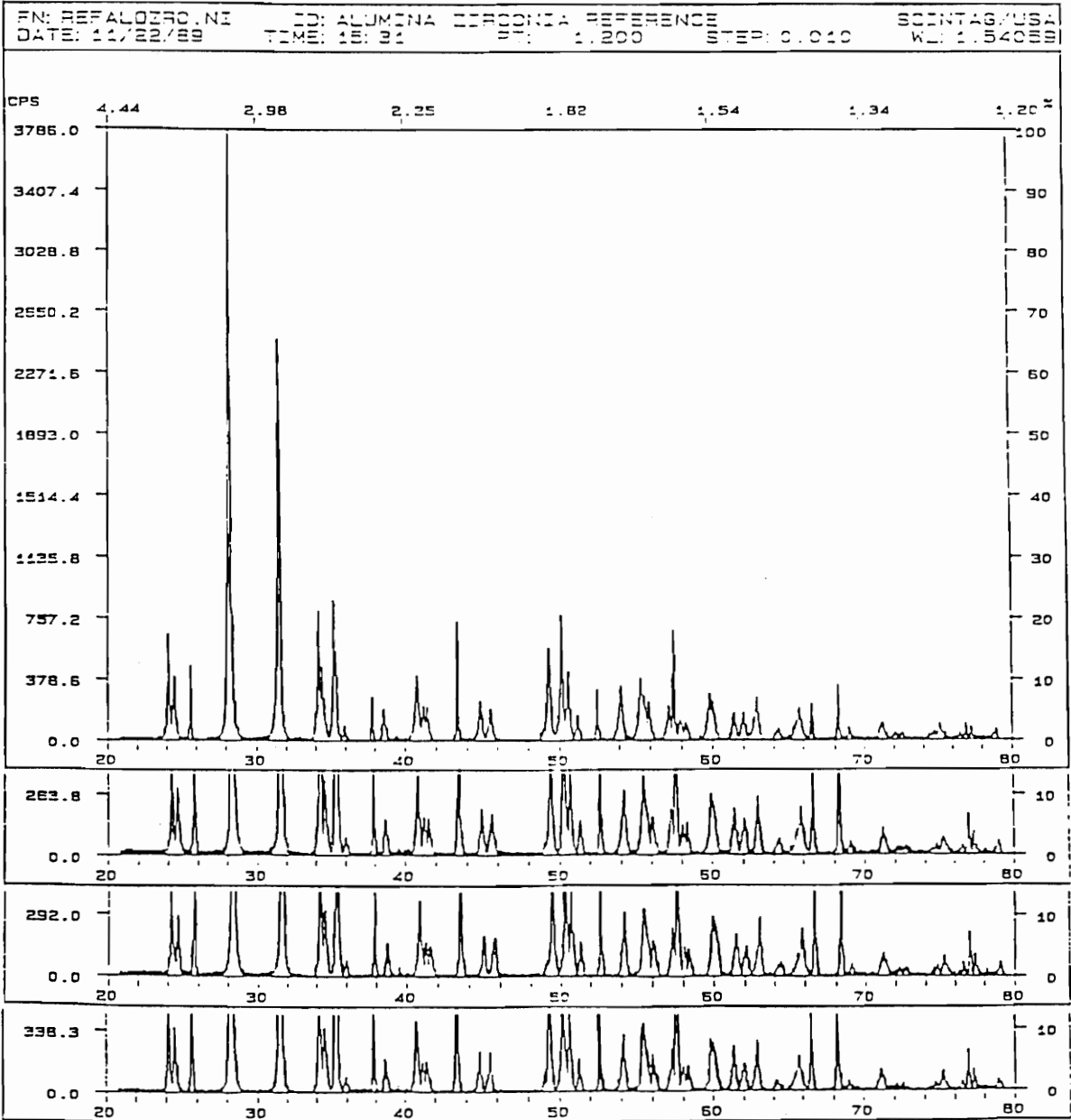


Figure 6.3 Alumina - Zirconia series

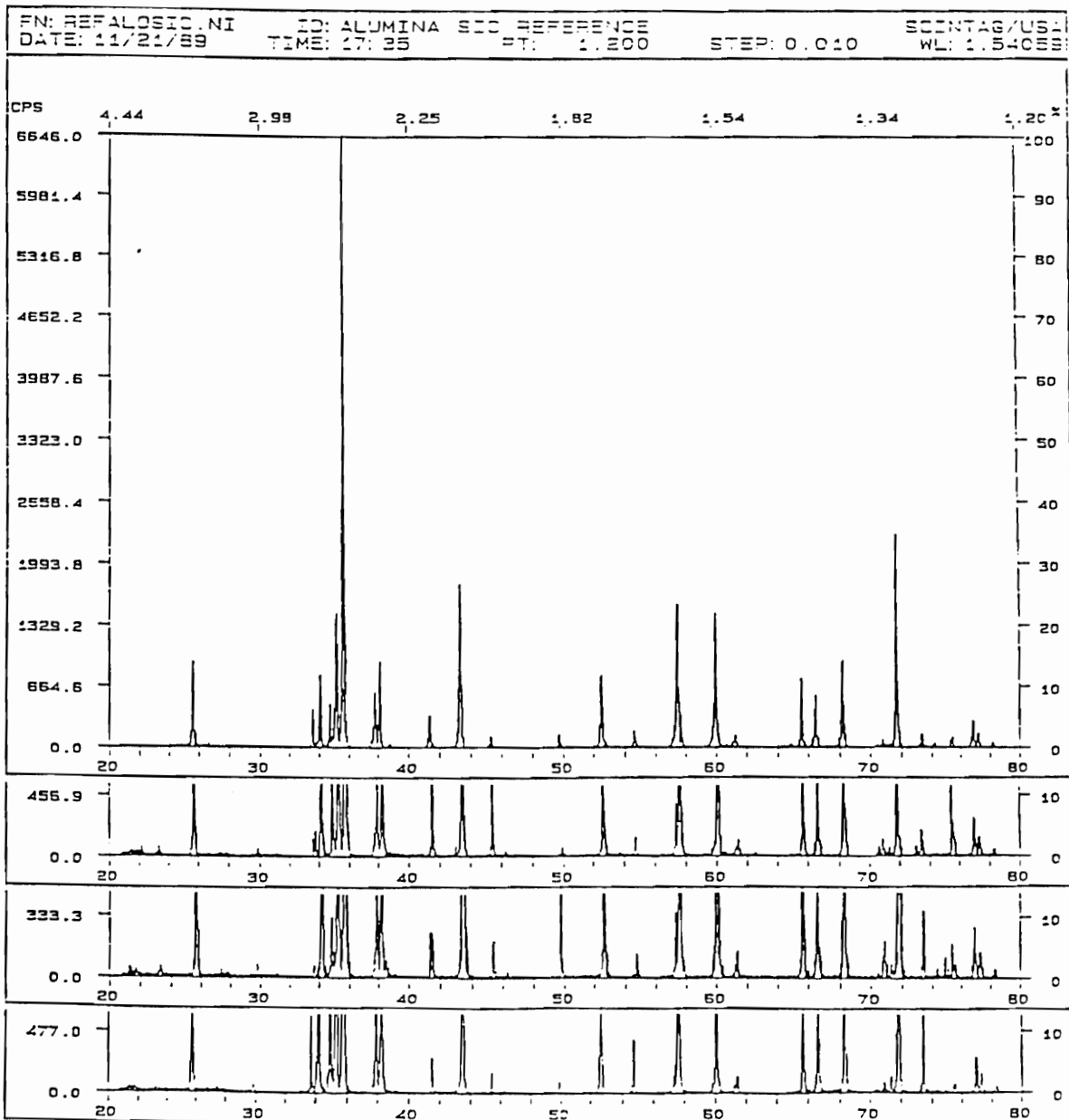


Figure 6.4 Silica - Silicon carbide series

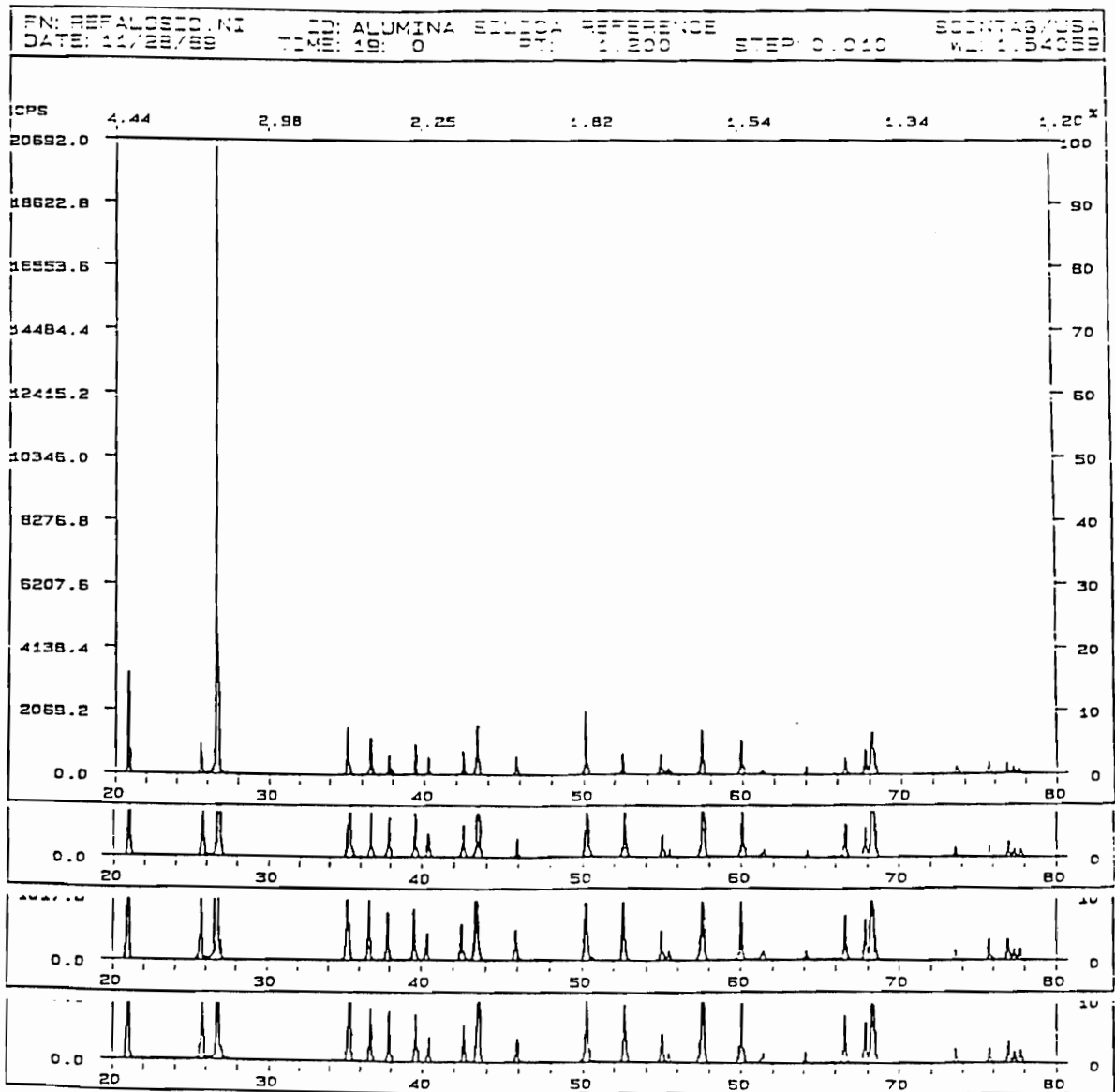


Figure 6.5 Silica - Zirconia series

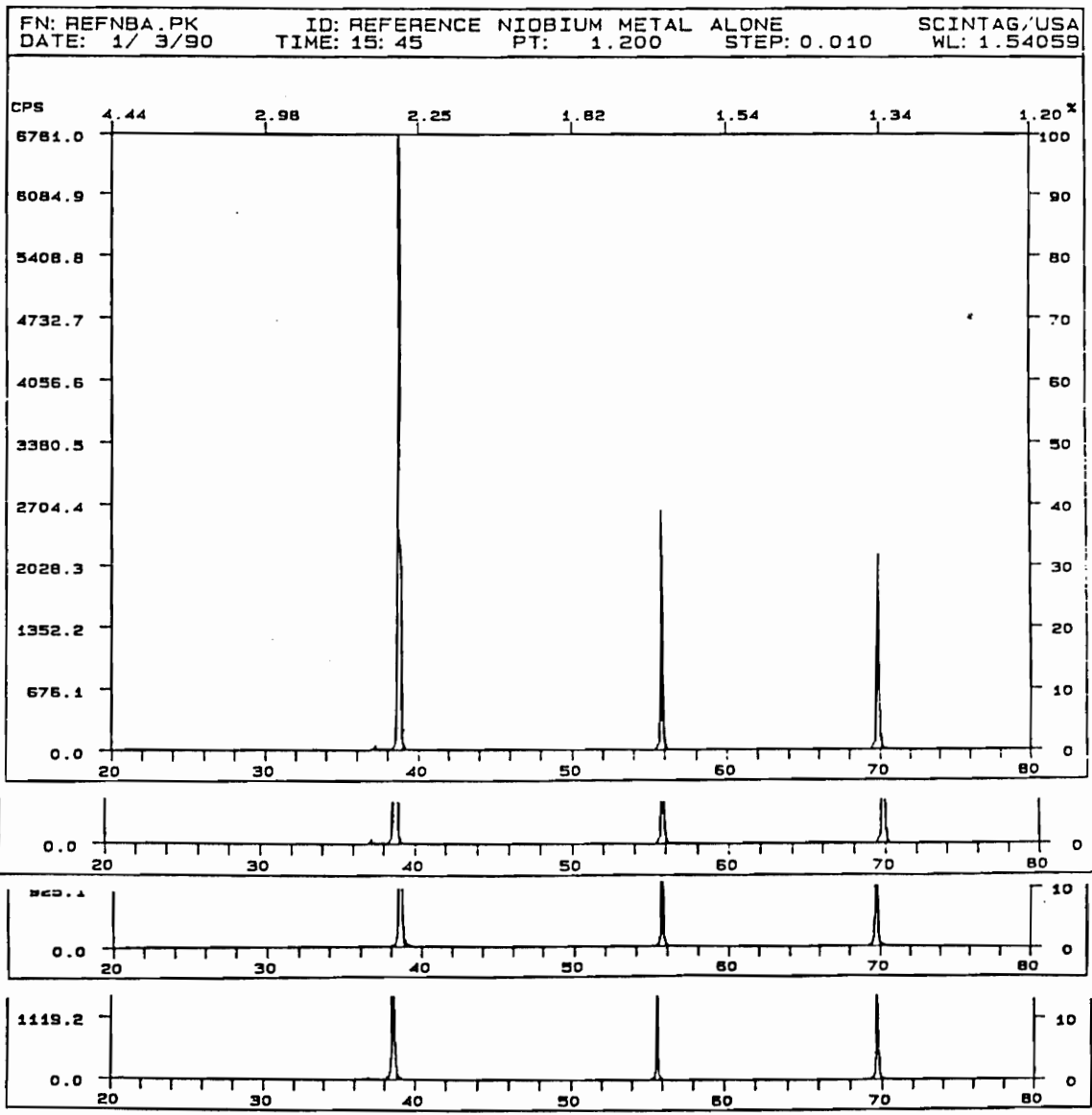
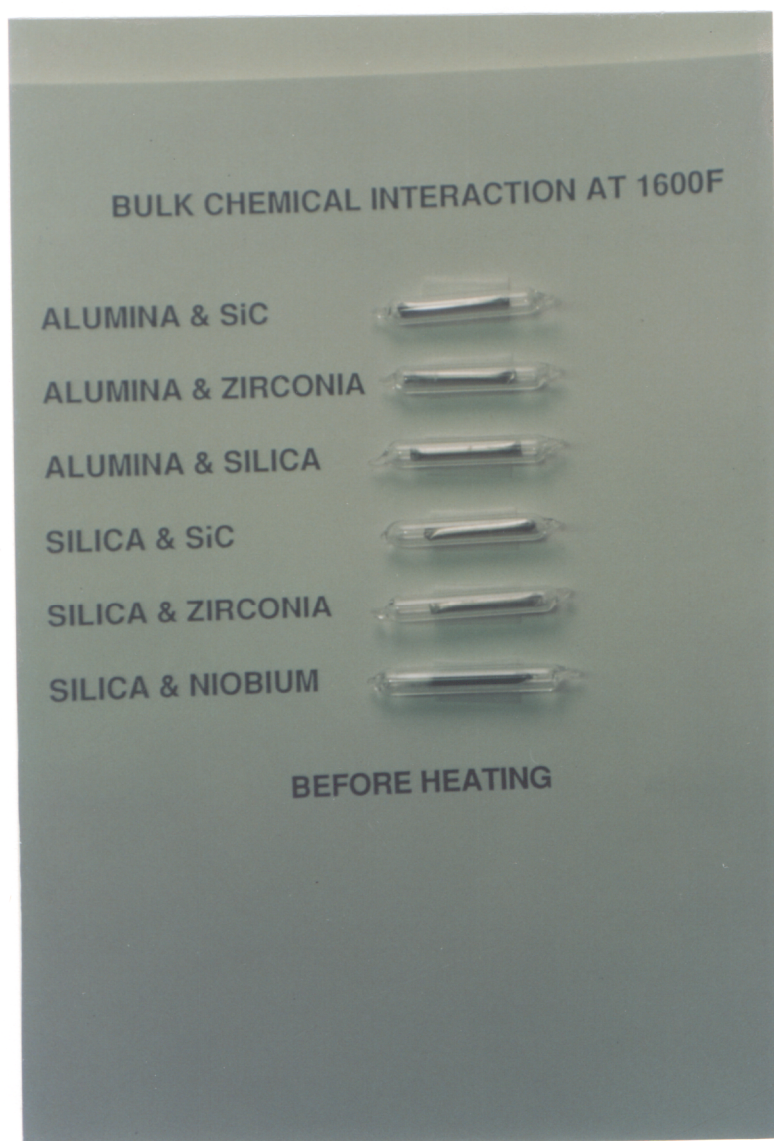


Figure 6.6

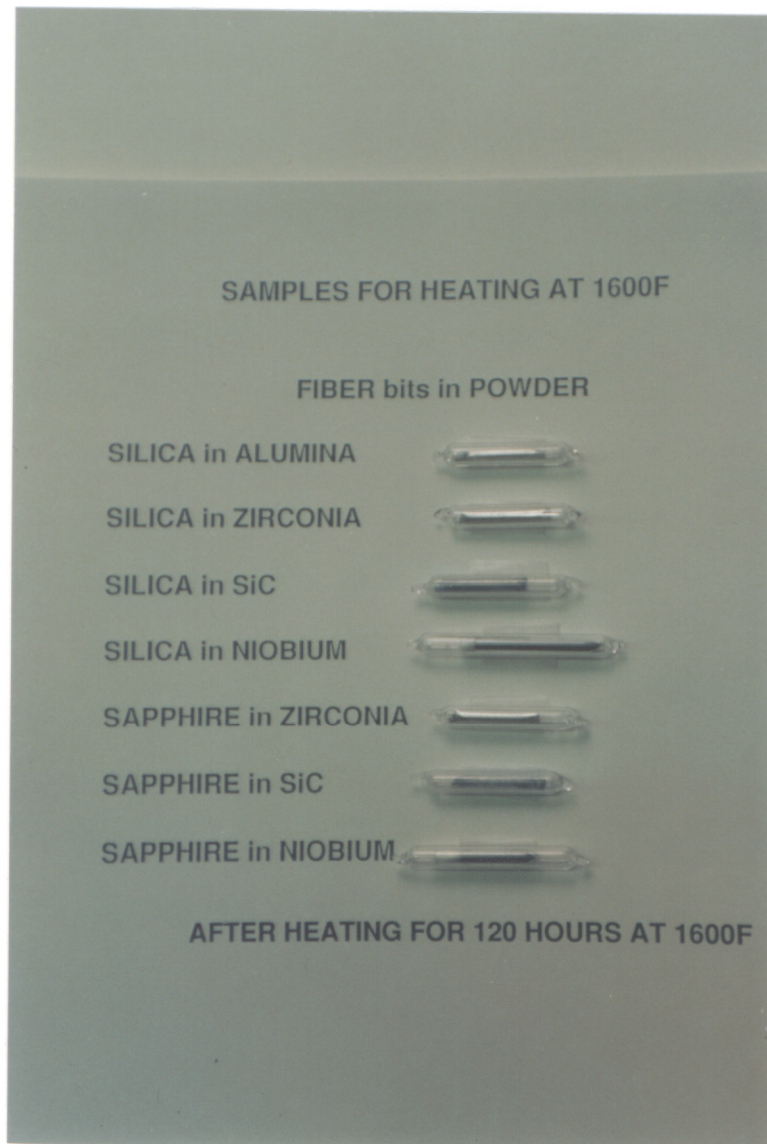
Silica - Niobium series

Material	Thermal Expansion (1000°C)	Melting Point	Structure
Alumina	$8.1 \times 10^{-6}/^{\circ}\text{C}$	2054°C	Hex
Sapphire	8.2 x 10 ⁻⁶ /°C per to C axis 9.2 x 10 ⁻⁶ /°C II to C axis	2053°C	Rhomb
Silica(Quartz) Fused Silica	$3 \times 10^{-6}/^{\circ}\text{C}$ $0.564 \times 10^{-6}/^{\circ}\text{C}$	1610°C	Hex
SiC	$5.8 \times 10^{-6}/^{\circ}\text{C}$	2830°C	fcc
Zirconia	$7.59 \times 10^{-6}/^{\circ}\text{C}$	— 2715°C 2600-2650°C	mono tetra stabilized
Niobium	$7.1 \times 10^{-6}/^{\circ}\text{C}$	2468°C	bcc

Figure 6.7 Comparative chart of the selected materials

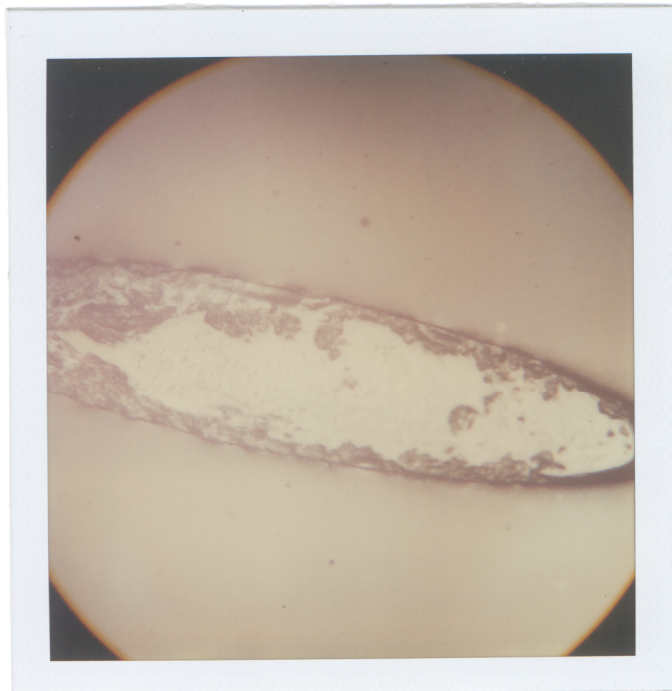


Appendix A Samples prepared for heat treatment



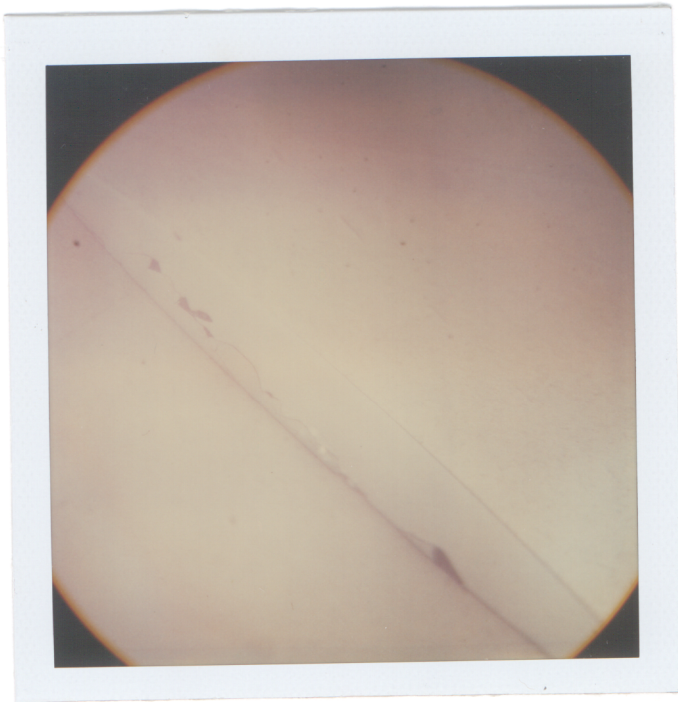
Appendix A Samples prepared for heat treatment

Sapphire Fiber

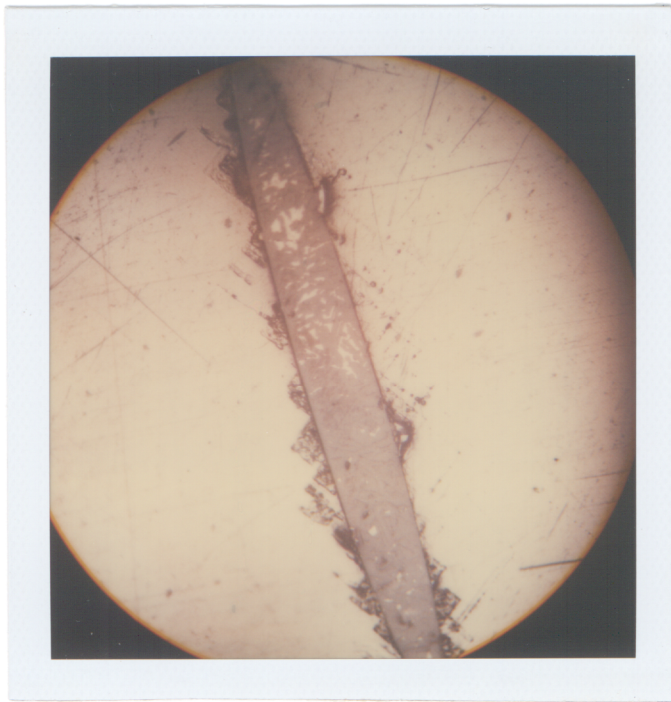


Appendix B Samples of fiber cross section for microprobe

Silica Fiber



Appendix B Samples of fiber cross section for microprobe



Appendix C Silica in silicon carbide cross section

Bibliography

- 1 Maria Gentile, *Alkali attack of coal gasifier linings*, MSMatE Thesis, Virginia Tech, 1985.
- 2 Kyoung - ho Lee *Alkali attack of coal gasifier linings*, MSMatE Thesis, Virginia Tech, 1988.
- 3 Rhonda Fae Hayden, *The study of the resistance of refractories to alkali vapours*, MSMatE Thesis, Virginia Tech, 1987.
- 4 P. W. Jayatilleke, *Carbon monoxide disintegration of coal gasifier refractories at elevated pressure* MSMatE Thesis, Virginia Tech, 1978.
- 5 M. M. Schwartz, *Composite Materials Handbook* (John Wiley & Sons) 1984.
- 6 Robert M. Jones, *Mechanics of Composite Materials*, Scripta Book Company 1975.
- 7 deGroot; J. J., dr ir J. J. deGroot, and ir J. A. J. M. van Vliet, *The high pressure sodium lamp*, (Phillips Technical Library, Kluwer Technischeboeken B. V., Deventer - Antwerpen), 1986.
- 8 R. J. Tiernam and J. E. Saunders, *Transient temperature emittance measurements on translucent aluminas*, Proceedings on the Symposium on high temp. lamp chem. Edited by E. G. Zubler, 1986, pp 206 - 219.
- 9 R. K. Datta, *Emission and Sealing Materials Chemistry of High Pressure Sodium (HPS) Lamp*, *ibid.* pp 220 - 223.
- 10 R. A. Snellgrove, *Seal Reactions at High Temperatures in Discharge Lamps*, *ibid.* pp 251-263.
- 11 A. J. H. M. Kock, *Surface Structure of Translucent Alumina, A Scanning Electron Microscopy Investigation*, *ibid.* pp 194 - 205.
- 12 Engineering property data on selected ceramics, Vol 3, Single oxides, MCIC report July 1981, (Metals and Ceramics Information Center).

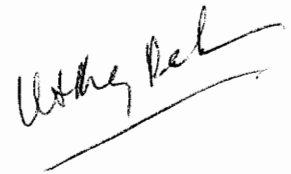
- 13 Martin Grayson (Editor), *Ceramics (Properties and Applications) - Encyclopedia of Composite materials and components*, reprint series (John Wiley & Sons), 1986, pp 300 - 323.
- 14 C-H Anderson and R. Warren, *Silicon Carbide Fibres and their Potential for Use in Composite Materials. Part I*“, *Composites*, Vol. 15, No 1, Jan 1984, pp 16 - 23.
- 15 R. Warren and C-H Anderson, *Silicon Carbide Fibres and their Potential for Use in Composite Materials. Part II* *ibid.* No 2, April 1984, pp 101 - 112.
- 16 Yasuharu Suematsu Ken-ichi Iga, *Introduction to Optical fiber communication*, (John Wiley & Sons), 1982.
- 17 H. E. LaBelle, Jr. and A. I. Mlavsky, *Growth of Controlled Profile Crystals from the Melt, Part I - Sapphire Filaments* , *Mat. Res. Bull.* Vol. 6, pp 571 - 580, 1971.
- 18 G. F. Hurley and T. T. A. Pollock, *Mechanical and Structural Characterisation of Sapphire Ribbons and Continuous Filaments* *Metallurgical Transactions*, Vol. 3, Feb. 1973, pp 397 - 402.
- 19 R. L. Mehan, *Stability of Single Crystal Sapphire in Nickel and Nickel Alloy Matrices*, *ibid.* April 1972, pp 897 - 904.
- 20 R. L. Crane and R. E. Tessler, *Effects of Surface Damage on the Strength of C-Axis Sapphire Filament* *J. Comp. Mat.* Vol. 5; Oct. 1971 pp 537 - 541.
- 21 R. H. Dhattman and M. W. Zemansky, *Heat and Thermodynamics* , (McGraw-Hill Book Company) 1979.
- 22 Hummel, F. A.; *Introduction to Phase Equilibria in Ceramic Systems*, (New York and Basel), 1985.
- 23 *Phase diagram for ceramists Vol 1 - 5*, Compiled at National Bureau of Standards (American Ceramics Society Inc.), 1984.
- 24 Thaddeus B. Massalski, Editor in Chief, *Binary Alloys Phase Diagrams, Vol 2*, (American Society for Metals, Metals Park, Ohio) 1986.

- 25 Patel, P. D.; Chandan, H. C.; Kalish, D.; *International Wire and Cable Proceedings*, 1981, pp 37 - 43.
- 26 Love, Roy E.; *Fiber and Integrated Optics*, SPIE Vol 77, pp 69 - 77.
- 27 M. J. Matthewson and C. R. Kurkjian, *J. Am. Ceram. Soc.* 71[3] pp 177 - 83, 1988.
- 28 S. T. Gulati, J. D. Helfinstine, G. S. Glaesemann, D. R. Roberts, E. Cuellar and L. M. Middleman, *Fiber Optic Reliability Benign and Adverse Environments*, SPIE, Vol. 842, 1987, pp 22 - 31.
- 30 M. J. Matthewson, C. R. Kurkjian, S. T. Gulati, *Strength Measurement of Optical Fiber by Bending*, *J. Am. Ceram. Soc.*, Vol. 69, No. 11, Nov. 1986, pp 815 - 821.
- 31 Robert D. Maurer, *Mat. Res. Bull.* Vol. 14, 14, 1979, pp 1305 - 1310,
- 32 T. W. Chou, A. Kelly, A. Okura, *Comp.* Vol. 16, No. 3, Jul. 1985, pp 187 - 205.
- 33 Saphikon Corp, Milford, NH, Standard Parts.
- 34 F. Donald Bloss, *Crystallography and Crystal Chemistry An Introduction*, VPI&SU (Holt, Rinehart and Winston, Inc), 1986.
- 35 Klaus Keil; *The Electron Microprobe X-ray Analyser and its Application in Mineralogy*, (National Aeronautics and Space Administration, Space Science Divisions, Ames Research Center, Moffett Field, California), 1975.

Vita

Ruby Raheem born in Kerala, India attended Presentation Convent Girls High School, Kodaikanal which is situated above 7000 feet above sea level in the Palni Hills of southern India. She received her undergraduate degree in Physics from Providence Women's College, Calicut, affiliated to Calicut University, India. In 1983 Marquette University Milwaukee, Wisconsin sponsored her for her graduate studies in Physics in the US and she received her Masters degree in Physics in 1985. She joined the department of Electrical Engineering at Virginia Tech, in the Fall of 1987 and in May 1990 she received her Masters in Electrical Engineering.

Besides applied physics, Ruby is interested in tennis, soccer, volley ball and hockey. She writes in her spare time and has published some of her work in college magazines. She enjoys meeting people of different cultural and ethnic background. She intends to take up writing seriously when she retires.

A handwritten signature in black ink, appearing to read 'Ruby Raheem', with a horizontal line underneath it.